國立臺灣大學生命科學院生化科學研究所

博士論文

Institute of Biochemical Sciences

College of Life Science

National Taiwan University

Doctoral Dissertation

# 研究類澱粉蛋白之調節蛋白 SERF1a 對阿茲海默症 Amyloid-β 和亨丁頓舞蹈症 HttpolyQ 纖維化的影響

# Investigating the Effect of an Amyloid Modifier SERF1a on Alzheimer's Amyloid-β and Huntington's HttpolyQ Fibrillization

蔡天穎

Tien-Ying Tsai

指導教授：陳韻如 博士，陳佩燁 博士

Advisor: Yun-Ru Chen, Ph.D., Rita P.-Y. Chen, Ph.D.

中華民國 112 年 8 月

August 2023

doi:10.6342/NTU202303164

# 中文摘要

隨著社會高齡化的現象，現今全球已有數千萬人受到神經退化性疾病的侵襲。在各種神經退化性疾病中，特定蛋白的聚集和堆積不僅使蛋白失去原本功能，也會產生神經毒性，進而造成神經功能的喪失。此類蛋白共同的特點為聚集後會形成由交叉β折疊所構成的纖維，即所謂類澱粉蛋白。近年，small EDRK-rich factor (SERF)蛋白被發現會促進類澱粉蛋白纖維化，因此被稱為類澱粉蛋白之調節蛋白。為了更進一步了解其機制，在此篇論文中，我們致力於研究 SERF1a 在阿茲海默症 Amyloid-β (Aβ)和亨丁頓舞蹈症 HttpolyQ 纖維化過程中所扮演的角色。我們利用硫代黃素-T (Thioflavin-T) 和圓二色光譜儀(circular dichroism spectroscopy)證明 SERF1a 加速了 Aβ 纖維化，而 Aβ 纖維量並不會因 SERF1a 有所差異。傅立葉轉換紅外光譜 (Fourier-transform infrared spectroscopy)和穿透式電子顯微鏡(transmission electron microscope)的結果顯示，SERF1a 會改變 Aβ 纖維的二級結構組成和型態。我們更進一步藉由電噴灑游離質譜法 (electrospray ionization mass spectrometry)、分析型超高速離心機(analytical ultracentrifugation)和核磁共振(nuclear magnetic resonance)發現，SERF1a 是利用其 N 端區域與 Aβ 形成 1:1 的結合。然而，SERF1a 會在改變 Aβ 後離開，並非成為纖維中的一部分。另外，細胞毒性測試結果顯示，SERF1a 會因加速 Aβ 纖維化而加重 Aβ 對細胞的毒性。此影響可利用 SERF1a 抗體阻斷 SERF1a 與 Aβ 的結合來排除。在 HttpolyQ 的研究中，實驗室前人發現 SERF1a 促進 HttpolyQ 纖維化，並以 α 螺旋的區域與 HttpolyQ 結合。接續其研究結果，為了針對蛋白結合做更進一步的探討，我們設計了一系列 HTT 短胜肽，並藉由等溫滴定量熱法(isothermal titration calorimetry)和小角度 X 光散射(small-angle X-ray scattering)發現，SERF1a 主要是與 HttpolyQ 的 N 端 17 個胺基酸以 1:2 的方式結合。除此之外，我們生產了 SERF1a 單株抗體，以應用在 SERF1a



doi:10.6342/NTU202303164

相關的研究中。整體而言，我們證實了 SERF1a 以不同機制對於 Aβ 和 HttpolyQ 纖維化產生影響，以提供未來阿茲海默症和亨丁頓舞蹈症療法的新方向。

**關鍵詞：**Amyloid-β、HttpolyQ、SERF1a、阿茲海默症、亨丁頓舞蹈症、纖維化、細胞毒性



doi:10.6342/NTU202303164

# ABSTRACT

Neurodegenerative disorders have impacted millions of people worldwide with no effective cure currently. Most proteins involved in neurodegenerative diseases are prone to aggregate and deposit in the brain, leading to the loss of neuronal functions. These aggregates show fibrillary structures with a highly ordered cross β-sheet and display the characteristics of amyloid-like protein assemblies. Modifier of aggregation 4 (MOAG-4)/small EDRK-rich factor (SERF) has been identified as an amyloid modifier that promotes the aggregations of amyloidogenic proteins. To further discover the underlying mechanisms, in this dissertation, we focused on the role of SERF1a in Amyloid-β, one of the hallmarks of Alzheimer's disease (AD), and HttpolyQ, involved in Huntington's disease (HD), fibrillization. We first monitored SERF1a effect on Aβ fibril formation by Thioflavin T assay and far-UV circular dichroism (CD) spectroscopy combined with filter-trap assay, immunogold labeling, and partition analysis. We found that SERF1a expedited Aβ aggregation in a dose-dependent manner without affecting the fibril amount and was excluded from Aβ fibrils. Using Fourier-transform infrared spectroscopy (FTIR) and transmission electron microscope (TEM), we showed that SERF1a changed the secondary structures and the morphology of Aβ fibrils. We also investigated the complex formation of SERF1a and Aβ by photo-induced cross-linking of unmodified proteins (PICUP), electrospray ionization mass spectrometry (ESI-MS), and analytical



doi:10.6342/NTU202303164

ultracentrifugation (AUC) and the results revealed that SERF1a and Aβ mainly formed a 1:1 complex. Moreover, the NMR experiment suggested that SERF1a interacted with Aβ via its N-terminal region. Cytotoxicity assay demonstrated that SERF1a-accelerated Aβ intermediates enhanced the Aβ toxicity in neuroblastoma and the effect could be blocked by SERF1a antibody. As for HttpolyQ, based on our previous findings that SERF1a promoted HttpolyQ fibrillization and interacted with HttpolyQ, in a way different from that observed for Aβ, via its helical regions, we further investigated the interaction between SERF1a and HttpolyQ. Here, by using isothermal titration calorimetry (ITC) and small-angle X-ray scattering (SAXS), the HTT peptide study showed that SERF1a preferentially bound to the region containing N-terminal 17 residues of HttpolyQ in a 1:2 ratio. In addition, we produced SERF1a monoclonal antibodies for further applications in our research. Altogether, our study demonstrated that SERF1a plays a promoting role in Aβ and HttpolyQ fibrillization and offers insight into the underlying mechanisms in which SERF1a accelerates the conformational changes of Aβ and HttpolyQ to be more aggregation-prone. Our work provides a new direction for the therapeutic development of both AD and HD.

**Keywords**: Alzheimer's disease, Amyloid-β, cytotoxicity, fibrillization, HttpolyQ, Huntington's disease, SERF1a



doi:10.6342/NTU202303164

# TABLE OF CONTENTS

**中文摘要** ..... **I**

**ABSTRACT** ..... **III**

**TABLE OF CONTENTS** ..... **V**

**LIST OF FIGURES** ..... **X**

**ABBREVIATIONS** ..... **XII**

**CHAPTER 1. INTRODUCTION** ..... **1**

1.1 Amyloid in neurodegenerative diseases ..... 1

1.2 Alzheimer's disease ..... 3

1.2.1 Overview of Alzheimer's disease ..... 3

1.2.2 Amyloid β ..... 4

1.3 Huntington's disease ..... 7

1.3.1 Overview of Huntington's disease ..... 7

1.3.2 Huntingtin protein ..... 7

1.4 Modifying factors ..... 9

1.4.1 Overview of modifying factors ..... 9

1.4.2 SERF protein ..... 10



doi:10.6342/NTU202303164

1.5 Motivation and Objectives ..... 13

**CHAPTER 2. MATERIALS AND METHODS ..... 15**

2.1 Materials ..... 15

2.1.1 Buffers ..... 15

2.1.2 Plasmids ..... 17

2.1.3 Brain lysates ..... 20

2.1.4 Antibodies ..... 20

2.1.5 Commercial reagents ..... 20

2.2 Methods ..... 21

2.2.1 Protein expression and purification ..... 21

2.2.2 Aβ peptide preparation ..... 24

2.2.3 Thioflavin T (ThT) assay ..... 25

2.2.4 Far-UV circular dichroism (CD) spectroscopy ..... 26

2.2.5 Filter-trap assay ..... 26

2.2.6 Transmission Electron Microscopy (TEM) ..... 27

2.2.7 Partition analysis ..... 28

2.2.8 Photo-Induced Cross-linking of Unmodified Proteins (PICUP) ..... 28



doi:10.6342/NTU202303164

2.2.9 Fourier-transform infrared spectroscopy (FTIR) ..... 29

2.2.10 Electrospray ionization mass spectrometry (ESI-MS) ..... 29

2.2.11 Analytical ultracentrifugation (AUC) ..... 30

2.2.12 Nuclear magnetic resonance (NMR) Spectroscopy ..... 31

2.2.13 MTT cytotoxicity assay ..... 32

2.2.14 HTT peptide preparation ..... 33

2.2.15 Isothermal titration calorimetry (ITC) ..... 33

2.2.16 Small-angle X-ray scattering (SAXS) ..... 34

2.2.17 Dot blot and western blot for antibody selection ..... 34

2.2.18 Enzyme-linked immunosorbent assay (ELISA) ..... 35

2.2.19 Cell transfection and collection ..... 35

2.2.20 Immunoprecipitation (IP) ..... 36

2.2.21 In-gel digestion ..... 36

2.2.22 Immunocytochemistry (ICC) ..... 38

**CHAPTER 3. RESULTS ..... 39**

Part I. Investigating the role of SERF1a in Aβ40 and Aβ42 fibrillization ..... 39



doi:10.6342/NTU202303164

3.1 SERF1a reduces the lag time of Aβ40 and Aβ42 fibril formation in a dose-dependent manner without change in the amount of fibrils ..... 39

3.2 SERF1a changes morphology and secondary structure of Aβ40 and Aβ42 fibrils without being incorporated into the fibrils ..... 46

3.3 SERF1a forms complexes with Aβ40 and Aβ42 primarily in a 1:1 stoichiometry ..... 52

3.4 SERF1a interacts with Aβ40 through its N-terminal region ..... 60

3.5 SERF1a enhances the cytotoxicity of Aβ40 and Aβ42 intermediates in neuroblastoma ..... 63

3.6 The cytotoxicity caused by SERF1a-induced Aβ42 intermediates can be rescued by SERF1a antibody ..... 67

Part II. Examining the effect of SERF1a on HttpolyQ fibrillization ..... 69

3.7 SERF1a binds to N-terminus of HTT peptides ..... 69

3.8 The expression level of SERF1a is higher in HD subjects ..... 77

Part III. SERF1a antibody production and application ..... 78

3.9 Production and selection of SERF1a antibodies ..... 78

3.10 Application and examination of SERF#2 ..... 81



doi:10.6342/NTU202303164

3.11 Examination of SERF#1 and SERF B5 ..... 86

3.12 Validation of SERF B1 ..... 90

**CHAPTER 4. DISCUSSION ..... 92**

4.1 Investigating the role of SERF1a in Aβ40 and Aβ42 fibrillization ..... 92

4.2 Examining the effect of SERF1a on HttpolyQ fibrillization ..... 97

**REFERENCES ..... 103**

**APPENDIX ..... 112**

List of antibodies ..... 112

List of commercial reagents ..... 113



doi:10.6342/NTU202303164

# LIST OF FIGURES

Figure 1. Sequence alignment of human SERF proteins. ..... 12

Figure 2. SERF1a accelerates Aβ fibrillization in a dose-dependent manner. ..... 42

Figure 3. SERF1a accelerates Aβ to form β-sheet structure. ..... 44

Figure 4. SERF1a does not affect the final amount of Aβ fibrils. ..... 45

Figure 5. SERF1a alters morphology and secondary structure of Aβ fibrils. ..... 48

Figure 6. SERF1a dissociates from Aβ after catalyzing fibril formation. ..... 50

Figure 7. SERF1a forms complexes with Aβ40 and Aβ42. ..... 55

Figure 8. SERF1a forms complexes with Aβ40 and Aβ42 in a 1:1 ratio. ..... 58

Figure 9. SERF1a forms complexes with Aβ40 and Aβ42 in a 1:1 ratio and disrupts Aβ42 oligomer formation in solution. ..... 59

Figure 10. SERF1a interacts with Aβ40 via N-terminal region. ..... 62

Figure 11. SERF1a increases Aβ cytotoxicity at intermediate stage in neuroblastoma. ..... 65

Figure 12. TEM images of 14-18 hr incubated Aβ40 and Aβ42 intermediates. ..... 66

Figure 13. SERF1a antibody blocks the effect of SERF1a on Aβ42 in human neuroblastoma. ..... 68

Figure 14. The primary sequence of the designed HTT peptides. ..... 72

Figure 15. Far-UV CD spectra of HTT peptides for the secondary structures. ..... 72



doi:10.6342/NTU202303164

Figure 16. ITC raw and fitted data of HTT peptides with SERF1a titration for the binding affinity. ..... 74

Figure 17. AUC analysis of HTT peptides. ..... 75

Figure 18. SAXS data and the extracted $R_g$ values of HTT peptides and SERF1a. .... 76

Figure 19. SERF1a protein level is elevated in HD plasma. ..... 77

Figure 20. The sequences of SERF1a N-terminus and C-terminus peptides used to immunize mice to produce SERF1a antibodies. ..... 79

Figure 21. Validation of the efficiency of SERF1a antibodies. ..... 80

Figure 22. Detection of SERF1a levels in AD brain (cortex) lysates by SERF#2. ..... 83

Figure 23. Examination of SERF1a expressed in cells. ..... 84

Figure 24. The band selection from IP for MS. ..... 85

Figure 25. Examination of the specificity of SERF1a antibodies in cells. ..... 87

Figure 26. Examination of the specificity and affinity of SERF1a antibodies in cells. ..... 88

Figure 27. Validation of SERF B1 by ELISA and western blot. ..... 91

Figure 28. Proposed model of SERF1a effect on Aβ aggregation. ..... 101

Figure 29. Mechanisms of SERF1a and HttpolyQ assembly. ..... 102



doi:10.6342/NTU202303164

# ABBREVIATIONS

| | |
|---|---|
| **Aβ** | amyloid-β |
| **ACN** | acetonitrile |
| **AD** | Alzheimer's disease |
| **AICD** | APP intracellular domain |
| **α-Syn** | α-synuclein |
| **ALS** | amyotrophic lateral sclerosis |
| **Amp** | ampicillin sodium salt |
| **APOE** | apolipoprotein |
| **APP** | amyloid precursor protein |
| **APS** | ammonium persulfate |
| **AUC** | analytical ultracentrifugation |
| **BACE1** | β-site APP-cleaving enzyme 1 |
| **BCA** | bicinchoninic acid |
| **β-ME** | β-mercaptoethanol |
| **BSA** | bovine serum albumin |
| **CD** | circular dichroism |
| **CSP** | chemical shift perturbation |
| **DMSO** | dimethyl sulfoxide |



doi:10.6342/NTU202303164

| | |
|---|---|
| **DTT** | dithiothreitol |
| **ECL** | enhanced chemiluminescence |
| **EDTA** | ethylenediaminetetraacetic acid |
| **ELISA** | enzyme-linked immunosorbent assay |
| **EOAD** | early-onset AD |
| **ESI-MS** | electrospray ionization mass spectrometry |
| **FBS** | fetal bovine serum |
| **FTIR** | Fourier-transform infrared spectroscopy |
| **HD** | Huntington's disease |
| **HFIP** | 1,1,1,3,3,3-Hexafluoro-2-propanol |
| **HPLC** | high performance liquid chromatography |
| **HRP** | horseradish peroxidase |
| **HSQC** | heteronuclear single quantum coherence |
| **ICC** | immunocytochemistry |
| **IP** | immunoprecipitation |
| **IPTG** | isopropyl ß-D-1-thiogalactopyranoside |
| **ITC** | isothermal titration calorimetry |
| **kDa** | kilodalton |
| **LB** | Luria-Bertani |



doi:10.6342/NTU202303164

| | |
|---|---|
| **LOAD** | late-onset AD |
| **MOAG-4** | modifiers of aggregation 4 |
| **NFT** | neurofibrillary tangle |
| **NMR** | nuclear magnetic resonance |
| **NT17** | N-terminal 17 amino acids (of HttpolyQ) |
| **PBS** | Phosphate-buffered saline |
| **PD** | Parkinson’s disease |
| **PICUP** | photo-induced cross-linking of unmodified proteins |
| **PQC** | protein quality control |
| **PRD** | proline-rich domain |
| **PSEN1** | presenilin-1 |
| **PSEN2** | presenilin-2 |
| **PVDF** | polyvinylidene fluoride |
| **rpm** | revolution per minute |
| **RuBpy** | Tris(2,2'-bipyridyl) dichlororuthenium(II) hexahydrate<br>(Tris(2,2'-bipyridyl)ruthenium(II) chloride hexahydrate) |
| **SAXS** | small-angle X-ray scattering |
| **SDS-PAGE** | sodium dodecyl sulfate-polyacrylamide gel electrophoresis |
| **SERF** | small EDRK-rich factor |



doi:10.6342/NTU202303164

| | |
|---|---|
| **SV** | sedimentation velocity |
| **TBS** | Tris-buffered saline |
| **TEM** | transmission electron microscopy |
| **TEMED** | N,N,N',N'-Tetramethyl ethylenediamine |
| **TFA** | trifluoroacetic acid |
| **ThT** | thioflavin T |
| **UA** | uranyl acetate |



doi:10.6342/NTU202303164

# CHAPTER 1. INTRODUCTION

## 1.1 Amyloid in neurodegenerative diseases

Neurodegenerative diseases become epidemic affecting millions of people worldwide nowadays as the elderly population is growing[1,2]. This kind of disease is characterized by slowly progressive neuronal damage and dysfunction that results in movement disorders and/or cognitive and behavioral disorders[3]. These neurodegenerative diseases such as Alzheimer's disease (AD), amyotrophic lateral sclerosis (ALS), Parkinson's disease (PD), and Huntington's disease (HD) share common molecular and cellular mechanisms including abnormal protein aggregation and deposition[4]. Normally, these unfolded/misfolded, aggregation-prone proteins can be monitored and eliminated by the protein quality control (PQC) system such as chaperon machinery, protein degradation, and protein compartmentalization to maintain protein homeostasis[3,5]. However, this protective system declines during aging which is the major risk factor for most neurodegenerative diseases[6]. With the faulty PQC system, the unfolded/misfolded proteins are unable to be efficiently removed and therefore accumulate and deposit in the cells leading to proteotoxicity. These toxic aggregates show fibrillary structures with a highly ordered cross β-sheet conformation in which the β-strands are stacked along the axis of the fibril to form parallel β-sheets by hydrogen bonds, termed amyloid[7,8]. In the



doi:10.6342/NTU202303164

nucleation phase of amyloid formation, monomeric precursors including intrinsically disordered, transiently unfolded, and, in rare cases, native proteins first assemble into oligomeric species with varied structures. Heterogeneous oligomers then associate to form either on-pathway fibril nucleus that can rapidly recruit other monomers into the aggregates or off-pathway assemblies that end the fibril formation. In the elongation phase, the existing fibrils can fragment to gain more fibril ends for the recruitment of monomers or other aggregation-prone species thereby facilitating fibril formation with exponential growth. The process enters the final stage, stationary phase, when all free materials assemble into fibrils. Fibrils can further associate with each other to form the larger amyloid plaques which is the hallmark of a wide range of neurodegenerative diseases[9,10]. Although amyloid fibrils have a common cross-β structure, the sequences and organization of the polypeptide chains vary the interactions between side chains contributing to the diversity of fibril structures with different physical, chemical, or biological properties[11]. The amyloid fibrils in different neurodegenerative disorders are composed of different proteins such as amyloid-β (Aβ) in AD, α-synuclein (α-Syn) in PD, and Huntingtin in HD, while one protein may be found in more than one disease and one disease may contain more than one amyloid deposit[3]. Amyloid aggregation also occurs in non-neurodegenerative diseases such as type II diabetes[12] and cataract[9].



doi:10.6342/NTU202303164

## 1.2 Alzheimer's disease

### 1.2.1 Overview of Alzheimer's disease

Alzheimer's disease is the most prevalent form of dementia. Currently, there are approximately 50 million patients worldwide and the number is predicted to reach even more than 150 million by 2050. AD not only impacts individuals but also results in family and financial burdens[13]. Generally, the clinical symptoms of AD can be divided into 4 stages including (1) pre-clinical stage with mild memory loss, (2) early stage with loss of concentration and memory, mood changes as well as disorientation of place and time, (3) moderate stage with an increased memory loss and difficulty in speaking, reading as well as writing, and (4) later stage with increasingly severe functional and cognitive impairments[14]. Since AD is a slowly progressive disorder, most cases occur after 65 years old, termed late-onset AD (LOAD), while less than 5% of the patients are affected earlier than age 65, known as early-onset AD (EOAD)[15,16]. AD is also a multifactorial disease causing by several risk factors such as, in addition to aging, head injuries, infections, genetic and environmental factors[14,17]. Genetically, mutations in *APP* (amyloid precursor protein, APP), *PSEN1* (presenilin-1, PS-1), and *PSEN2* (presenilin-2, PS-2) lead to rare early-onset familial AD accounting for less than 1% of AD cases[15]. *APOE* ε4 allele (apolipoprotein E4) constitutes the primary genetic risk factor for late-onset familial and sporadic AD, where the latter accounts for the majority of AD cases[18,19]. The presence of



doi:10.6342/NTU202303164

extracellular amyloid-β (Aβ) plaques and intracellular hyperphosphorylated tau protein-formed neurofibrillary tangles (NFTs) is considered as the key pathological hallmark in AD[1]. There are several hypotheses proposed for the causality of AD such as the Aβ hypothesis, the tau hypothesis, the cholinergic hypothesis, and the dendritic hypothesis[20]. Although the Aβ hypothesis has been debated for a long time, it is still the most well-known and recognized one nowadays. This hypothesis is based on the strong relationship between Aβ deposition in the central nervous system and the onset of dementia. It suggests that AD is caused by an imbalance between production and degradation of Aβ, which may result from abnormally increased production due to genetic mutations and/or decreased degradation owing to aging[14,20].

### 1.2.2 Amyloid β

Aβ peptides, the major component of amyloid plaques in the brain of AD, are generated from amyloid precursor protein (APP), a type I transmembrane protein, through proteolytic cleavages. There are two proteolytic processing pathways[21-23]. One is non-amyloidogenic pathway in which APP is first cleaved by α-secretase, including ADAM9, 10, and 17 (members of a disintegrin and metalloprotease family)[24], at a site between Lys16 and Leu17 of Aβ domain yielding an extracellularly released soluble APPsα and a membrane-bound APP carboxy-terminal fragment called αCTF or C83[25-27], the latter is



doi:10.6342/NTU202303164

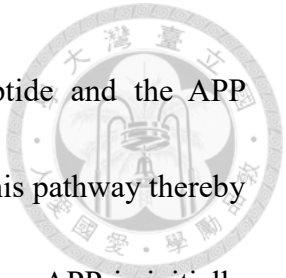

further cleaved by γ-secretase to release an extracellular p3 peptide and the APP intracellular domain (AICD). The majority of APP is processed via this pathway thereby preventing Aβ generation. The other is amyloidogenic pathway where APP is initially cleaved by β-secretase, also known as β-site APP-cleaving enzyme 1 (BACE1), to generate an extracellularly released soluble APPsβ and a membrane-bound βCTF (C99). The subsequent cleavage of βCTF by γ-secretase releases Aβ peptides extracellularly and the AICD intracellularly. The Aβ peptides produced by this pathway are diverse in length ranging from 38 to 43 residues, while Aβ40 and Aβ42 are the two most common isoforms in the human brain[23]. Aβ peptides are intrinsically disordered and are prone to assemble into amyloid fibrils with cross-β structures. It has been reported that Aβ42 is the principal component of amyloid plaques and the major neurotoxic species[28-30], although the levels of Aβ40 in cerebrospinal fluid is much higher than that of Aβ42[31]. This fact may result from the higher susceptibility of Aβ42 to aggregation as the addition of two residues, isoleucine and alanine, at the C terminus makes Aβ42 more hydrophobic than Aβ40. Therefore, the Aβ42 levels and the Aβ42/Aβ40 ratio play a pivotal role in AD pathogenesis. Increasing the Aβ42/Aβ40 ratio, not total Aβ levels, induces not only Aβ aggregation but also tau pathology and consequent neurodegeneration[14]. Mutations in APP and presenilin (PS-1 or PS-2), the catalytic subunit of γ-secretase, affect the generation of Aβ species and the Aβ42/Aβ40 ratio[32-34]. Several mutations in APP



doi:10.6342/NTU202303164

influence the cleavage site of γ-secretase and therefore increase the Aβ42/Aβ40 ratio. PS-1 and PS-2 mutations also increase the Aβ42/Aβ40 ratio by reducing Aβ40 levels and elevating Aβ42 levels, respectively[35,36]. Between soluble monomers and insoluble fibrils, Aβ has several different intermediate states during the aggregation, including soluble oligomers and larger protofibrils. Except for monomers, soluble intermediates and insoluble fibrils exhibit neurotoxicity in different levels[21]. Aβ causes cytotoxicity via several mechanisms, such as increasing oxidative stress by reducing metal ions[37], leading to synaptic dysfunction by disturbing the synaptic transmission[38], interacting with various neurotransmitters receptors[39], and resulting in mitochondrial dysfunction by inhibiting the production of mitochondrial ATP[40]. In addition to the neurotoxic role in AD pathogenesis, accumulated evidence suggests that Aβ has several physiological functions[21]. For instance, it has been demonstrated that blocking or reducing endogenous Aβ in animal models impairs long-term potentiation and memory, and the impairments can be rescued by exogenously applied Aβ42 with the physiological dose, low picomolar range, indicating the essential role of soluble Aβ in synaptic plasticity and memory[41]. Moreover, monomeric Aβ has been found to positively regulate synaptic transmission[42] and maintain neuronal glucose homeostasis[43]. Accordingly, the synaptic failure and neuronal loss in AD can also be caused by loss of function of Aβ monomers due to the aggregation.



doi:10.6342/NTU202303164

## 1.3 Huntington's disease

### 1.3.1 Overview of Huntington's disease

Huntington's disease is another neurodegenerative disorder and is also the most well-known polyglutamine (polyQ) disease[44], which results from abnormal expansion of CAG trinucleotide repeats, coding for a polyQ stretch. The dominantly inherited CAG repeat expansion in HD occurs in exon 1 of the huntingtin gene (*HTT*) encoding huntingtin protein (Htt). Normally, CAG units range from approximately 10 to 35 repeats in healthy subjects, while 36 or more repeats lead to progressive HD and the number of repeats is negatively correlated with the age of onset[45,46]. The symptoms that may begin from childhood to old age with an average at around 45 years old include involuntary muscle movements, behavioral and mental disorders, and dementia.

### 1.3.2 Huntingtin protein

The *HTT* gene containing 67 exons encodes a large Htt protein composed of 3,144 amino acids, 348 kDa[47]. In human, Htt protein is ubiquitously expressed throughout most tissues with different levels. Within the nervous system where Htt expression is higher than in other tissues, this protein can be found not only in the striatum, the most vulnerable region to HD pathology, but also in the cortex, hippocampus, and cerebellum[48,49]. Htt is present in both nucleus and cytoplasm and shuttles between these two regions through its nuclear export and nuclear localization sequences[50-52]. Numerous studies suggest that



doi:10.6342/NTU202303164

wild-type Htt is involved in various cellular processes[47]. For instance, Htt plays a role in the regulations of organelle transport in axons and dendrites within neurons[53-55], transcription[56,57], and endocytosis[58,59] by interacting with the molecular motor machinery, transcription factors and transcriptional regulators, and the certain proteins involved in endocytosis, respectively. Htt is also essential for embryonic brain development[60,61], tissue maintenance[62], cell morphology[63,64], and cell survival[65,66]. Therefore, the mutant Htt protein caused by CAG repeat expansion impacts many cellular functions of Htt, resulting in cell death. The very N-terminal region encoded by *HTT* exon 1 has been widely studied since the pathogenic mutation occurs in this region, while the rest of the protein containing amino acids 69 to 3,144 is poorly characterized[47]. Human Htt exon 1 (Httex1) protein consists of N-terminal 17 amino acids (NT17), a central expanded polyQ tract, and C-terminal proline-rich domain (PRD). NT17 acting as a nuclear export signal is important for Htt trafficking and localization. It also plays critical role in regulating the aggregation and toxicity of Httex1[51]. PRD, in contrast to NT17, protects Httex1 from aggregation, while its effect is outweighed by NT17. Structurally, the study using X-ray crystallography demonstrated that Htt17Q-EX1 is composed of an α-helical NT17, a flexible poly17Q region adopting α-helix, random coil, and extended loop, and a polyproline helix [67]. An NMR study showed that NT17 and the connecting part of polyQ tract partially form α-helical structure[68]. Another NMR study combining with



doi:10.6342/NTU202303164

computational methods revealed that an α-helical structure propagates from part of NT17 into the polyQ region at low pH, while these regions become unstructured at neutral pH[69]. Pathologically, mutant Httex1 with more than 35 glutamine residues may undergo a conformational shift that is susceptible to aggregation and formation of amyloid fibrils that eventually deposit as inclusions in the neuronal cytoplasm and nucleus, leading to the loss of neuron and progressive dysfunction of brains [70-73].

## 1.4 Modifying factors

### 1.4.1 Overview of modifying factors

Amyloid formation is a complicated process with multiple stages, and aggregates are diverse in structure, morphology, stability, and cytotoxicity. In addition to the properties of protein itself, the aggregation process and final products can also be affected by many modifying factors including intrinsic factors such as mutations and expression levels and extrinsic factors such as metal ions, small molecules, and chaperones[74]. For instance, it has been shown that copper, zinc, iron, and aluminum ions influence Aβ aggregation mechanisms by promoting the formation of different types of oligomers[75]. Also, aberrantly high levels of $Cu^{2+}$, $Zn^{2+}$, and $Fe^{3+}$ are found in the senile plaques and colocalize with Aβ in AD brains[76]. Copper was also found to facilitate Httex1-polyQ oligomerization and aggregation. Moreover, some small molecules, such as



doi:10.6342/NTU202303164

epigallocatechin gallate[77] and curcumin[78], have been reported to inhibit Aβ fibrillization and neurotoxicity by promoting the formation of nontoxic oligomers. Chaperone proteins play a protective role that can assist protein folding, prevent aggregation, disassemble fibrils, and facilitate protein degradation[74]. In addition to the above-mentioned factors, a protein we are interested in and further investigated in our studies is introduced in more detail below.

### 1.4.2 SERF protein

Small EDRK-rich factor (SERF) is one of the names for the 4F5 family of proteins which is widely conserved in all sequenced eukaryotic organisms. The members in this protein family are generally less than 10 kDa in size and contain abundant charged residues with pI values higher than 10, as indicated by the name, small EDRK-rich factor[79]. A role for the family was first identified to be related to spinal muscular atrophy in 1998[80], while the role in amyloid aggregation and cytotoxicity was first found in 2010. By a chemical mutagenesis screen in polyQ-expressing *C. elegans* model, *moag-4* (*modifiers of aggregation 4*) encoding protein MOAG-4 was identified to modulate protein aggregation where deletion or mutation of *moag-4* reduced the aggregation of polyQ, whereas overexpression of *moag-4* promoted the aggregation[81]. Human orthologs of MOAG-4, SERF1a and SERF2, were also found to promote the aggregation and



doi:10.6342/NTU202303164

toxicity of polyQ proteins. Human SERF1a protein has two isoforms including the short one with 62 amino acids and the long one with 110 residues, while human SERF2 protein has four isoforms (Figure 1). They consist of a highly conserved N-terminal region which is partially disordered and a less conserved C-terminal region with more helical structure[79]. In addition, SERF1a showed aggregation-promoting effect specifically on amyloid proteins *in vitro* including α-Syn, HttpolyQ, Aβ40, and prion protein, but not on nonamyloid proteins[82]. In the study of underlying mechanisms, it has been proposed that the positively charged N-terminus of MOAG-4 competes with N-terminus of α-Syn for the negatively charged C-terminus of α-Syn, and the protected hydrophobic central region of α-Syn is therefore exposed to facilitate the aggregation[83]. Similarly, another study by NMR/SAXS analysis demonstrated that the charge-driven binding of SERF1a to α-Syn resulted in the partial exposure of α-Syn amyloid nucleation site[84]. The transcript of human SERF1a short isoform is ubiquitously expressed with higher levels in testis and heart, and that of SERF1a long isoform is predominantly expressed in heart, skeletal muscle, and brain. Both of these isoforms are expressed throughout the central nervous system[80]. However, the physiological function of SERF1a protein is still obscure. It has been proposed that SERF1a, in normal condition, serves as an RNA-chaperone to mediate the functional integration of RNA in the nucleolus. However, it is released from the nucleolus to cytosol in response to stressors such as heat and oxidative stress[85]. Given the



doi:10.6342/NTU202303164

fact that SERF1a is considered a general modifier for amyloid fibrillization, it is essential to elucidate the underlying mechanisms and SERF1a functions for developing the therapeutic strategies for neurodegenerative diseases.

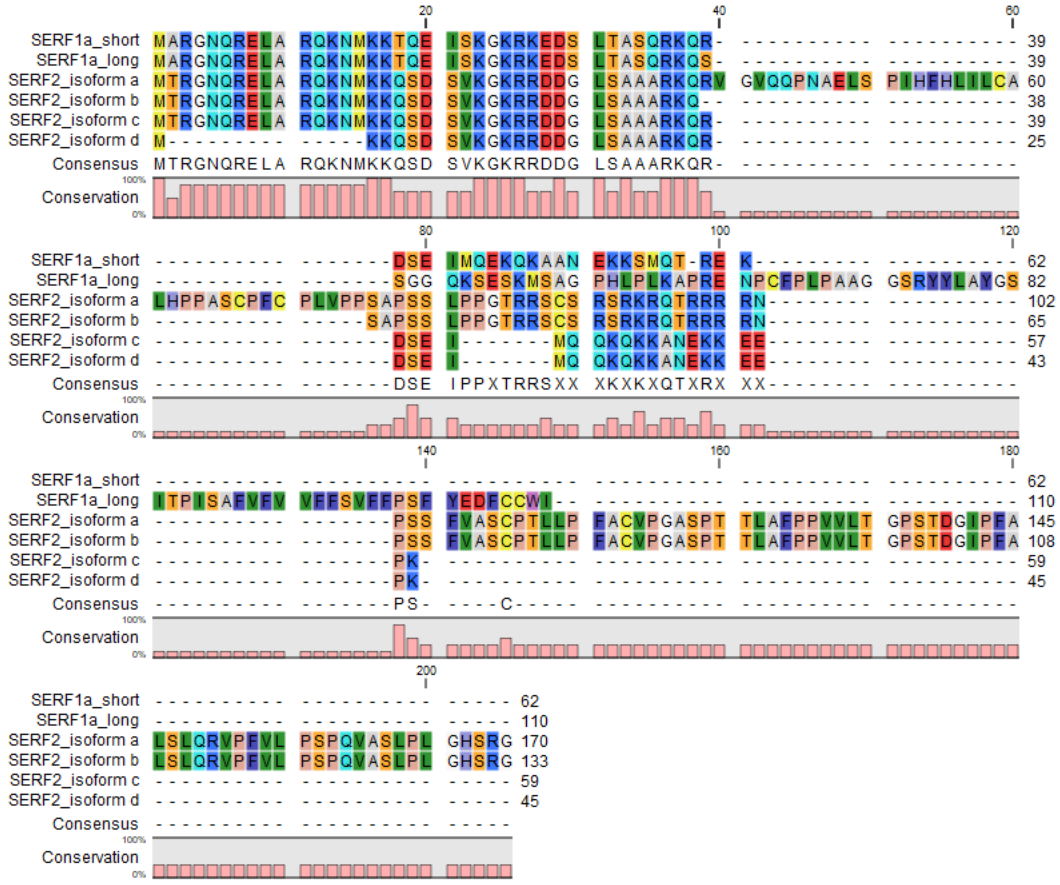


**Figure 1. Sequence alignment of human SERF proteins.**

The sequences of SERF proteins were from National Center for Biotechnology Information website. The alignment was performed by using CLC Sequence Viewer 8.0 software. A highly conserved N-terminal region and a less conserved C-terminal region were shown.



doi:10.6342/NTU202303164

## 1.5 Motivation and Objectives

Nowadays, the lives of millions of people and their families are impacted by neurodegenerative diseases in the whole world and the number is dramatically increasing. However, even though there are a cornucopia of studies focusing on the underlying mechanisms and developing the treatments, no effective treatments or cures are available to date. Therefore, it is imperative to discover potential therapies for neurodegenerative disorders. MOAG-4/SERF protein is an emergent amyloid modifier found in the last decade. Since it has been reported to affect the process of amyloid formation, manipulating this protein may help for therapeutic development.

To investigate the underlying mechanisms by which human SERF protein influences the fibrillization of amyloid proteins, our study focused on the effect of SERF1a short form on Aβ and HttpolyQ fibril formation.

In the first part of this study, we aimed to examine the role of SERF1a in Aβ40 and Aβ42 aggregation and the underlying mechanism. The effect of SERF1a on Aβ fibril growth was monitored by ThT assay, far-UV circular dichroism (CD) spectroscopy, and filter-trap assay. The effect on Aβ fibril morphology and secondary structure were detected by transmission electron microscopy (TEM) and Fourier-transform infrared spectroscopy (FTIR), respectively. The complex of SERF1a and Aβ was investigated by photo-induced cross-linking (PICUP), electrospray ionization mass spectrometry (ESI-



doi:10.6342/NTU202303164

MS), and analytical ultracentrifugation (AUC). The binding sites of Aβ on SERF1a was determined by nuclear magnetic resonance (NMR) spectroscopy. The effect of SERF1a on Aβ cytotoxicity and the effect of blocking agent, SERF1a antibody, were examined in human neuroblastoma cell line, BE(2)-C, and the cell viability was measured by MTT assay.

On the basis of our previous findings that SERF1a facilitates HttpolyQ fibrillization and the interaction between SERF1a and HttpolyQ may be via coiled-coils that consists of multiple α-helices, the second part of this study therefore aimed to further confirm the coiled-coil interaction. The tested HTT peptides were designed according to the prediction of the coiled coil position using DrawCoil. The secondary structure of these peptides was checked by far-UV CD spectroscopy. The species of these HTT peptides was assessed by AUC. The binding affinity of SERF1a to the peptides was examined by isothermal titration calorimetry (ITC) and small-angle X-ray scattering (SAXS).

The last part of this study aimed to generate SERF1a monoclonal antibodies for further applications. The affinity of the antibodies was validated by dot blot, western blot, and enzyme-linked immunosorbent assay (ELISA). The specificity of the antibodies was examined by immunoprecipitation (IP) and immunocytochemistry (ICC).



doi:10.6342/NTU202303164

# CHAPTER 2. MATERIALS AND METHODS

## 2.1 Materials

### 2.1.1 Buffers

**Purification of recombinant Aβ42**

Lysis buffer: 20 mM Tris, pH 8.0, 150 mM NaCl, and 1 mM DTT

Solubilization buffer: 20 mM Tris, pH 11.0, 150 mM NaCl, and 8 M urea

Binding buffer (A): 20 mM Tris, pH 8.0, 150 mM NaCl, and 5 M urea

Eluting buffer (B): 20 mM Tris, pH 8.0, 150 mM NaCl, 5 M urea, and 0.5 M imidazole

HPLC buffer A: 20% ACN and 0.1% TFA

HPLC buffer B: 90% ACN and 0.1% TFA

**Purification of recombinant SERF1a and $^{15}$N-SERF1a**

Lysis buffer: 20 mM Tris, pH 7.9, 0.5 M NaCl, 5 mM imidazole, and protease inhibitor

Buffer for HisPrep FF 16/10

Binding buffer (A): 20 mM Tris, pH 7.9, 500 mM NaCl, and 5 mM imidazole

Eluting buffer (B): 20 mM Tris, pH 7.9, 500 mM NaCl, and 250 mM imidazole

Thrombin cutting buffer: 20 mM Tris, pH 8.4, and 150 mM NaCl

Buffer for Mono S$^{TM}$ 5/50 GL

Binding buffer (A): 20 mM Tris, pH 8.0, 0.2 mM EDTA, 0.5 mM DTT, and 5 mM NaCl



doi:10.6342/NTU202303164

Eluting buffer (B): 20 mM Tris, pH 8.0, 0.2 mM EDTA, 0.5 mM DTT, and 0.5 M NaCl

SERF1a storage buffer: 50 mM Tris, pH 6.8, and 20 mM NaCl

$^{15}$N-SERF1a storage buffer: 50 mM Tris, pH 6.5, and 50 mM NaCl

**Purification of synthetic Aβ40**

HPLC buffer A: 10% ACN and 0.05% TFA

HPLC buffer B: 90% ACN and 0.05% TFA

**Purification of synthetic HTT peptides**

HPLC buffer A: 10% ACN and 0.1% TFA

HPLC buffer B: 90% ACN and 0.1% TFA

**Tricine SDS-PAGE**

10X running buffer (Anode): 1 M Tris, pH 8.9

10X running buffer (Cathode): 1 M Tris, pH 8.3, 1M Tricine, 1% SDS

3X gel buffer: 3 M Tris, pH 8.45, 0.3% SDS

5X sample buffer: 250 mM Tris (pH 6.8), 50% glycerol, 10% SDS, 0.05% bromophenol blue, 5% β-ME

Stain buffer: 0.25% Coomassie Brilliant Blue R250, 50% methanol, 10% acetic acid

Destain buffer: 7% acetic acid, 25% ethanol



doi:10.6342/NTU202303164

Tricine gel formula

| | Separating (13%) | Spacing (10%) | Stacking (4%) |
|---|---|---|---|
| 30% Acrylamide/Bis (37.5:1) | 1.67 | 0.5 | 0.2 |
| 3X gel buffer | 1.25 | 0.4 | 0.5 |
| dd$H_2O$ | 0.83 | 0.6 | 0.8 |
| 10% APS | 0.04 | 0.012 | 0.024 |
| TEMED | 0.008 | 0.0024 | 0.0048 |
| Loading volume | 3 ml | 0.7 ml | 1 ml |

**Western blot**

Transfer buffer: 25 mM Tris, 192 mM glycine, 10% methanol

Tris-Buffered Saline (TBS): 50 mM Tris, pH 7.4, 200 mM NaCl

TBST: 50 mM Tris, pH 7.4, 200 mM NaCl, 0.05% Tween20

**Phosphate-Buffered Saline (PBS)**

137 mM NaCl, 2.7 mM KCl, 1.8 mM $KH_2PO_4$, 10 mM $Na_2HPO_4$, pH 7.6

### 2.1.2 Plasmids

(1) pET14b-SERF1a

Vector: pET14b

Insert:

CCATGGGCAGCAGCCATCATCATCATCATCACAGCAGCGGCCTGGTGCCG



doi:10.6342/NTU202303164

CGCGGCAGCCATATGGCCCGTGGAAATCAACGAGAACTTGCCCGCCAGA

AAAACATGAAGAAAACCCAGGAAATTAGCAAGGGAAAGAGGAAAGAGG

ATAGCTTGACTGCCTCTCAGAGAAAGCAGAGGGACTCTGAGATCATGCA

AGAAAAGCAGAAGGCAGCTAATGAGAAGAAGTCTATGCAGACAAGAGA

AAAGTGAGAGGATCC

Restriction sites: NcoI and BamHI

(2) HisUb-Abeta42_pCOLADuet™-1 (provided by Dr. Chun Chung Chan's lab)

Vector: pCOLADuet™-1

Insert:

CATATGCATCACCATCACCATCACATGCAAATCTTCGTCAAAACGCTGACC

GGCAAAACCATCACGCTGGAAGTGGAACCGTCCGATACCATCGAAAACG

TCAAAGCGAAAATTCAGGATAAAGAAGGTATCCCGCCGGACCAGCAACG

TCTGATTTTTGCCGGTAAACAGCTGGAAGATGGCCGCACCCTGAGCGACT

ATAACATCCAAAAAGAATCTACGCTGCATCTGGTTCTGCGTCTGCGCGGC

GGTGGTACCGAAAATCTGTATTTTCAGGATGCAGAATTCCGTCACGACAG

TGGCTACGAAGTGCATCACCAAAAACTGGTGTTTTTCGCGGAAGATGTGG

GCTCAAACAAAGGTGCGATTATTGGTCTGATGGTTGGCGGCGTCGTTATT

GCGTAACTCGAG

Restriction sites: Ndel and XhoI



doi:10.6342/NTU202303164

(3) pFLAG-CMV-6-SERF1a

Vector: pFLAG-CMV-6a

Insert:

GAATTCAACCGTGGCCCGTGGAAATCAACGAGAACTTGCCCGCCAGAAA

AACATGAAGAAAACCCAGGAAATTAGCAAGGGAAAGAGGAAAGAGGAT

AGCTTGACTGCCTCTCAGAGAAAGCAGAGGGACTCTGAGATCATGCAAG

AAAAGCAGAAGGCAGCTAATGAGAAGAAGTCTATGCAGACAAGAGAAA

AGTGAGAGGATCC

Restriction sites: EcoRI and BamHI

(4) pEGFP-SERF1a

Vector: pEGFP-C1

Insert:

GAATTCAACCGTGGCCCGTGGAAATCAACGAGAACTTGCCCGCCAGAA

AAACATGAAGAAAACCCAGGAAATTAGCAAGGGAAAGAGGAAAGAGG

ATAGCTTGACTGCCTCTCAGAGAAAGCAGAGGGACTCTGAGATCATGCA

AGAAAAGCAGAAGGCAGCTAATGAGAAGAAGTCTATGCAGACAAGAGA

AAAGTGAGAGGATCC

Restriction sites: EcoRI and BamHI



doi:10.6342/NTU202303164

### 2.1.3 Brain lysates

The brain lysates of control and AD patients were provided by Dr. Lee-Way Jin (UC Davis)

### 2.1.4 Antibodies

The antibodies used in this study are listed in appendix.

### 2.1.5 Commercial reagents

The commercial reagents used in this study are listed in appendix.



doi:10.6342/NTU202303164

## 2.2 Methods

### 2.2.1 Protein expression and purification

*Recombinant SERF1a and $^{15}$N-SERF1a*

The plasmid containing a pET14b vector and human SERF1a short isoform was transformed into *Escherichia coli* strain BL21 (DE3), and SERF1a protein with N-terminal His-tag and a thrombin-cutting site was expressed. The cells were grown in sterile Luria-Bertani (LB) medium with 100 μg/ml ampicillin at 37°C, shaking at 200 rpm, and induced by 1 mM IPTG for 5 hr. The cells were then harvested by centrifugation at 4°C, 7,000 rpm for 15 min. The pellet was resuspended in lysis buffer consisting of 20 mM Tris, pH 7.9, 5 mM imidazole, 500 mM NaCl, and protease inhibitor and lysed by a microfluidizer. After centrifugation at 4°C, 20,000 rpm for 30 min, the supernatant was collected and loaded onto a HisPrep FF column (GE Healthcare) for purification using FPLC. The column was first equilibrated with the loading buffer containing 20 mM Tris, pH 7.9, 500 mM NaCl, and 5 mM imidazole. After sample application, the column was washed with the same loading buffer, and the protein was then eluted with one-step gradient from 0% to 100% eluting buffer containing 20 mM Tris, pH 7.9, 500 mM NaCl, and 250 mM imidazole. After checking on SDS-PAGE, the fractions containing the protein of interest were collected for concentration and buffer exchange to thrombin-cutting buffer consisting of 20 mM Tris, pH 8.4, and 150 mM NaCl. N-terminal His-tag



doi:10.6342/NTU202303164

of SERF1a was removed by incubating with thrombin at room temperature overnight. The mixtures were then loaded onto a Mono-S Sepharose column (GE Healthcare) which was equilibrated with the loading buffer containing 20 mM Tris, pH 8, 0.2 mM EDTA, 0.5 mM DTT, and 5 mM NaCl. After sample application, the column was washed with the same loading buffer, and the protein was eluted with three-step gradient from 0% to 100% eluting buffer containing 20 mM Tris, pH 8, 0.2 mM EDTA, 0.5 mM DTT, and 500 mM NaCl. The purity of SERF1a protein was verified by SDS-PAGE. The fractions containing the pure protein were pooled, concentrated, dialyzed into 50 mM Tris, pH 6.8, 20 mM NaCl buffer, and stored at -20°C. $^{15}$N-SERF1a protein was produced similarly to SERF1a, but induced in M9 medium with $CaCl_2$, $MgSO_4$, $^{15}$N-$NH_4Cl$, and glucose. The final pure $^{15}$N-SERF1a protein was stored in buffer containing 50 mM Tris, pH 6.5, and 50 mM NaCl at -20°C.

*Synthetic Aβ40*

Synthesis of Aβ40 peptides were performed by using solid phase peptide synthesis (SPPS) system by Peptide Synthesis Facility in Genomics Research Center (GRC), Academia Sinica, Taiwan. The crude peptides were purified by reversed-phase HPLC equipped with UG120-C18 column (Shiseido). Buffer A containing 10% acetonitrile (ACN) and 0.05% trifluoroacetic acid (TFA) and buffer B containing 90% ACN and



doi:10.6342/NTU202303164

0.05% TFA were used. The final products were validated by MALDI-TOF-MS in GRC Mass Core Facility.

*Recombinant Aβ42*

The plasmid containing a pCOLADuet™-1 vector and Aβ42 was transformed into *Escherichia coli* strain BL21 (DE3), and Aβ42 with N-terminal His-tag, ubiquitin, and a TEV protease cleavage site was expressed. Cells were cultured in LB medium with 50 μg/ml kanamycin at 37°C with shaking at 200 rpm until the $OD_{600}$ reached 0.8-1.0 and then induced by 1 mM IPTG for 18-20 hr. Cells were harvested by centrifugation at 7,000 rpm for 15 min and the pellet was resuspended in lysis buffer containing 20 mM Tris, pH 8, 150 mM NaCl, and 1 mM DTT. Cells were then lysed by a sonicator (Misonix S3000) (1 cycle: on: 1 s (total 8 min), off: 3 s, power: 30W). After centrifugation to collect the proteins, the supernatant was discarded, while the pellet was resuspended in solubilization buffer containing 20 mM Tris, pH 11, 150 mM NaCl, and 8 M urea to increase solubility and sonicated for 1 hr on ice. After centrifugation again, the supernatant was collected and HisUb-Aβ42 was purified by HisTrap HP 5 ml column (GE Healthcare) on a FPLC systems ÄKTA PURE (GE Healthcare). The column bound with proteins was washed with loading buffer containing 20 mM Tris, pH 8, 150 mM NaCl, and 5 M urea mixed with 6% eluting buffer containing additional 500 mM imidazole. To further elute the



doi:10.6342/NTU202303164

proteins, the loading buffer and eluting buffer were mixed for one-step gradient from 6% to 100% of the latter. After checking on SDS-PAGE, the fractions including HisUb-Aβ42 were collected and concentrated. For TEV protease cleavage, the urea concentration was lowered down to 1 M by adding lysis buffer and the N-terminal His-tag and ubiquitin was removed from Aβ42 by incubation with TEV in 30°C water bath overnight. The post proteolysis products were then brought back to 8 M urea and the pH value was adjusted to 11 with NaOH followed by standing at room temperature for at least 1 hr. For Aβ42 purification, the proteins were loaded into HisTrap HP 5 ml column again following the method mentioned above to separate HisUb and Aβ42. After verified by SDS-PAGE, the fractions containing pure Aβ42 were collected and concentrated for further purification using PROTO 300 C18 column (Higgins Analytical, Inc.) on reversed-phase HPLC systems with 20% ACN and 0.1% TFA buffer and 90% ACN and 0.1% TFA buffer. The final products were validated by MALDI-TOF-MS (GRC Mass Spectrometry Facility).

### 2.2.2 Aβ peptide preparation

The purified Aβ peptides, 0.1 mg, were treated with 100 μl of hexafluoroisopropanol (HFIP) at room temperature for at least 1 hr to dissociate preformed Aβ aggregates. HFIP was then removed by using freeze dryer or SpeedVac vacuum concentrator. After that, for ThT assay, partition analysis, ESI-MS, and PICUP, the Aβ peptides were dissolved in



doi:10.6342/NTU202303164

10 μl of dimethyl sulfoxide (DMSO) which was then transferred into 10 mM Tris (Trizma base for ESI-MS) buffer, pH 7.4 and well-mixed by vortex. For CD, FTIR, AUC, and NMR, the Aβ peptides were dissolved in 100 μl of 3 mM NaOH and lyophilized, followed by the addition of 10 mM PB, pH 7.4 (50 mM Tris, pH 6.5, and 50 mM NaCl for NMR) and mixed by vortex. After centrifugation at 4℃ and 15,000 rpm for 10 min to exclude precipitates, the supernatant was collected and the concentrations of Aβ stock were measured by Bicinchoninic acid (BCA) assay kit.

### 2.2.3 Thioflavin T (ThT) assay

The Aβ40 and Aβ42 were freshly prepared as described in Aβ peptide preparation. Aβ with a final concentration of 25 μM, the given concentration of SERF1a, and 5 μM ThT were well-mixed and loaded into a Corning 384-well black plate for incubation. By using SpectraMax M3/M5 Multi-Mode Microplate Reader (Molecular Devices, Sunnyvale, CA, USA), the samples were incubated at 25℃ under 10-sec agitation per hour and ThT fluorescence was recorded at 485 nm with excitation wavelength of 442 nm. The data were fitted according to the following equation[86]:

$$Y = y_i + m_i x + \frac{y_f + m_f x}{1 + e^{-[\frac{x - x_o}{\tau}]}}$$

where $Y$ is the intensity of ThT fluorescence, $x$ is the time for incubation, and $x_o$ is the time for the fluorescence intensity reaching 50% of maximum. The lag time is given by



doi:10.6342/NTU202303164

$x_o$ - 2$\tau$. The apparent rate constant $k_{app}$ for the fibril growth is defined by 1/$\tau$.

### 2.2.4 Far-UV circular dichroism (CD) spectroscopy

Twenty-five μM Aβ40 or Aβ42 was incubated in the absence or presence of 2.5 μM SERF1a at 25°C and shaken for 10 sec per hour as in ThT assay but without ThT. At each time point, the samples were collected and loaded into a 1-mm path length quartz cuvette (120-QS, Hellma, Germany) for the measurement. Far-UV spectra between 195 nm and 250 nm were recorded by a J-815 CD spectropolarimeter (Jasco Inc., Easton, MD, USA) at room temperature. The spectrum of buffer control was subtracted from that of Aβ alone, and the spectrum of SERF1a alone was subtracted from that of the mixture of Aβ with SERF1a. Twenty μM synthetic HTT peptides in 10 mM PB were also examined in this way.

### 2.2.5 Filter-trap assay

The endpoint products of ThT assay were loaded on 0.8 μm cellulose acetate membranes (Advantec) by using a Bio-Dot SF microfiltration apparatus (Bio-Rad, Hercules, CA, USA) equipped with a central vacuum system. The membranes were blocked with 10% skim milk/TBS at room temperature for 2 hr and probed with the primary antibody OC (1:5,000) at 4°C overnight. After that, the secondary antibody,



doi:10.6342/NTU202303164

horseradish peroxidase (HRP) conjugated anti-mouse IgG (1:5,000; GeneTex) was applied and incubated at room temperature for another 2 hr. The membrane was then developed with Chemiluminescent HRP Substrate (Millipore) and the signals were detected by ImageQuant LAS 4000.

### 2.2.6 Transmission Electron Microscopy (TEM)

Ten μl of the end-point products of ThT assay were placed on 400-mesh Formvar/carbon-coated copper grids (Electron Microscopy Sciences, Hatfield, PA, USA). After 10 minutes, the excess liquids of the samples were removed with filter paper, and the grids were washed with ultrapure water twice. The samples were then stained with 10 μl of 1% uranyl acetate (UA) for 30 sec, blotted, washed, and air-dried. For immunogold labeling, the procedure was similar to the above-mentioned steps, while before UA staining, the grids were incubated with the primary antibody SERF#1 (1:100; monoclonal antibody) in 0.1% bovine serum albumin (BSA)/TBS for 2 hr at room temperature. After washing, the 10 nm gold-conjugated secondary anti-mouse IgG antibody (1:500; Abcam) in TBS was applied to the grids for 1 hr. The samples were then fixed by using 1% glutaraldehyde in PBS for 10 min. After being washed a few times with ultrapure water, the grids were stained with 1% UA. The images were then observed with a FEI Tecnai G2 F20 S-TWIN transmission electron microscope at 120 kV accelerating voltage.



doi:10.6342/NTU202303164

### 2.2.7 Partition analysis

The samples were prepared as described in Aβ peptide preparation. Forty μM Aβ40 or Aβ42 was incubated in the absence or presence of the equimolar SERF1a, as the conditions in ThT assay but without ThT, for at least 5 days for fibril formation. After incubation, the supernatant and the pellet were ultracentrifuged at 25℃ and 100,000 rpm for separation. Then, the pellet was washed with PBS, pH 7.6, three times, and resuspended in the same buffer. Ten μl of each sample (10 μl of 10 M urea was added into the pellet fractions of Aβ42) was subjected to SDS-PAGE and western blot. For western blot, the primary SERF#1 antibody (1:100; monoclonal antibody) and the secondary anti-mouse antibody (1:5,000; GeneTex) were used.

### 2.2.8 Photo-Induced Cross-linking of Unmodified Proteins (PICUP)

Eighteen μl of freshly prepared Aβ and SERF1a was cross-linked by adding freshly prepared 1 μl of 1 mM Ru(Bpy) and 1 μl of 20 mM ammonium persulfate (APS). The mixtures were then irradiated with LED blue light for 30 sec (Aβ40) or 60 sec (Aβ42). The reaction was immediately quenched with 5 μl of 5x SDS-containing sample buffer and the samples were subjected to SDS-PAGE by using a 13% Tris/tricine separating gel with 10% spacing gel and 4% stacking gel. For the following western blot, the proteins were transferred from the gel to 0.2 μm polyvinylidene fluoride (PVDF) membrane (GE)



doi:10.6342/NTU202303164

which was then probed with the primary antibody 4G8 and 6E10 mixture (1: 2,500; BioLegend) or SERF#1 (1:200; monoclonal antibody) and the secondary antibody, horseradish peroxidase (HRP) conjugated anti-mouse IgG (1:5,000; GeneTex). Blots were visualized with Chemiluminescent HRP Substrate (Millipore).

### 2.2.9 Fourier-transform infrared spectroscopy (FTIR)

The samples were prepared as described in Aβ peptide preparation. Aβ40 and Aβ42 were incubated with and without SERF1a at 25℃ with constant agitation at 300 rpm for a least 10 days by ThermoMixer C (Eppendorf) to form fibrils. Two μl of the resuspended fibrils was deposited on top of the ZnSe crystal of ATR sampling accessory (PIKE MIRacle) and dried by nitrogen gas. This step was repeated five times for each sample to increase the fibril concentrations. The absorbance spectra of the samples were measured on a Nicolet 6700 FTIR spectrometer (Thermo Electron Corporation) and recorded at a resolution of 2 $cm^{-1}$ and accumulation of 100 scans. The spectrum of buffer control was subtracted from that of each sample.

### 2.2.10 Electrospray ionization mass spectrometry (ESI-MS)

The indicated concentrations of freshly prepared Aβ working solution were mixed with equimolar SERF1a without further incubation before being subjected to ESI-MS.



doi:10.6342/NTU202303164

Aβ alone and SERF1a alone were also examined as the control groups. The high-resolution ESI-MS experiments were performed on a Waters Synapt G2 HDMS instrument with a LockSpray ESI source, the parameters used were as follows: ESI capillary voltage, 3.0 kV; sample cone voltage, 20-60 V; extraction cone voltage, 0-4.0 V; trap collision energy (CE), 4.0 V; transfer CE, 0 V; desolvation gas flow, 500 L/h (nitrogen); source temperature, 30℃; and desolvation temperature, 30℃. The samples were infused into the ESI source by a syringe pump (KDS-100, KD Scientific) at a flow rate of 5 μL/min. The data were then analyzed using MassLynx 4.1 program provided by Waters.

### 2.2.11 Analytical ultracentrifugation (AUC)

Sedimentation velocity (SV) experiments were carried out in a ProteomeLab XLI analytical ultracentrifuge (Beckman Coulter, USA) equipped with an An-60 Ti rotor at 25°C. Twenty-five μM freshly prepared Aβ were mixed with equimolar SERF1a without further incubation before injecting into a double-sector centerpiece. For Aβ40 and Aβ42 experiments, all samples were centrifuged at 30,000 rpm and monitored under the absorbance at 231 nm except for the mixture of Aβ40 and SER1a which was monitored at 234 nm. For HTT peptides, 50 μM NT-17 and HTT-3 and 30 μM HTT-0, HTT-1, HTT-2, HTT-4, and HTT-5 in 10 mM PB, pH 7.4 were centrifuged at 42,000 rpm. The moving



doi:10.6342/NTU202303164

boundary was monitored continuously under the absorbance at 220 nm for NT17 and HTT-0, 225 nm for HTT-1 and HTT-2, and 230 nm for HTT-3, HTT-4, and HTT-5. The data was analyzed in SEDFIT program using continuous c(s) distribution model with the parameters obtained from SEDNTERP program.

### 2.2.12 Nuclear magnetic resonance (NMR) Spectroscopy

The NMR measurements were conducted at 298K on a Bruker Avance 600MHz NMR spectrometer equipped with 5 mm triple resonance cryoprobe with Z-axis gradient. Sequence specific backbone resonance assignment was performed based on the analysis of HNCA, HN(CO)CA, HNCO, HN(CA)CO, CBCA(CO)NH, and HNCACB spectra[87]. $^{1}H$ chemical shifts were externally referenced to 0 ppm methyl resonance of the 2,2-dimthyl-2-silapentane-5-sulfonate (DSS), and $^{13}C/^{15}N$ chemical shifts were indirectly referenced according to the IUPAC recommendations[88]. Aβ40 at final concentrations of 35 and 50 μM was added to 50 μM $^{15}N$-labeled SERF1a in 50 mM Tris, pH 6.5, and 50 mM NaCl. $^{1}H$, $^{15}N$-HSQC spectra were collected and processed using software Topspin2.1 (Bruker, Germany) and further analyzed by Sparky version 3.114 (Goddard and Kneller). The chemical shift perturbation for combined $^{1}H$ and $^{15}N$ resonances of SERF1a was calculated by using the following equation[89]:

$$\Delta ppm = [(5*\Delta^{1}H)^{2} + (\Delta^{15}N)^{2}]^{1/2}$$



doi:10.6342/NTU202303164

The intensity changes for each residue were calculated as I (bound)/ I (free).

### 2.2.13 MTT cytotoxicity assay

Human neuroblastoma BE(2)-C cells were seeded with 2-4 x $10^4$ cells per well in DMEM/F12 medium without phenol red and with 2% FBS in a 96-well ELISA plate. After 24 hr, the samples were added into the wells to get a final concentration of 3 μM and incubated with the cells for another 24 hr. An MTT stock solution was prepared as 5 mg/ml in ddH2O and filtered through a 0.22 μm filter. The cells of each well were then treated with 5 μl of the MTT solution and incubated in the dark for 3 hr at 37ºC. The medium was removed and 100 μl of DMSO was added per well to dissolve the remained formazan crystals. The absorbance of the solution was measured at a wavelength of 570 nm and 690 nm using SpectraMax M3/M5 Multi-Mode Microplate Reader (Molecular Devices, Sunnyvale, CA, USA). The absorbance at 690 nm as the background signal was subtracted from that at 570 nm and all sample groups were normalized to the buffer control. The data was analyzed by GraphPad Prism9. For SERF1a antibody rescuing experiment, SERF1a was first pre-incubated with SERF B1 for 2 hr at room temperature followed by the addition of Aβ42. The samples were then incubated as described in ThT assay but without ThT for 14.5 hr before treating the cells.



doi:10.6342/NTU202303164

### 2.2.14 HTT peptide preparation

NT17, HTT-0, HTT-1, HTT-2, HTT-3, and HTT-4 peptides were synthesized and purified by peptide synthesis facility in Genomics Research Center, Academia Sinica. HTT-5 peptide was purchased from Scientific Biotech. The peptides, 0.1–0.2 mg for ITC and AUC experiments and 0.3–1 mg for SAXS, were dissolved in 20 μl of 100% TFA at room temperature overnight to dissociate preformed aggregates. TFA was eliminated by using SpeedVac vacuum concentrator. The dried peptides were dissolved in 10 μl of 1% TFA which were then added into 480 μl of 10 mM PB, pH 7.4, with 16.5 μl of 100 mM NaOH. All peptides were centrifuged at 4℃ and 15,000 rpm for 10 min to exclude precipitates. The supernatant was collected and the concentration was quantified by BCA assay.

### 2.2.15 Isothermal titration calorimetry (ITC)

ITC experiments were performed in 10 mM PB, pH 7.4, at 26°C by using MicroCal iTC200 (GE). For HTT-0, HTT-1, HTT-2, HTT-4, and HTT-5, 300 μM SERF1a in the syringe was titrated into 30 μM HTT peptides in the cell. The volume of each injection was 2 μl with a total of 19 injections. For HTT-3 and NT17, 250 μM SERF1a was titrated into 50 μM HTT peptides. The volume of each injection was 1.5 μl with a total of 25 injections. ITC analysis software (GE Healthcare) was used for data analysis.



doi:10.6342/NTU202303164

### 2.2.16 Small-angle X-ray scattering (SAXS)

HTT peptide stocks were prepared as described in HTT peptide preparation. SERF1a was in 10 mM PB, pH 7.4, with the same concentrations of TFA and NaOH as in HTT peptides. For SAXS measurements, NT17 at 129.2 μM, SERF1a at 60.7 μM, and their mixture in 2:1 molar ratio was prepared. HTT-3 at 203.3 μM, SERF1a at 95.4 μM, and their mixture in 2:1 molar ratio was also prepared. SAXS data were measured and collected at TPS 13A BioSWAXS end station using a 15 keV beam and an Eiger X 9M detector[90,91]. The data was analyzed using the ATSAS package [92].

### 2.2.17 Dot blot and western blot for antibody selection

For dot blot, the indicated amounts of recombinant SERF1a (2 μl) were dotted on the 0.45 μm nitrocellulose membrane. For western blot, the indicated samples were loaded into the wells of a 13% Tris/tricine separating gel with 10% spacing gel and 4% stacking gel for SDS-PAGE and transferred to 0.2 μm PVDF membranes. After incubating with 10% skim milk/TBS, the membranes were then separately probed with the primary SERF1a antibodies followed by the secondary HRP-conjugated anti-mouse antibody (1:5,000, GeneTex). The membranes were finally developed with ECL reagent (Millipore) and the signals were visualized by ImageQuant LAS 4000.



doi:10.6342/NTU202303164

### 2.2.18 Enzyme-linked immunosorbent assay (ELISA)

Ninety μl of serially diluted recombinant SERF1a was coated in a 96-well ELISA plate and incubated at 4°C overnight. The next day, the uncoated SERF1a was removed, and the plate was washed with TBST and blocked with 5% BSA in TBS at room temperature for 2 hr. The primary SERF1a antibodies were separately applied to the plate and incubated at 4°C overnight. Then, the secondary HRP-conjugated anti-mouse antibody was added to the plate and incubated at room temperature for 1.5 hr. Finally, the signal was developed using TMB microwell peroxidase substrate by incubating at room temperature for 10-20 min, followed by the addition of 250 mM HCl to stop the reaction. The absorbance at 450 nm was measured by using SpectraMax M5 microplate reader (Molecular Devices). For HD plasma, 100 μl of 10-fold PBS-diluted normal and HD plasma was coated and followed the method mentioned above. The primary antibody was SERF#1 (1:100) and the secondary antibody was HRP-conjugated anti-mouse antibody (1:5,000; GeneTex).

### 2.2.19 Cell transfection and collection

Neuro-2A cells or HEK293T cells were transfected with 2.5 μg of EGFP-SERF1a or Flag-SERF1a by using Lipofectamine 2000 Reagent (Invitrogen) according to the manufacturer's protocol. The next day, the cells were collected and lysed with RIPA



doi:10.6342/NTU202303164

buffer (50 mM Tris-HCl, pH 8.0, 150 mM NaCl, 0.1% SDS, 1% Triton X-100, 2 mM EDTA, 0.5% sodium deoxycholate) by sonication for 10 sec. After centrifugation at 15,000 rpm, 4°C for 10 min, the supernatant was collected for western blot and IP.

### 2.2.20 Immunoprecipitation (IP)

Fifty μl of protein G magnetic beads (GE Healthcare) was equilibrated with 500 μl TBST before use. Ten μg of the primary antibody, SERF#2, diluted with 300 μl of TBST was mixed with the beads and incubated using end-over-end rotator for 1 hr at room temperature. At the same time, the sample was added into the other tube containing beads for precleaning and incubated using end-over-end rotator for 1 hr at 4°C. After incubation, the beads were washed with TBST for 3 times. The precleaned sample was mixed with the antibody-bound beads and incubated using end-over-end rotator at 4°C overnight. The beads were then washed with TBST for 4 times and incubated with sample buffer at 95°C for 10 min. After removing the beads, the sample was subjected to SDS-PAGE.

### 2.2.21 In-gel digestion

The gel with the protein of interest was sliced and covered by 100 μl of 50 mM $NH_4HCO_3$. After incubation with shaking for 10 min at room temperature, the gel was diced by using a micro-pestle and incubated with 200 μl of a 1:1 mixture of 50 mM



doi:10.6342/NTU202303164

$NH_4HCO_3$ and 100% ACN for 10 min to remove Coomassie blue or salts in the gel. The supernatant was removed and the gel was incubated with 50 μl of 100% ACN for 10 min. Then, the gel was washed one more time as described above. After that, the gel was dried by SpeedVac and incubated with 75 μl of 10 mM DTT in 50 mM $NH_4HCO_3$ at 55°C for 1 hr. The supernatant was removed and the gel was incubated with 75 μl of 50 mM iodoacetamide in 50 mM $NH_4HCO_3$ for 30 min in the dark. The gel was further incubated with 100 μl of 50 mM $NH_4HCO_3$ for 10 min and followed by 50 μl of 100% ACN for another 10 min. This step was repeated twice. So far, the supernatant was spun down and removed after each incubation. The gel was dried by SpeedVac and incubated with Glu-C endoproteinase (1 μg of the enzyme for 20 μg of the sample) in 50 mM $NH_4HCO_3$ with shaking at 37°C overnight. The next day, 50 μl of ddH2O was added into the tube which was then shaken for 5 min. The supernatant was collected into a new tube. The gel was incubated with 100 μl of 50% ACN with 5% formic acid for 5 min. The supernatant was combined into the same tube. This step was repeated twice and followed by 100 μl of 100% ACN for 5 min. The supernatant was combined and mixed well. The sample was then dried by SpeedVac and finally subjected to linear trap quadrupole - Fourier transform (LTQ-FT) in GRC Mass Core Facility.



doi:10.6342/NTU202303164

### 2.2.22 Immunocytochemistry (ICC)

Neuro-2A cells were seeded at $1.2 \times 10^5$ cells per well at 12-well plate for 24 hr and transfected with Flag-SERF1a using Lipofectamine 3000 Reagent (Invitrogen) according to the manufacturer's protocol. After 24 hr, cells were fixed with 4% formaldehyde (Invitrogen) and subjected to fluorescence imaging. Flag-SERF1a expression was detected by the primary SERF1a antibodies and anti-flag antibody (1:800; D6W5B, rabbit, Cell Signaling) and the secondary Alexa Fluor 594 anti-mouse (1:1,000; Invitrogen) and Alexa Fluor 488 anti-rabbit (1:1,000; Invitrogen) antibody. Nucleus was stained with Hoechst dye (1:1,000; Invitrogen). Cells were imaged using confocal microscopy (Leica TCS-SP5-MP-SMD).



doi:10.6342/NTU202303164

# CHAPTER 3. RESULTS

## Part I. Investigating the role of SERF1a in Aβ40 and Aβ42 fibrillization

### 3.1 SERF1a reduces the lag time of Aβ40 and Aβ42 fibril formation in a dose-dependent manner without change in the amount of fibrils

First, to examine the promoting effect of SERF1a on Aβ aggregation shown in previous study[82], we monitored the process of Aβ40 and Aβ42 amyloid formation by means of a fluorescent dye thioflavin T (ThT), which gives a bright fluorescence signal at the excitation of 450 nm and the emission of 482 nm upon binding to amyloid fibrils and is commonly used for monitoring the kinetics of aggregation[93]. Monomeric Aβ40 or Aβ42 was incubated with and without various concentrations of SERF1a at 25℃ under 10 sec agitation per hour (Figure 2). We found that, in the absence of SERF1a, the half time of fibril formation for Aβ40 was 52.6 hr and the initial lag phase was 49 hr. SERF1a efficiently accelerated Aβ40 aggregation by reducing the half time of conversion and the lag phase to 43.6 hr and 39 hr, respectively, at very low molar ratio of Aβ40 to SERF1a (1:0.001) (Figure 2a-2c). The half time and the lag time were reduced upon increasing the dose of SERF1a, while the accelerating effect nearly reached the maximum at a molar Aβ40 to SERF1a ratio of 1:0.01 to the half time 20 hr and the lag time 16.6 hr. The molar ratio of Aβ40 to SERF1a at 1:0.1 or 1:1 did not further show obvious decrease in the half time and the lag time. In addition, we also calculated the apparent rate constant ($k_{app}$) for



doi:10.6342/NTU202303164

fibril growth rate which showed fluctuation, indicating that SERF1a concentration was unrelated to the rate of Aβ40 aggregation (Figure 2d). This efficiently accelerating effect we found in Aβ40 aggregation was also shown in Aβ42 amyloid formation in which the half time of conversion and the lag phase were SERF1a dose-dependently reduced (Figure 2e-2g). Unlike that observed for Aβ40, the $k_{app}$ of Aβ42 was enhanced upon increasing the SERF1a concentration with more obvious effect at a molar Aβ42 to SERF1a ratio of 1:0.1 and 1:1 showing a positive correlation with SERF1a doses (Figure 2h). Moreover, we performed the time-course experiment by using Far-UV CD spectroscopy to monitor the conversion of the secondary structures of Aβ40 and Aβ42 with and without SERF1a (Figure 3). The sample incubation was the same as in ThT assay but no ThT was added. The results revealed that Aβ40 adopted random coils with a minimum at 198 nm in the beginning, and gradually transformed to β-sheet structure until 72 hr, while SERF1a accelerated the conformational conversion of Aβ40 from random coils to β-sheet structure starting before 18 hr (Figure 3a). Similarly, SERF1a also accelerated the conformational changes of Aβ42 starting before 6 hr compared to that of Aβ42 alone starting after 6 hr (Figure 3b). These results were in line with the ThT assay. To know whether SERF1a also affects the final amount of fibrils, we collected the endpoint products of Aβ40 and Aβ42 from the ThT assays to conduct filter trap assay (Figure 4). By using a fibril-specific antibody, OC antibody[94,95], we found that the intensity of bands showing the fibril amount



doi:10.6342/NTU202303164

had no dose-dependent difference. After quantification of the band intensity, the results revealed that the final levels of Aβ40 and Aβ42 fibrils were not related to the SERF1a concentration. Collectively, these findings demonstrated that SERF1a reduces the lag time of both Aβ40 and Aβ42 fibrillization in a concentration-dependent manner without influencing the fibril amount.



doi:10.6342/NTU202303164

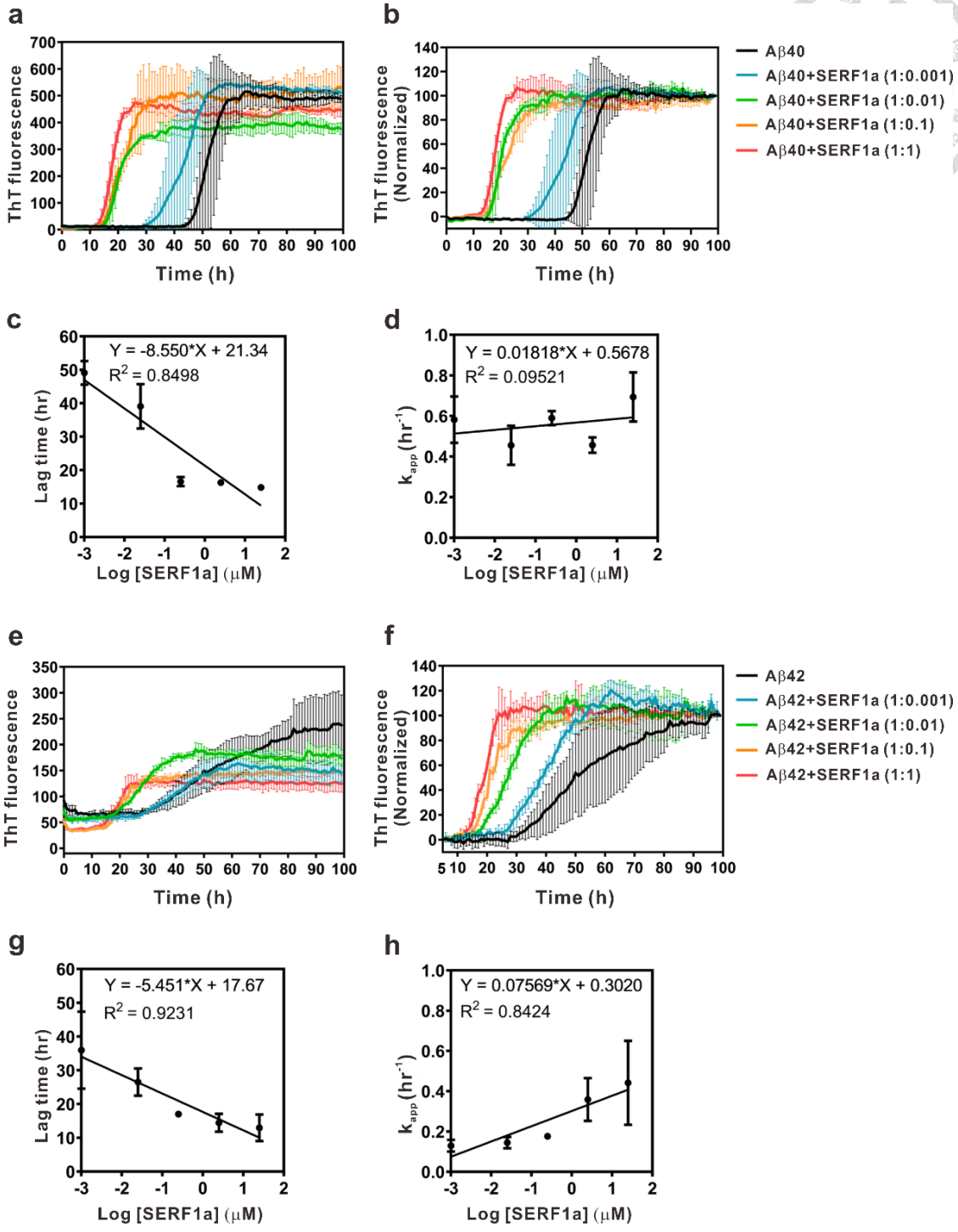


**Figure 2. SERF1a accelerates Aβ fibrillization in a dose-dependent manner.**

ThT aggregation assay of Aβ40 and Aβ42 in the absence or presence of different concentrations of SERF1a. The kinetics of fibril formation for 25 μM Aβ40 **(a-d)** or 25



doi:10.6342/NTU202303164

μM Aβ42 **(e-h)** at 25°C without SERF1a or with different molar ratio of Aβ to SERF1a from 1:0.001 to 1:1 were measured (a, e) and normalized (b, f). Trendlines of the lag time (c, g) and $k_{app}$ for fibril growth rate (d, h) are shown. The points at -3 log concentration of SERF1a denote the absence of SERF1a. The error bars indicate the standard deviation.



doi:10.6342/NTU202303164

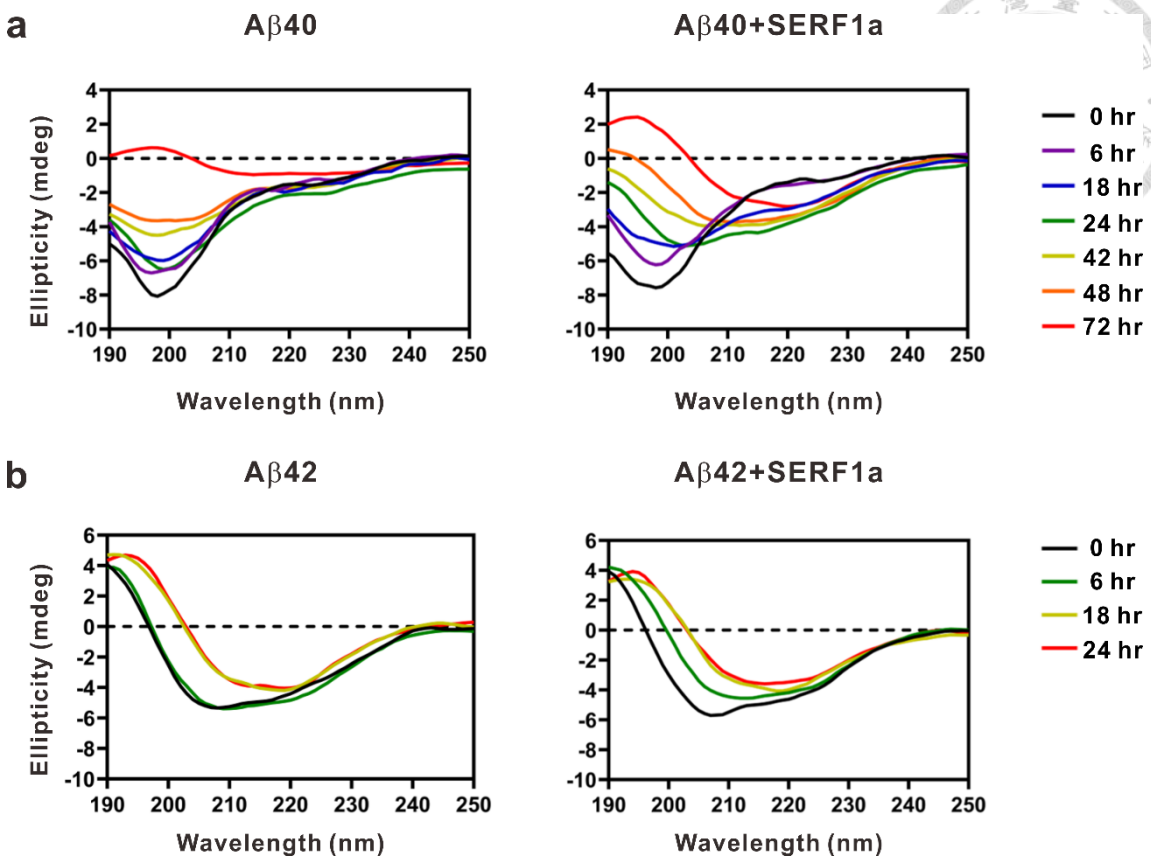


**Figure 3. SERF1a accelerates Aβ to form β-sheet structure.**

CD spectra of 25 μM Aβ40 **(a)** and Aβ42 **(b)** with and without 2.5 μM SERF1a at different time points of the incubation. The spectrum of 2.5 μM SERF1a alone was subtracted from that of Aβ40/Aβ42 with SERF1a coincubation.



doi:10.6342/NTU202303164

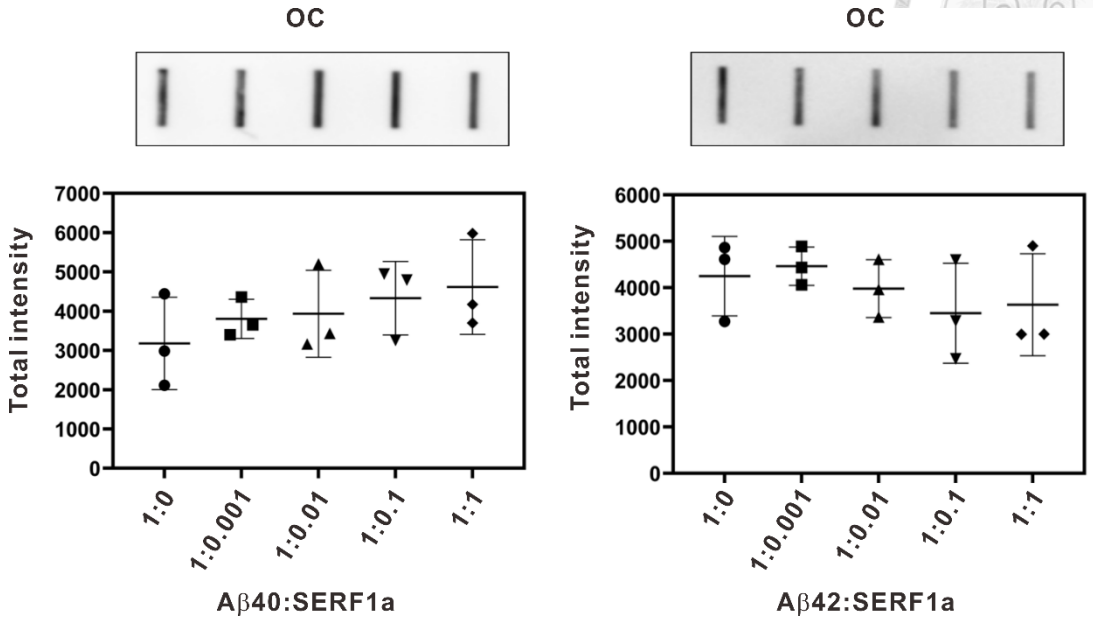


**Figure 4. SERF1a does not affect the final amount of Aβ fibrils.**

The endpoint products of Aβ40 and Aβ42 in the ThT assay were collected and subjected to filter trap assay. The Aβ aggregates trapped on the membrane were probed by an anti-amyloid fibril antibody, OC. The representative images for the membranes were shown on the top. The intensity of signals (n=3) was quantified by ImageJ. The error bars indicate the standard deviation.



doi:10.6342/NTU202303164

## 3.2 SERF1a changes morphology and secondary structure of Aβ40 and Aβ42 fibrils without being incorporated into the fibrils

To know how SERF1a affects the aggregation time of Aβ, we next investigated the effect of SERF1a on the Aβ fibrils through measuring the morphology and secondary structures of the fibrils. The Aβ fibrils taken from the end point of ThT assay were subjected to TEM and the images showed that, in the absence of SERF1a, both Aβ40 and Aβ42 formed thin and long fibrils, while the fibrils became thicker and clumping upon increasing SERF1a concentrations (Figure 5a). This result suggested more Aβ fibril association in the presence of SERF1a.

By using FTIR, we also measured the secondary structure of the Aβ fibrils incubated with and without SERF1a. In the spectrum of Aβ40 fibrils, one major peak at 1627 $cm^{-1}$ typical of β-sheet content[96,97] and a small peak at 1663 $cm^{-1}$ representing the β-turn[98] or irregular secondary structure were shown[99] (Figure 5b). The spectrum of SERF1a alone displayed a single peak at ~ 1650 $cm^{-1}$ indicative of α-helix structure. Coincubation of Aβ40 with SERF1a eliminated the peak of β-turn at 1663 $cm^{-1}$ from Aβ40 fibrils (Figure 5b and 5c), suggesting the conformational change in the presence of SERF1a. The FTIR spectrum of Aβ42 fibrils also revealed two peaks, one at 1628 $cm^{-1}$ for β-sheet and the other at ~1678 $cm^{-1}$ indicative of β-turn[96,97,99] (Figure 5d). In a way similar to that observed for Aβ40, the large peak at 1678 $cm^{-1}$ for β-turn in Aβ42 fibrils was eliminated



doi:10.6342/NTU202303164

upon coincubation of Aβ42 and SERF1a (Figure 5d and 5e). Taken together, these results implied that SERF1a accelerates the Aβ40 and Aβ42 aggregation through influencing the association and conformation of Aβ fibrils.

To investigate whether SERF1a is incorporated into Aβ fibrils, the end-point products of ThT assay were subjected to immunogold labeling and visualized by TEM (Figure 6a). A monoclonal antibody, SERF#1, produced in house with an epitope at the C-terminus of SERF1a, served as the primary antibody to detect SERF1a. The validation of SERF#1 is described in Part III section. By using 10 nm gold-conjugated secondary antibody to bind to SERF#1, the TEM images showed that very few numbers of nanogold remained on the fibrils, indicating that SERF1a affects Aβ amyloid formation without being a part of the fibrils. This finding was further supported by Aβ fibril partition analysis (Figure 6b). Aβ40 or Aβ42 was incubated in the absence or presence of SERF1a for fibril formation, and the end-point products were then centrifuged to separate the soluble proteins in the supernatant and the insoluble fibrils in the pellet. We performed western blot with SERF1a antibody and SDS-PAGE for the soluble and insoluble fractions and found that SERF1a was predominantly shown in the soluble fractions in both Aβ40 and Aβ42 cases with a negligible band in the pellet fraction of Aβ40 and SERF1a mixture, suggesting the dissociation of most SERF1a from Aβ fibrils.



doi:10.6342/NTU202303164

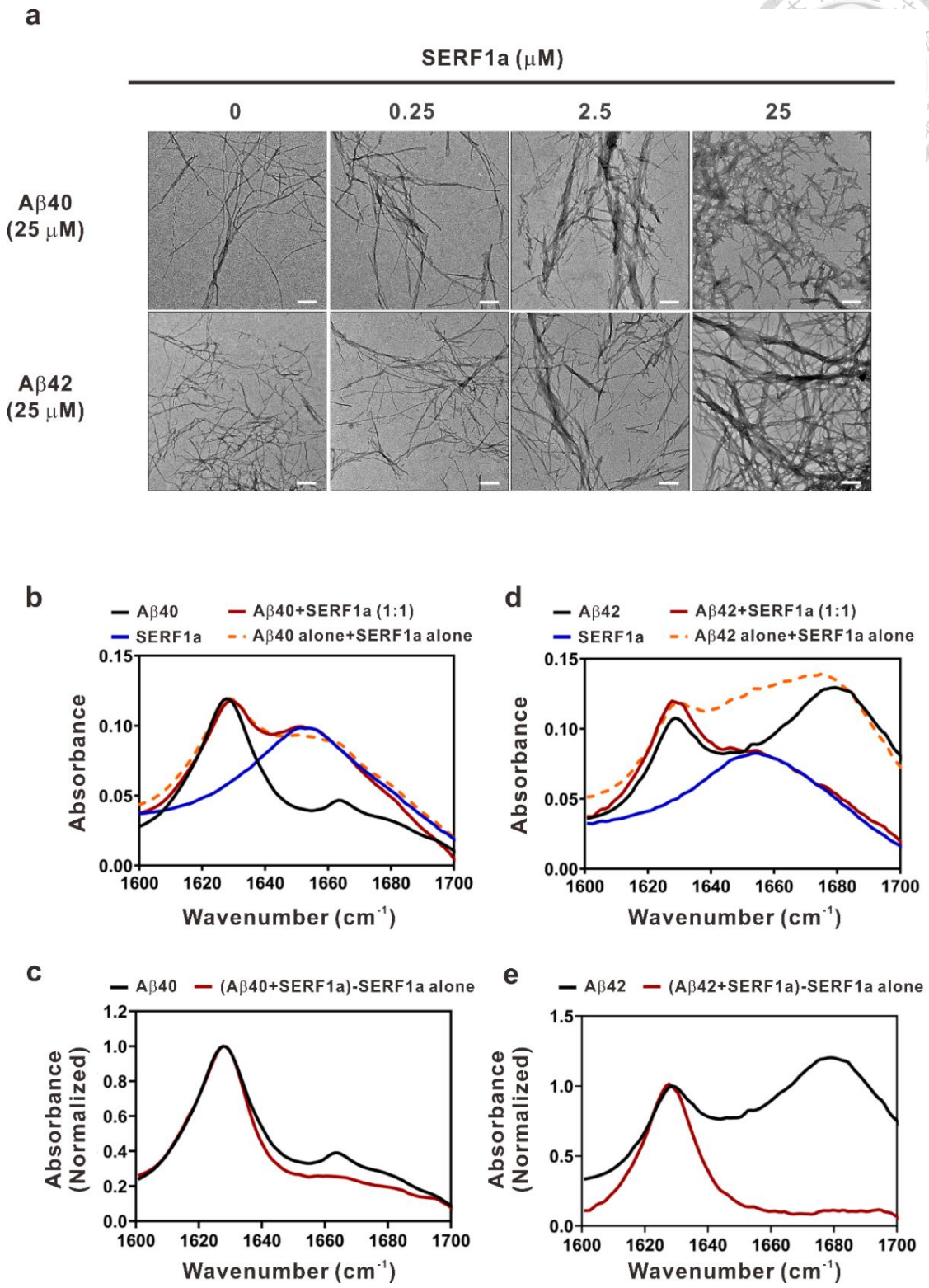


**Figure 5. SERF1a alters morphology and secondary structure of Aβ fibrils.**



doi:10.6342/NTU202303164

**(a)** TEM images of the endpoint products of Aβ40 and Aβ42 with different SERF1a concentrations from ThT assays. The scale bars are 200 nm. **(b-e)** FTIR analysis of Aβ40 (b, c) and Aβ42 (d, e) in the absence or presence of SERF1a after incubation.



doi:10.6342/NTU202303164

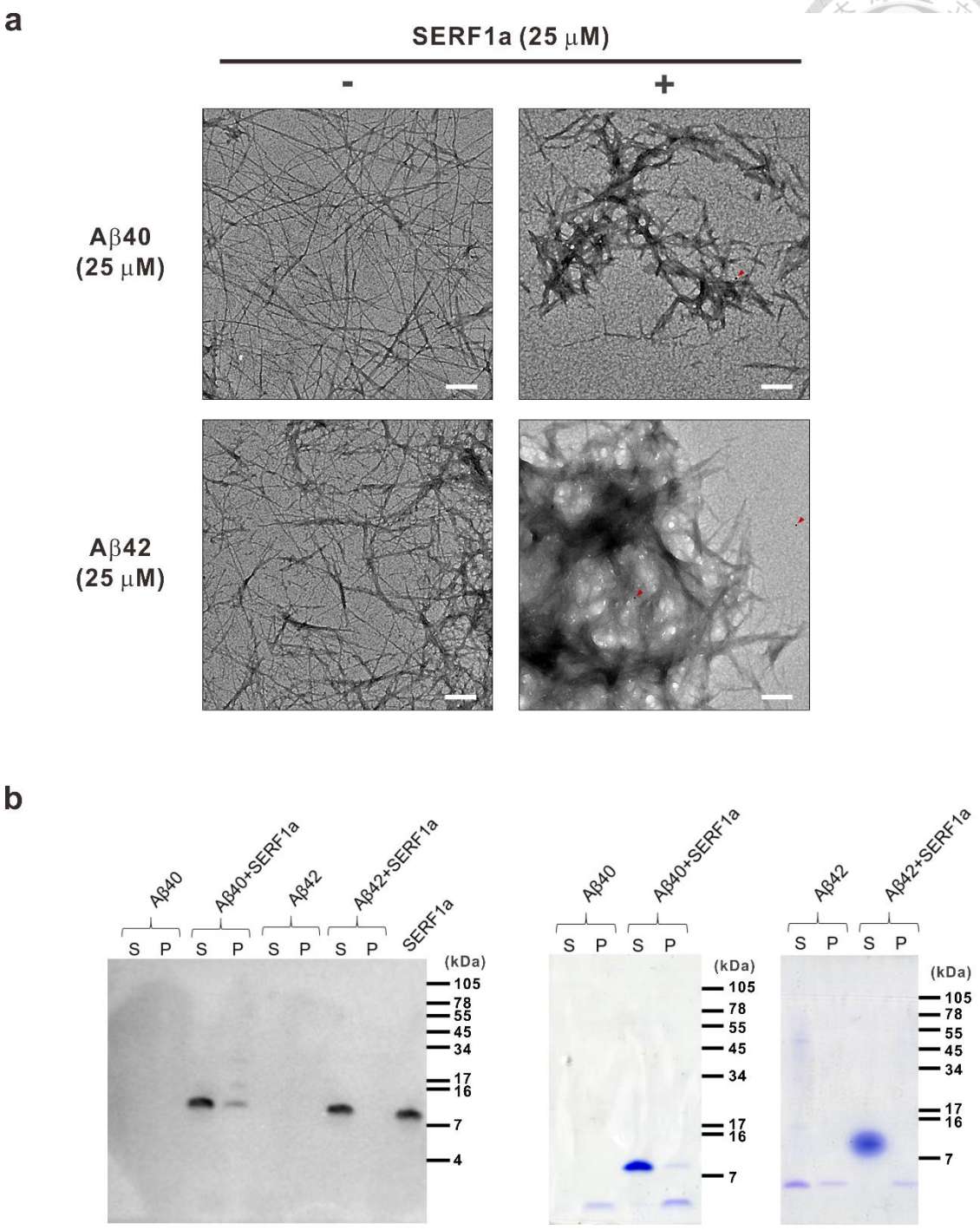


**Figure 6. SERF1a dissociates from Aβ after catalyzing fibril formation.**

**(a)** Immuno-EM images of Aβ40 and Aβ42 fibrils with and without SERF1a. The 10 nm golds are pointed out by red arrows. The scale bars are 200 nm. **(b)** Western blot (left)



doi:10.6342/NTU202303164

and SDS gel (right) of Aβ fibril partition analysis. The soluble and insoluble portions of incubated products were separated by ultracentrifugation at 100,000 rpm. SERF#1 antibody (1:100) was used for western blot. S: supernatant; P: pellet.



doi:10.6342/NTU202303164

## 3.3 SERF1a forms complexes with Aβ40 and Aβ42 primarily in a 1:1 stoichiometry

Having demonstrated the effect of SERF1a on Aβ fibril formation, we next wanted to know how SERF1a interacts with Aβ. To this end, we first examined the complex of SERF1a and Aβ by PICUP which has been applied for Aβ oligomerization and interaction with other binding partners[100]. In this experiment, Aβ and SERF1a were cross-linked by RuBpy under a blue light exposure. The samples were subjected to western blot probed by a mixture of Aβ antibody 4G8 and 6E10, which recognized Aβ residues 17 to 24 and residues 1 to 16, respectively, as well as the SERF1a antibody SERF#1. We found that, in both Aβ40 and Aβ42 cases, several bands in the Aβ and SERF1a mixtures were shown in both 4G8/6E10 and SERF#1 probing membranes, pointing to the cross-linked interacting complex of Aβ and SERF1a (Figure 7). The bands marked with one red asterisk indicated the complex formed by one Aβ and one SERF1a, and that was the predominant species. In addition, the bands for the complex of two Aβ and two SERF1a marked with two red asterisks and other species were also shown. The bands for complexes became more noticeable upon increasing the concentration of SERF1a, further confirming the formation of Aβ and SERF1a complexes. Furthermore, the self-assembled Aβ40 dimers, trimers, tetramers, and Aβ42 dimers were gradually reduced upon the addition of SERF1a.



doi:10.6342/NTU202303164

Next, to more accurately determine the complex composition, we performed ESI-MS and sedimentation velocity (SV)-AUC for Aβ, SERF1a, and the mixtures of Aβ and SERF1a. ESI-MS has been commonly used for the detection of noncovalent protein complexes[101-103]. The ESI-MS results revealed that, by comparing with the spectra of Aβ40 alone and SERF1a alone, extra peaks were shown in the spectrum of the equimolar Aβ40 and SERF1a mixture, attesting the formation of Aβ40/SERF1a complex (Figure 8a). The complex of Aβ40 and SERF1a produced three charge states including 7+ (m/z 1727.3), 8+ (m/z 1511.5), and 9+ (m/z 1343.8). After calculation, the complex was around 12 kDa that should consist of one Aβ40 (4.3 kDa) and one SERF1a (7.3 kDa). In Aβ42 case, the ESI-MS spectrum of Aβ42 and SERF1a mixture also displayed the peaks for the complex yielding only one charge state, 6+ (m/z 2045.7) (Figure 8b). Similarly, the complex was composed of one Aβ42 (4.5 kDa) and one SERF1a (7.3 kDa). However, the spectrum of SERF1a alone showed a peak at m/z 1342.1646 which should not be the peak for SERF1a. Also, a peak at m/z 2052.7144 was present in the spectra of both Aβ42 alone and SERF1a alone. These peaks were probably caused by solvent, buffer, or contaminants due to the high sensitivity of ESI-MS.

In support of ESI-MS results, SV-AUC data revealed that, for the mixture of equimolar Aβ40 and SERF1a, a broad peak at 1.2 S corresponding to the molecular weight around 11.6 kDa was shown and that was nearly the sum of the peaks for Aβ40



doi:10.6342/NTU202303164

monomers (4.3 kDa) and SERF1a monomers (7.4 kDa), attesting the complex of Aβ40 and SERF1a in a 1 to 1 ratio (Figure 9a). Being different from Aβ40 alone which kept monomeric, Aβ42 alone formed trimers (13.5 kDa) and oligomers (236 kDa) during the experiment. However, the addition of SERF1a prevented Aβ42 from the self-assembly of trimers as well as oligomers and formed the one-to-one complex (11.9 kDa) instead (Figure 9b). Indeed, the self-formed dimers, trimers, and tetramers of Aβ were also observed in PICUP assay and were gradually reduced upon increasing the concentration of SERF1a (Figure 7). Collectively, these results suggested that SERF1a influences Aβ fibril formation by forming a one-to-one complex with Aβ monomer.



doi:10.6342/NTU202303164

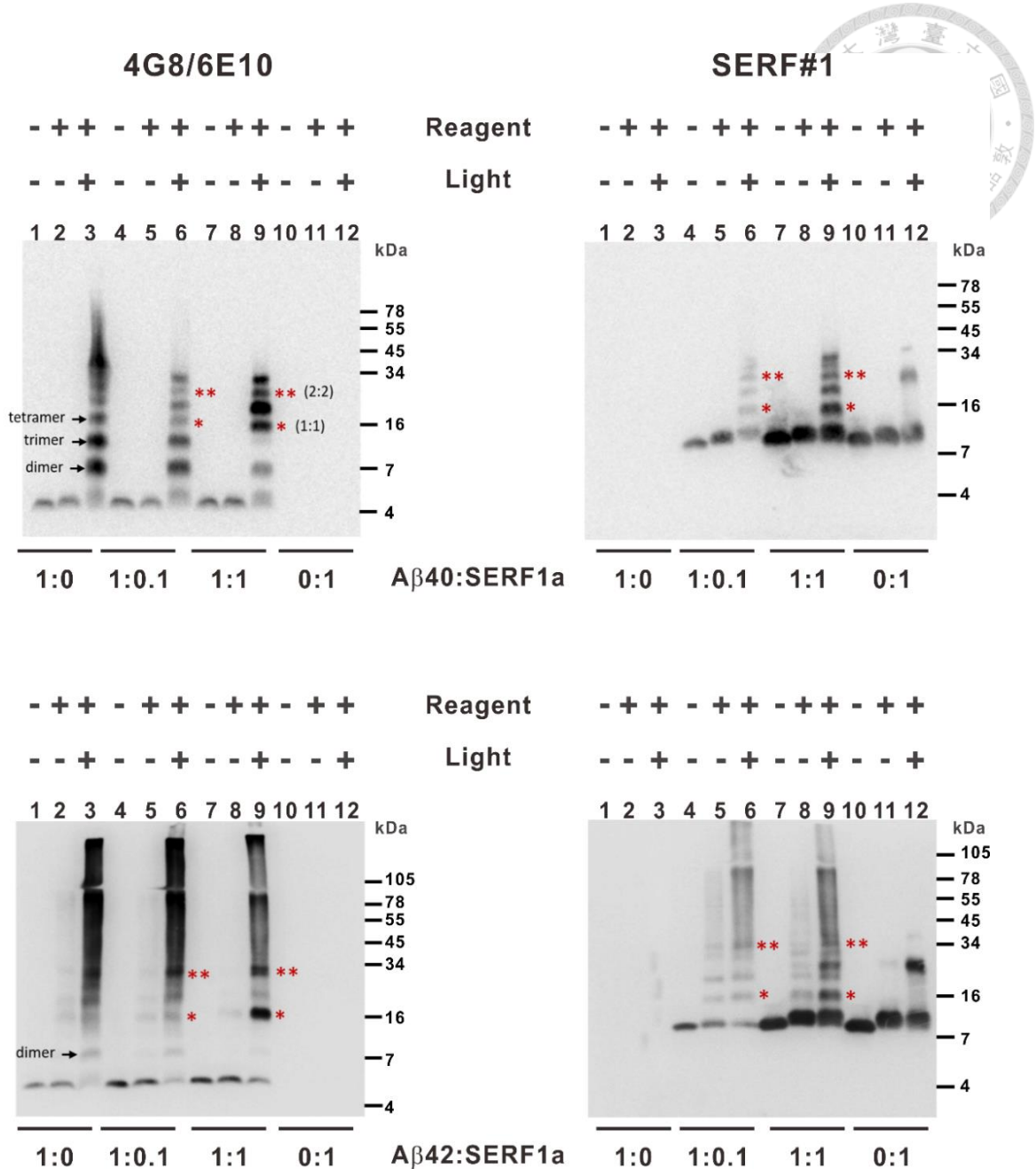


**Figure 7. SERF1a forms complexes with Aβ40 and Aβ42.**

PICUP assay combined with western blot for 25 μM Aβ40 and Aβ42 in the absence or presence of SERF1a at 1:0.1 or 1:1 ratio. Aβ40 and Aβ42 were probed by the mixture of 4G8 and 6E10 antibodies, and SERF1a protein was recognized by SERF#1 antibody. The bands for 1:1 complex of SERF1a and Aβ40 or Aβ42 are indicated by one red asterisk.



doi:10.6342/NTU202303164

The bands for 2:2 complex of SERF1a and Aβ40 or Aβ42 are marked with two red asterisks. The bands for Aβ dimers, trimers, and tetramers are also pointed out.



doi:10.6342/NTU202303164

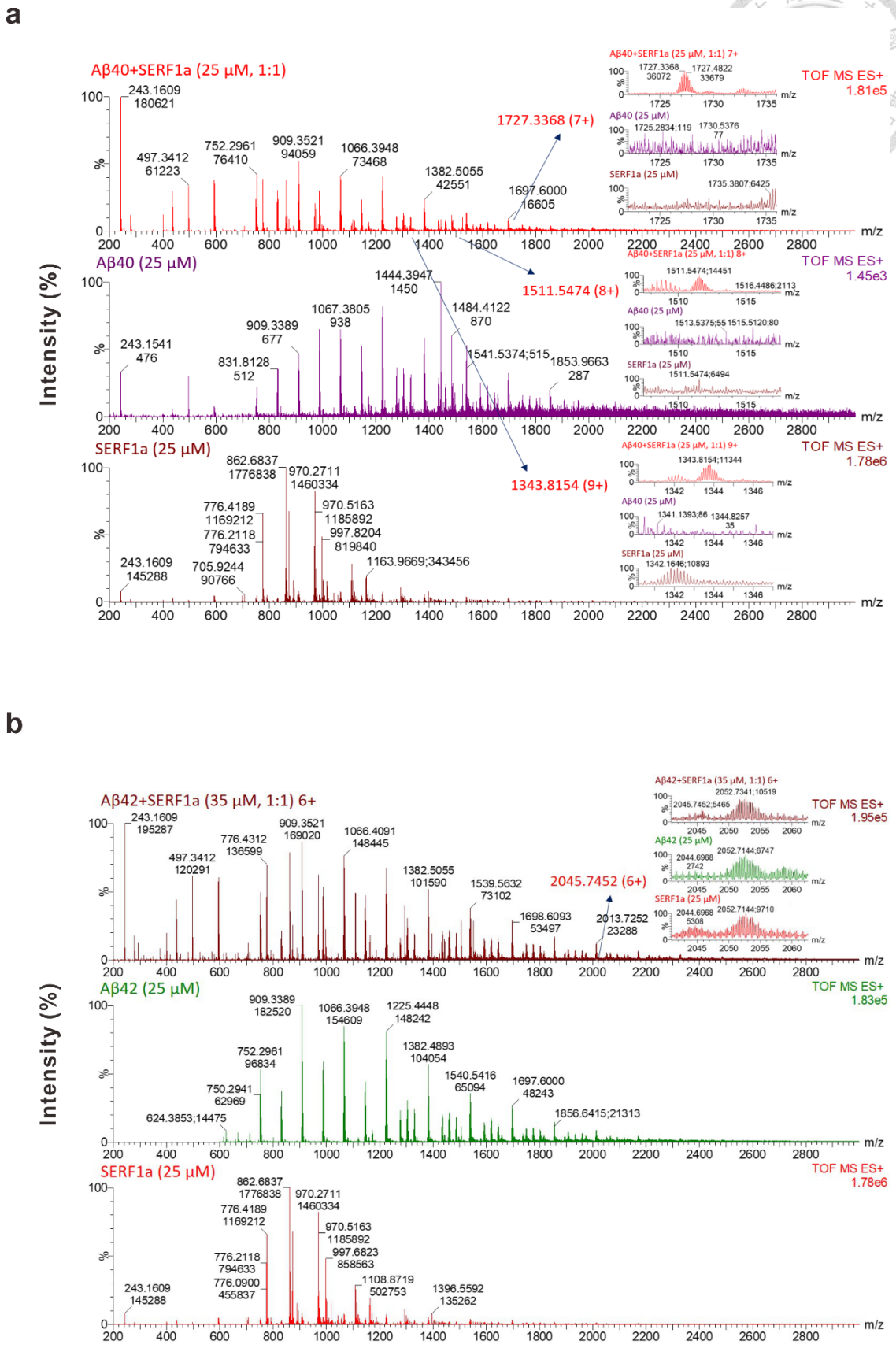




doi:10.6342/NTU202303164

**Figure 8. SERF1a forms complexes with Aβ40 and Aβ42 in a 1:1 ratio.**

**(a, b)** ESI-MS spectra of Aβ40 (a), Aβ42 (b), SERF1a, and the mixtures. The extra peaks appeared in the spectra of equimolar Aβ and SERF1a mixtures when compared to that of Aβ alone and SERF1a alone, pointing to the complexes of Aβ and SERF1a.



doi:10.6342/NTU202303164

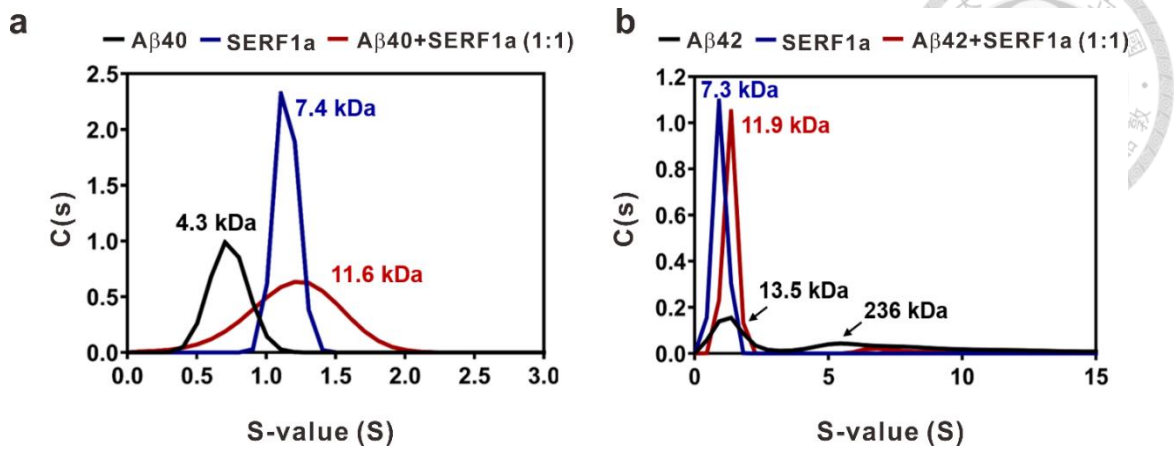


**Figure 9. SERF1a forms complexes with Aβ40 and Aβ42 in a 1:1 ratio and disrupts Aβ42 oligomer formation in solution.**

**(a, b)** SV-AUC data of 25 μM Aβ40 (a) and Aβ42 (b) in the absence or presence of equimolar SERF1a was fitted and analyzed by the continuous c(s) distribution model in SEDFIT software. The sedimentation coefficients (S-value) were acquired. On the basis of the given molecular weight, the complexes consist of one Aβ40 or Aβ42 and one SERF1a.



doi:10.6342/NTU202303164

## 3.4 SERF1a interacts with Aβ40 through its N-terminal region

To further identify the Aβ binding site on SERF1a, we generated $^{15}$N-labeled SERF1a and conducted the heteronuclear single quantum coherence (HSQC) experiment by using NMR spectroscopy. We fixed the $^{15}$N-SERF1a concentration at 50 μM and mixed with 35 μM and 50 μM Aβ40 respectively to detect the chemical shift perturbation (CSP) and intensity changes in $^{15}$N-SERF1a amide signals. We found that, upon the addition of Aβ40, some of the $^{15}$N-SERF1a residues revealed noticeable CSP and intensity drop (Figure 10a). According to the equation given in Method, the peaks for residues A2, R3, N5, and N14 exhibited larger CSP (> or ≈ 0.1 ppm) in comparison to that for other residues (Figure 10b). The intensity drop in almost all residues might be owing to the line broadening upon binding to Aβ40, while residues G4, N5, Q6, N14, K23, S34, S56, and M57 exhibited more significant intensity drop (≥ 70%), indicating the major possible interacting residues (Figure 10c). Taken together, these data suggested that the Aβ40 binding site is mainly located in the N-terminal region of SERF1a (Figure 10d).



doi:10.6342/NTU202303164

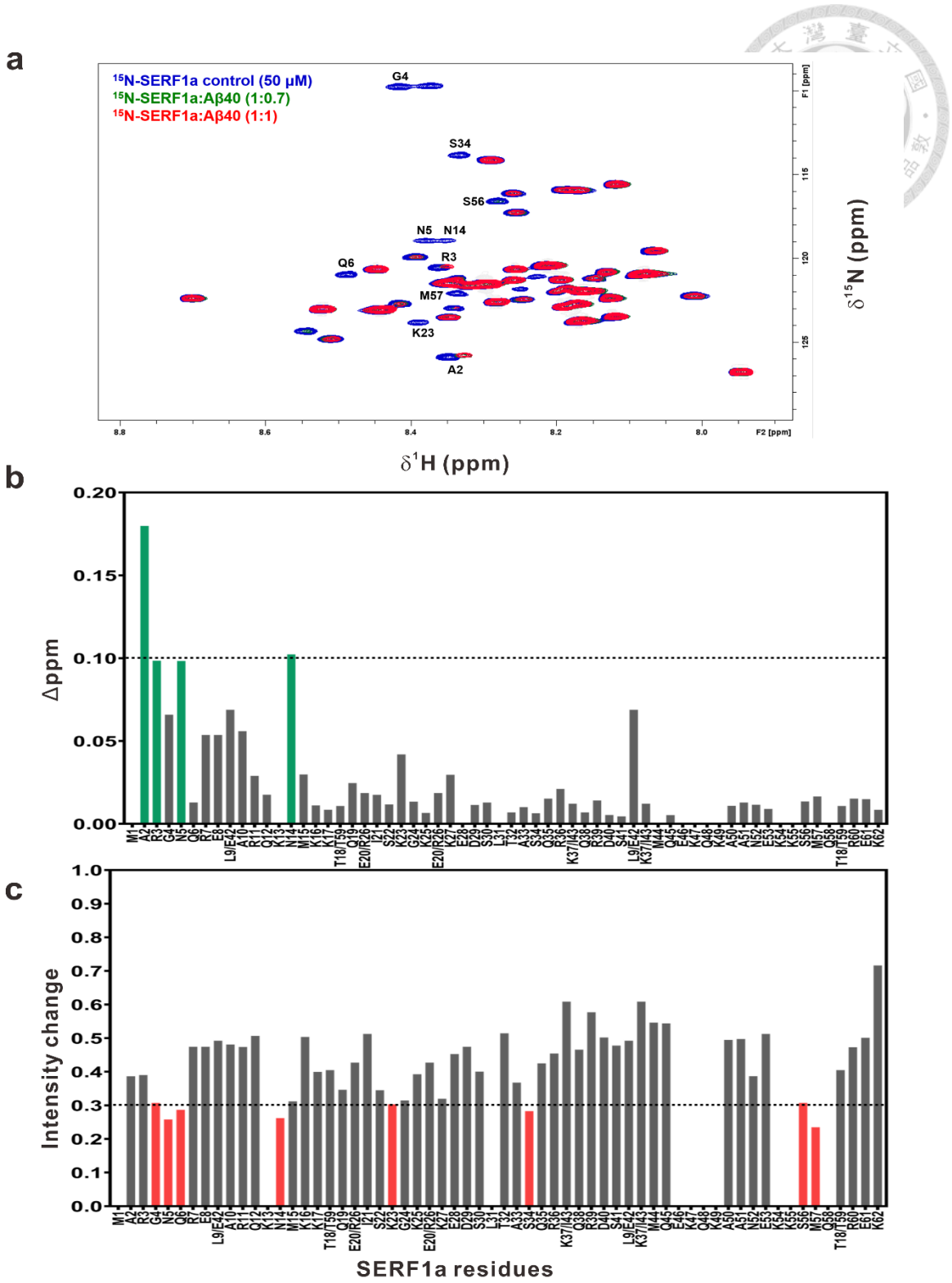




doi:10.6342/NTU202303164

**Figure 10. SERF1a interacts with Aβ40 via N-terminal region.**

**(a)** Overlay of HSQC spectra of $^{15}$N-labeled SERF1a with different Aβ40 concentrations. Peaks for $^{15}$N-SERF1a alone and $^{15}$N-SERF1a with Aβ40 at a molar ratio of 1:0.7 and 1:1 were labeled in blue, green, and red, respectively. **(b)** CSP and **(c)** intensity change between $^{15}$N-SERF1a alone and $^{15}$N-SERF1a with Aβ40 (1:1). The signals of residues L9/E42, T18/T59, and E20/R26 were overlapped and difficult to be distinguished. The bars for the residues with CSP > or ≈ 0.1 ppm were labeled in green. The bars for the residues with intensity drop ≥ 70% were labeled in red. **(d)** Secondary structure of SERF1a idnetified by chemical shift index (CSI 3.0). Amino acids with CSP > or ≈ 0.1 ppm or with intensity drop ≥ 70% were marked as black dots. C = coil, H = helix.



doi:10.6342/NTU202303164

## 3.5 SERF1a enhances the cytotoxicity of Aβ40 and Aβ42 intermediates in neuroblastoma

Considering the effect of SERF1a on Aβ fibrillization which is related to neuronal toxicity, we further investigated whether SERF1a affects Aβ toxicity in neuroblastoma. Here, we examined three different samples including (1) Aβ monomers with and without SERF1a at time 0, (2) Aβ intermediates incubated with and without SERF1a for 14-18 hr, and (3) Aβ fibrils collected from the end point of ThT assay. These samples were treated to human neuroblastoma cell line, BE(2)-C, for approximately 24 hr and the cell viability was then measured by MTT assay. The results showed that, in both Aβ40 and Aβ42 cases, Aβ monomers with and without SERF1a at time 0 had no statistical significance in cytotoxicity with around 90% or more cell viability (Figure 11a and 11b). For the samples incubated for 14-18 hr, we found that Aβ intermediates incubated with SERF1a showed a significantly higher toxicity to the cells (Figure 11c and 11d). These Aβ intermediates were imaged by TEM (Figure 12). This result might be caused by the amyloid-accelerating effect of SERF1a on Aβ monomers to facilitate the formation of more toxic on-pathway oligomers. Intriguingly, despite the finding that SERF1a changed the conformation of Aβ fibrils, the samples from the end point of ThT assay did not show difference in cytotoxicity, indicating that SERF1a-induced conformational changes of Aβ fibrils does not influence the Aβ toxicity in neuroblastoma (Figure 11e and 11f).



doi:10.6342/NTU202303164

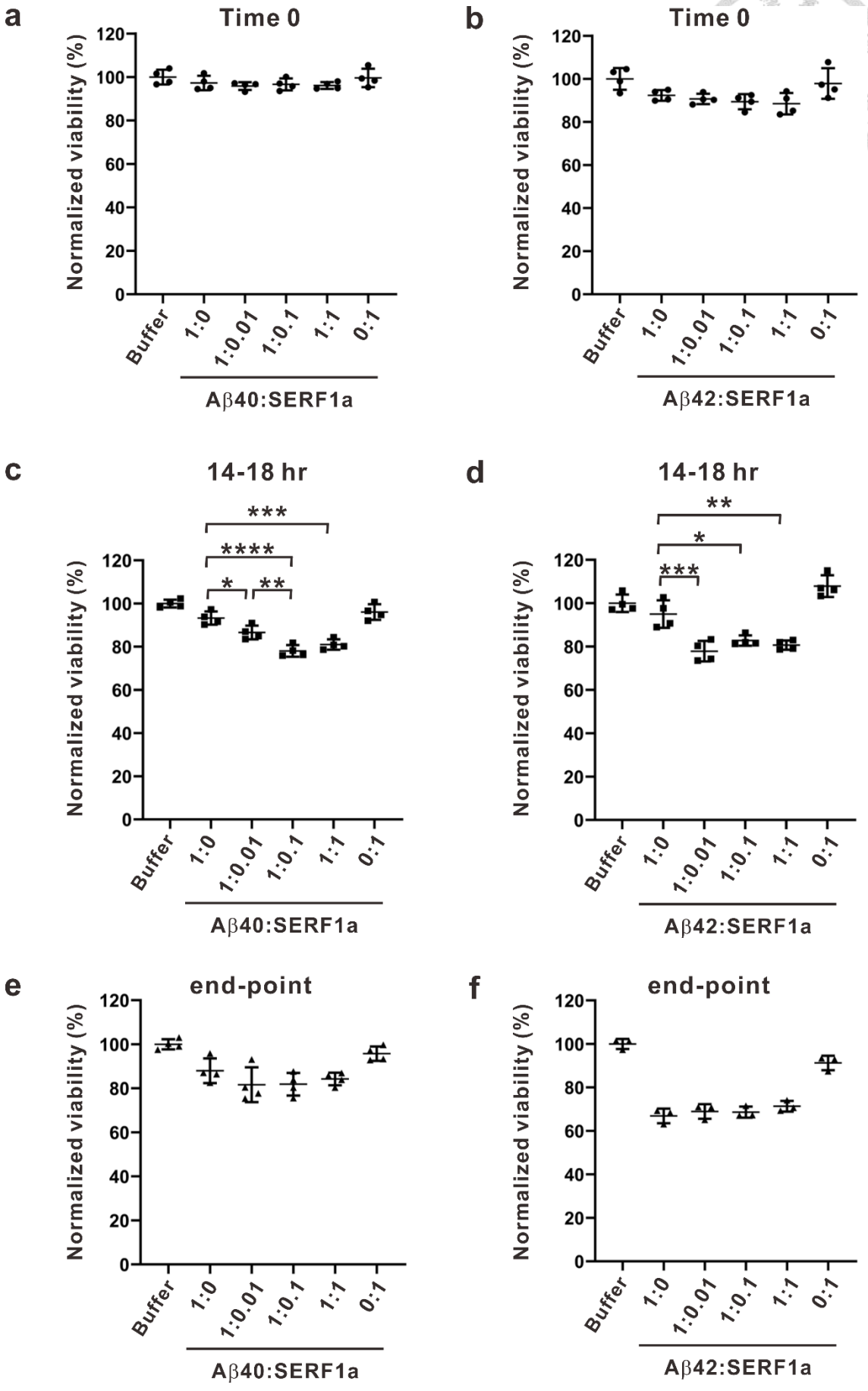




doi:10.6342/NTU202303164

**Figure 11. SERF1a increases Aβ cytotoxicity at intermediate stage in neuroblastoma.**

**(a, b)** Freshly prepared Aβ40 and Aβ42 monomers at time 0, **(c, d)** Aβ40 and Aβ42 intermediates incubated for 14-18 hr, and **(e, f)** Aβ40 and Aβ42 fibrils from the end point of ThT assay with and without SERF1a were treated to the BE(2)-C cells for 20-24 hr. The final concentration of Aβ was 3 μM in the cell culture media. The cell viability was assessed by MTT and normalized to the buffer control. Statistical analysis was calculated by one-way ANOVA, $*P < 0.1$, $**P < 0.01$, $***P < 0.001$, and $****P < 0.0001$; n = 4 for Aβ monomers, intermediates, and Aβ40 fibrils; n = 3 for Aβ42 fibrils. Only statistical analysis of Aβ with and without SERF1a was shown. The error bars denote standard deviation.



doi:10.6342/NTU202303164

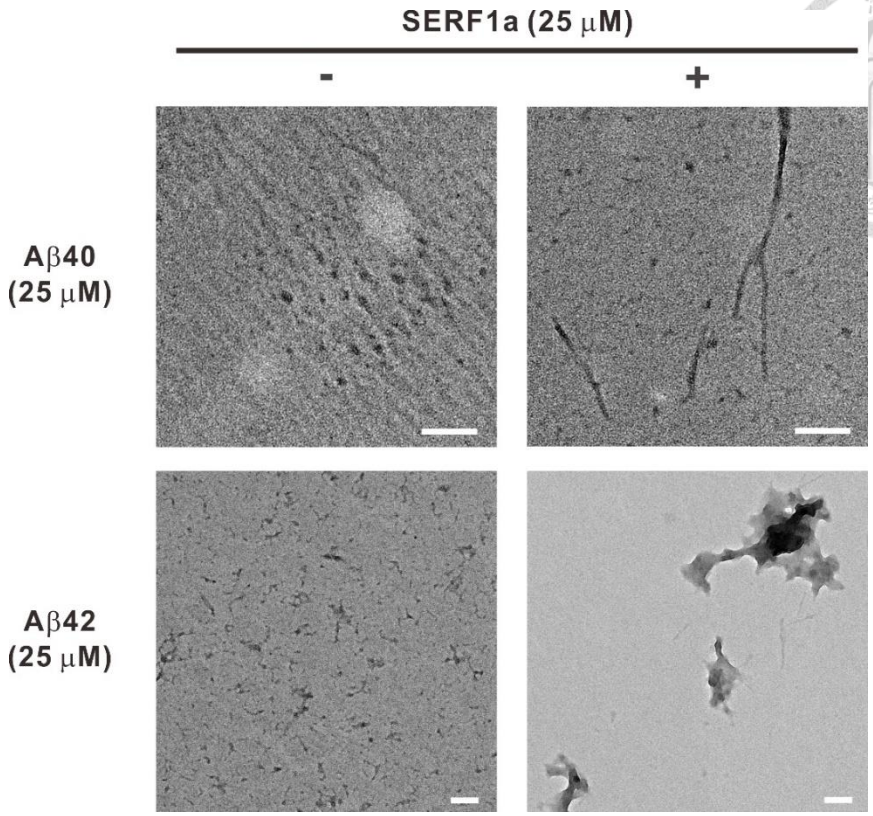


**Figure 12. TEM images of 14-18 hr incubated Aβ40 and Aβ42 intermediates.**

Twenty-five μM Aβ40 or Aβ42 was incubated in the absence or presence of the equimolar SERF1a for 14-18 hr to form Aβ intermediates. The scale bars are 100 nm.



doi:10.6342/NTU202303164

## 3.6 The cytotoxicity caused by SERF1a-induced Aβ42 intermediates can be rescued by SERF1a antibody

On the basis of our data that SERF1a exacerbated the cytotoxicity of Aβ intermediates, we then wanted to develop a blocking agent to hinder the interaction between Aβ and SERF1a, thereby eliminating the effect of SERF1a on Aβ. Since SERF1a binds to Aβ via N-terminal region, we used a monoclonal SERF1a antibody, SERF B1, with an epitope at the N-terminus of SERF1a, to prevent the binding of SERF1a and Aβ42. The validation of SERF B1 is described in Part III section. We first pre-incubated SERF1a with and without SERF B1 for 2 hr prior to the addition of Aβ42 monomers to the mixtures for further incubation. After around 15 hr, the samples were then treated to BE(2)-C cells and incubated for another 24 hr. As measured by MTT, the results revealed approximately 85% cell viability in Aβ42 alone treatment, while coincubation of Aβ42 and SERF1a increased the cytotoxicity with only around 74% cell viability (Figure 13). The effect of SERF1a on Aβ42 was eliminated by co-incubating with SERF B1 which impeded the interaction between SERF1a and Aβ42 and therefore rescued the cell viability back to 84%. This result suggested that blocking the effect of SERF1a on Aβ should be beneficial for cell survival.



doi:10.6342/NTU202303164

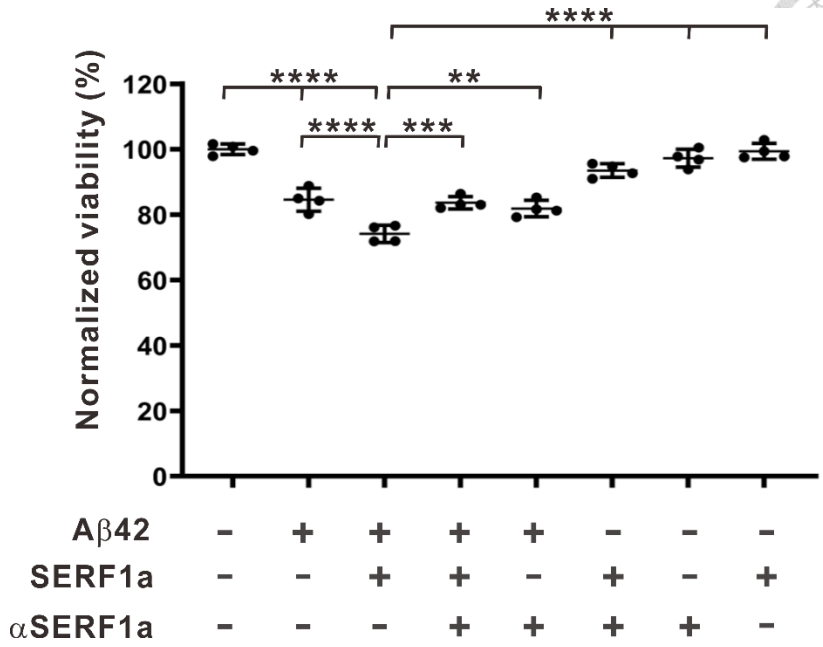


**Figure 13. SERF1a antibody blocks the effect of SERF1a on Aβ42 in human neuroblastoma.**

After incubation of Aβ42 and SERF1a with and without SERF B1 to form the toxic intermediates, the samples were then added into the media to treat the human neuroblastoma BE(2)-C cells for 24 hr. The final concentration of Aβ42 was 3 μM in cell culture media. The ratio of Aβ42 to SERF1a was 1:0.01 and to SERF B1 was 1:0.005. SERF1a antibody, SERF B1, is marked as αSERF1a. The cell viability was measured by MTT and normalized to the buffer control. Statistical analysis was calculated by one-way ANOVA, $^{**}P < 0.01$, $^{***}P < 0.001$, and $^{****}P < 0.0001$, n = 4. The error bars denote standard deviation.



doi:10.6342/NTU202303164

## Part II. Examining the effect of SERF1a on HttpolyQ fibrillization

### 3.7 SERF1a binds to N-terminus of HTT peptides

On the basis of our previous findings that SERF1a promoted fibril formation of mutant HttpolyQ by interacting with mutant HttpolyQ via its helical regions, and the interaction was enhanced upon increasing the level of helical content, we would like to further know whether these two proteins interact via coiled-coils (CC), which plays an important role in protein-protein interactions and has been found in the aggregation of polyQ and Q/N-rich protein interactors[104]. To this end, we designed several HTT peptides comprising N-terminal 17 amino acids of HttpolyQ, a 14-polyQ repeat, and the additional 2 residues at C-terminus (Figure 14). According to the prediction of possible coiled coil a/d positions on the wild-type HTT-0 peptide by DrawCoil[105], five HTT peptides including HTT-1, -2, -3, -4, and -5 were designed with replacement of residues in a/d positions for CC-enhancement and CC-disruption. In HTT-1 and HTT-2, the residues in a/d within the polyQ region were replaced with leucines for CC-enhancing effect, while the residues in a/d within the N-terminal region of HTT-2 were replaced with prolines for CC-destabilizing effect. In HTT-3 and HTT-4, by contrast, the residues in a/d within the polyQ region were replaced by prolines for CC-destabilizing effect, and HTT-4 had additional prolines in a/d within the N-terminal region to substitute for leucines. HTT-5



doi:10.6342/NTU202303164

retained glutamines in a/d within the polyQ region but the residues in a/d within the N-terminal region were replaced with prolines. In addition to these 33-residue peptides, we also generated a shorter peptide consisting of N-terminal 17 amino acids of HTT, named NT17, for the following investigations.

We first assessed the secondary structures of these HTT peptides by using far-UV CD spectroscopy (Figure 15). The spectra revealed that the wild-type HTT-0 showed a partial α-helix structure. HTT-1 with CC-enhancement in the polyQ region revealed a standard α-helical structure, while HTT-2 with additional CC-disruption in the N-terminal region showed a partially α-helical structure similar to HTT-0. The peptides, HTT-3, -4, and -5, with CC-disruption in the N-terminus, polyQ region, or both showed random coils. NT17 showed a partial α-helix in line with previous studies[73,106].

Next, we examined the binding affinity of SERF1a on these HTT peptides by ITC in which SERF1a was titrated into HTT (Figure 16). After analysis and fitting of the raw data, the ITC results revealed that SERF1a and NT17 had the strongest interaction with a $K_A$ value of $1.38 \times 10^7 \pm 6.01 \times 10^6$ $M^{-1}$ ($K_D = 7.25 \times 10^{-8}$ M, 0.0725 μM). SERF1a also bound to HTT-3 with a $K_A$ value of $3.01 \times 10^6 \pm 9.67 \times 10^5$ $M^{-1}$ ($K_D = 3.32 \times 10^{-7}$ M, 0.33 μM). The binding stoichiometry of SERF1a to both NT17 and HTT-3 was nearly 0.5, suggesting a complex of one SERF1a protein and two NT17 or HTT-3. However, except for these two peptides, other peptides including HTT-0, HTT-1, HTT-2, HTT-4, and HTT-



doi:10.6342/NTU202303164

5, did not show interaction with SERF1a. This result indicated that NT17 region containing the first 17 residues of HttpolyQ protein plays a critical role in the interaction with SERF1a; therefore, the peptides with disrupted N-terminus such as HTT-2, HTT-4, and HTT-5 were incapable of binding to SERF1a. Surprisingly, the wild-type HTT-0 and HTT-1 with undisturbed N-terminus did not interact with SERF1a. Considering that self-association of the HTT peptides may block the binding site in the N-terminus, we further assessed the species of the peptides using SV-AUC and found that NT17, HTT-2, HTT-3, HTT-4, and HTT-5 were preponderantly monomers, while HTT-0 formed dimers and HTT-1 predominantly formed oligomers including pentamers and octamers (Figure 17). To further verify the binding of SERF1a with NT17 and HTT-3, we performed SAXS for NT17, HTT-3, and the respective mixtures with SERF1a (Figure 18). The results revealed that the absolute x-ray scattering intensity $I(0)$ of the co-incubated NT17 and SERF1a mixture ($R_g$ = 20.6 Å) was much higher than the sum of respective $I(0)$ values of NT17 monomer ($R_g$ = 11.6 Å) and SERF1a monomer ($R_g$ = 24.0 Å), suggesting a more massive complex formed by NT17 and SERF1a (Figure 18a). Similar conduct of the SAXS $I(0)$ values was also found in HTT-3 monomer ($R_g$ = 16.7 Å), SERF1a monomer, and their mixture ($R_g$ = 21.4 Å), indicating a complex formation of HTT-3 and SERF1a (Figure 18b). These results supported the ITC data, attesting that HTT-3 interacts with SERF1a mainly through the NT17 domain.



doi:10.6342/NTU202303164


**Figure 14. The primary sequence of the designed HTT peptides.**

The possible coiled coil a/d positions was predicted by DrawCoil. Residue substitution in a/d positions were highlighted in green. Leucine was for CC-enhancing effect and proline was for CC-destabilizing effect.

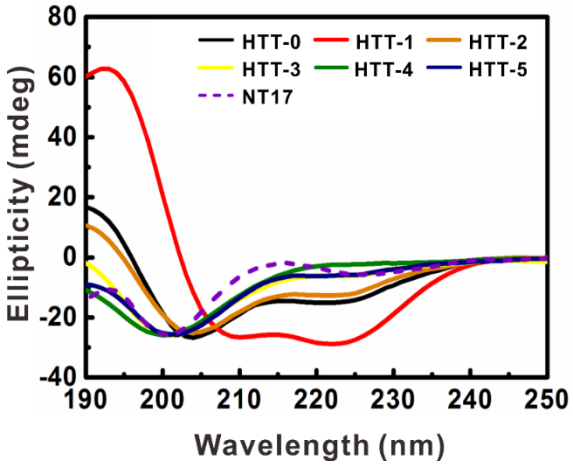


**Figure 15. Far-UV CD spectra of HTT peptides for the secondary structures.**

HTT0, HTT-2, and NT17 showed partial α-helical structures. HTT-1 adopted a classic α-helical structure. HTT-3, HTT-4, and HTT-5 displayed random coils.



doi:10.6342/NTU202303164

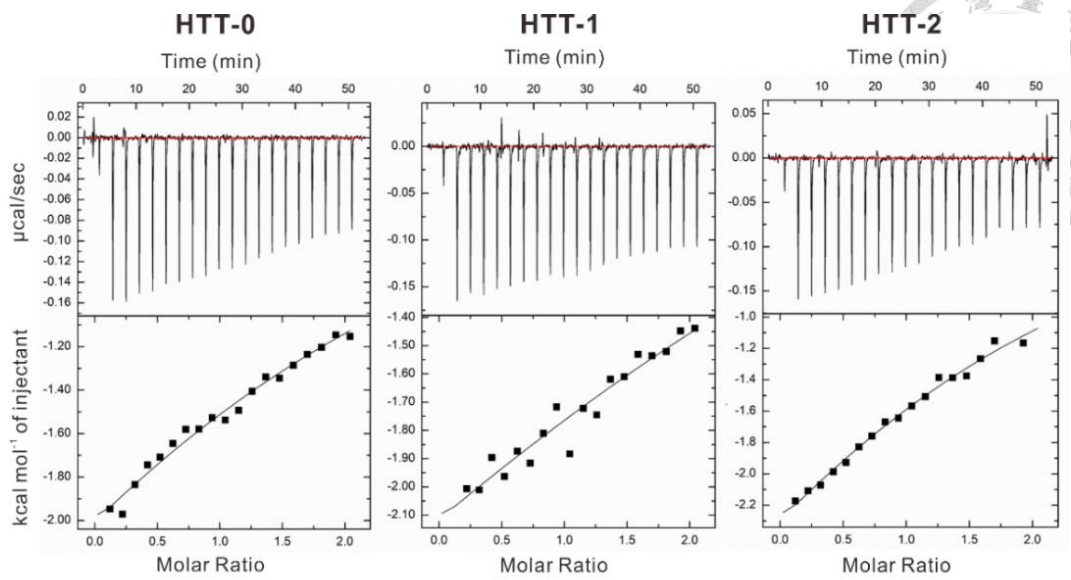


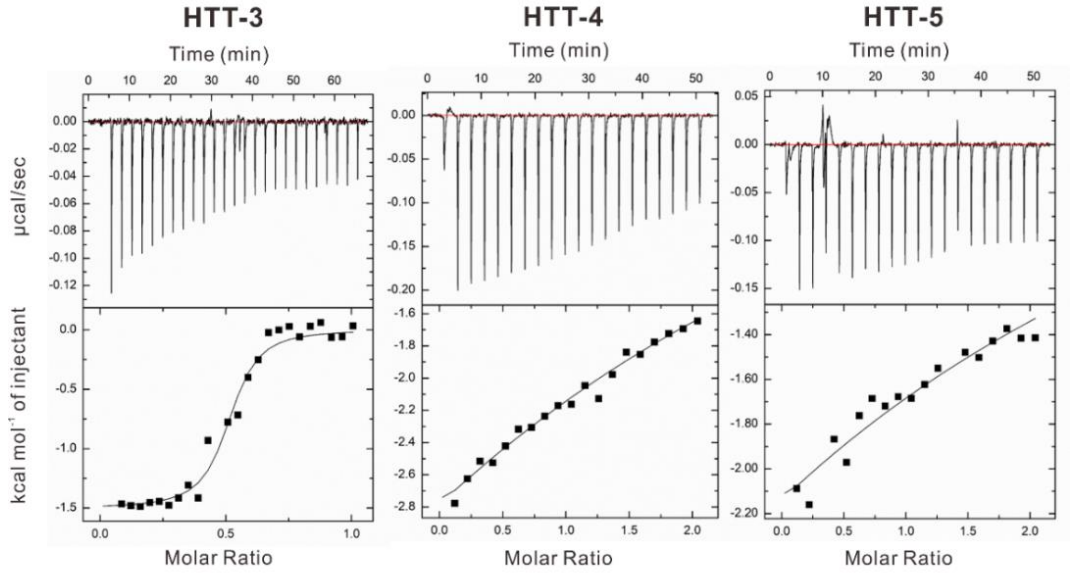


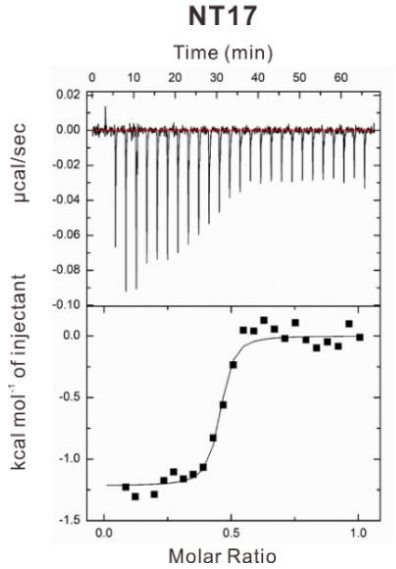




doi:10.6342/NTU202303164

**Figure 16. ITC raw and fitted data of HTT peptides with SERF1a titration for the binding affinity.**

HTT-3 and NT17 showed the stronger interactions with SERF1a. The binding of HTT-3 showed a $K_A$ value of $3.01 \times 10^6 \pm 9.67 \times 10^5$ $M^{-1}$. The binding of NT17 showed a $K_A$ value of $1.38 \times 10^7 \pm 6.01 \times 10^6$ $M^{-1}$. The binding stoichiometry of SERF1a to both HTT-3 and NT17 was nearly 0.5.



doi:10.6342/NTU202303164

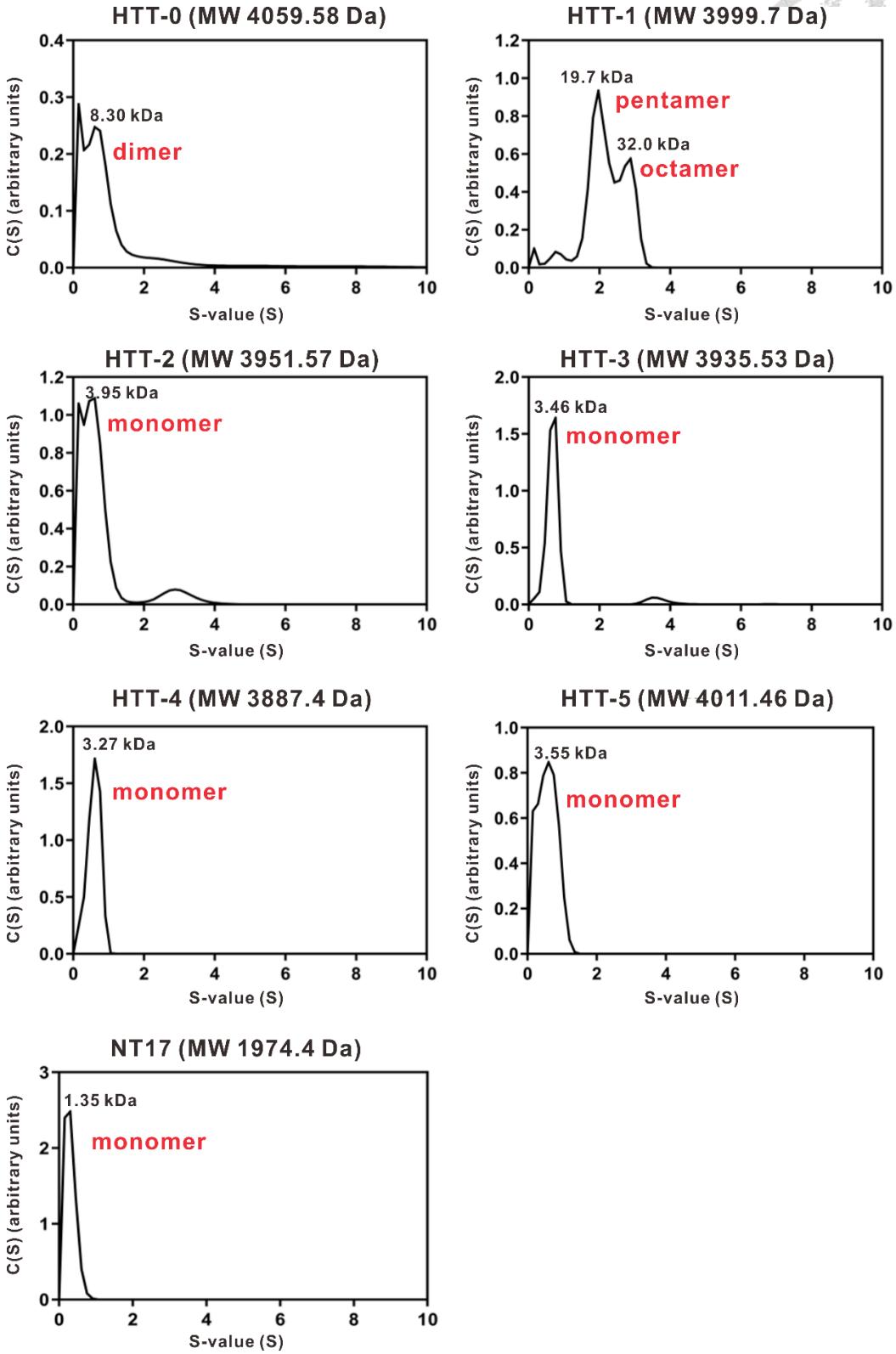


**Figure 17. AUC analysis of HTT peptides.**

According to the concentrations used in ITC, NT17 and HTT-3 at 50 μM and HTT-0,



doi:10.6342/NTU202303164

HTT-1, HTT-2, HTT-4, and HTT-5 at 30 μM were centrifuged at 42,000 rpm for 24 h at 25°C. The theoretical molecular weights of each peptide were indicated on the top.

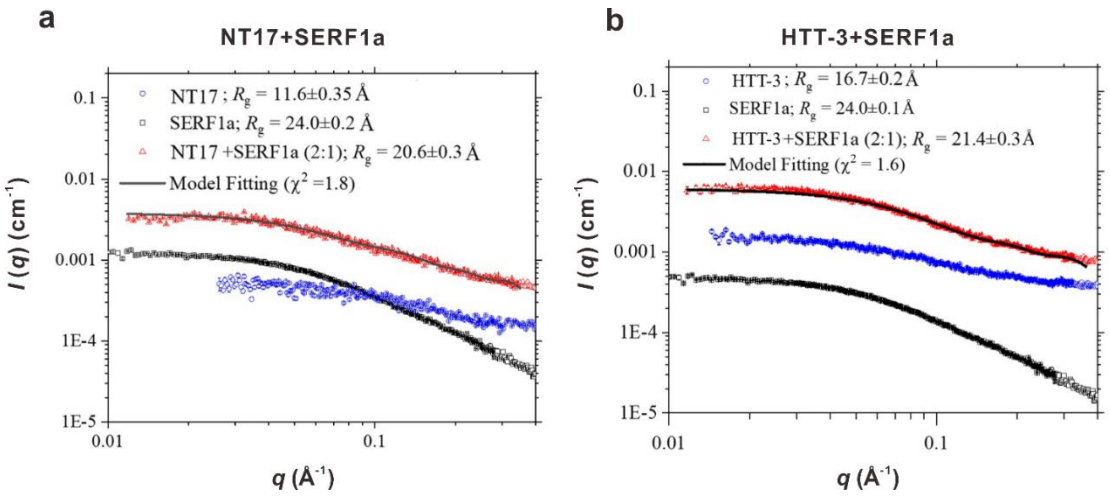


**Figure 18. SAXS data and the extracted $R_g$ values of HTT peptides and SERF1a.**

**(a)** NT17, SERF1a, and the mixture in 2:1 molar ratio. **(b)** HTT-3, SERF1a, and the mixture in molar ratio of 2:1. Data of the mixture was fitted by a DAMMIN model.



doi:10.6342/NTU202303164

## 3.8 The expression level of SERF1a is higher in HD subjects

Our previous data showed that SERF1a transcript levels were higher in HD transgenic mice and human HD iPSCs than in the normal control by using real-time quantitative PCR (Q-PCR). Here, we further compared the SERF1a expression levels in plasma of normal subjects and HD patients by ELISA (Figure 19). Using SERF1a antibody, SERF#1, we found that SERF1a protein level was significantly higher in HD patients' plasma with ~221.9 ng/ml than in the normal control with ~ 152.4 ng/ml. Therefore, this result supports our Q-PCR data, suggesting a disease role of SERF1a in HD.

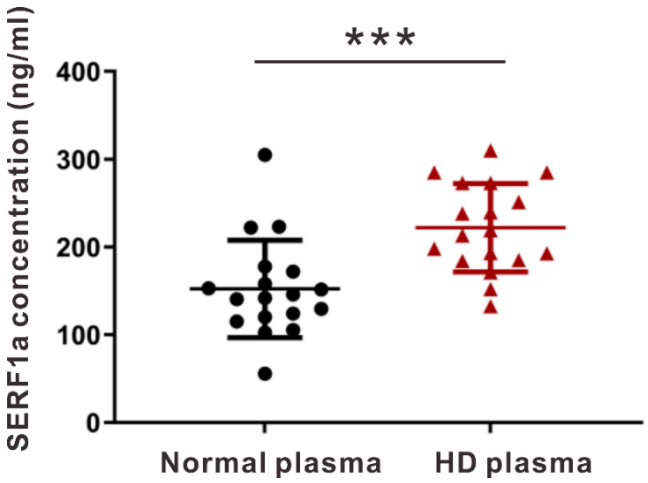


**Figure 19. SERF1a protein level is elevated in HD plasma.**

Normal plasma, n=18; HD plasma, n=18. Data was analyzed using unpaired Student's t-test, ***$P < 0.001$. The error bars denote standard deviation.



doi:10.6342/NTU202303164

## Part III. SERF1a antibody production and application

### 3.9 Production and selection of SERF1a antibodies

To extend our study, we produced SERF1a monoclonal antibodies for further applications. Monoclonal antibody, generated by the same clone of B cells, has high specificity to a single epitope and therefore can be a useful tool for the investigation[107]. We first provided the peptides of SERF1a N-terminus and C-terminus synthesized by GRC peptide synthesis core facility, as shown in Figure 20, to LTK BioLaboratories. In LTK, 100 mg of SERF1a N-terminus and 100 mg of C-terminus peptides were simultaneously injected into a mouse every 2 weeks for 6 times in total. After the treatment, 8 single clones of hybridomas were selected and the antibodies were purified using Protein G Sepharose 4 Fast Flow beads. The affinity of the antibodies was then measured by dot blot (Figure 21a). The epitopes of most of these SERF1a antibodies are at the C-terminus of SERF1a except for B1 whose epitope is at the N-terminus of SERF1a. The result of dot blot revealed that clone #1, #2, #4, and B5 were more effective while clone B1, B3, B4, and B10 had no signals shown. Next, we further examined the efficiency of SERF#1, #2, #4, and B5 by western blot and ELISA. Although all four clones showed similar efficiency in the western blot (Figure 21b), SERF#2 had highest



doi:10.6342/NTU202303164

intensity in ELISA (Figure 21c). Based on these results, we used SERF#2 for our experiments.

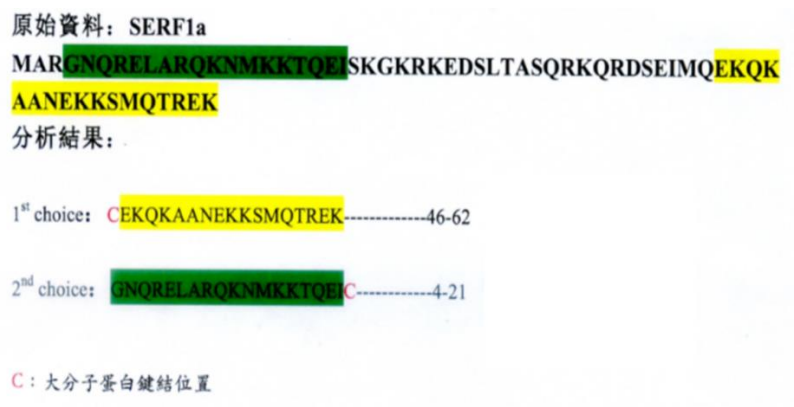


**Figure 20. The sequences of SERF1a N-terminus and C-terminus peptides used to immunize mice to produce SERF1a antibodies.**



doi:10.6342/NTU202303164

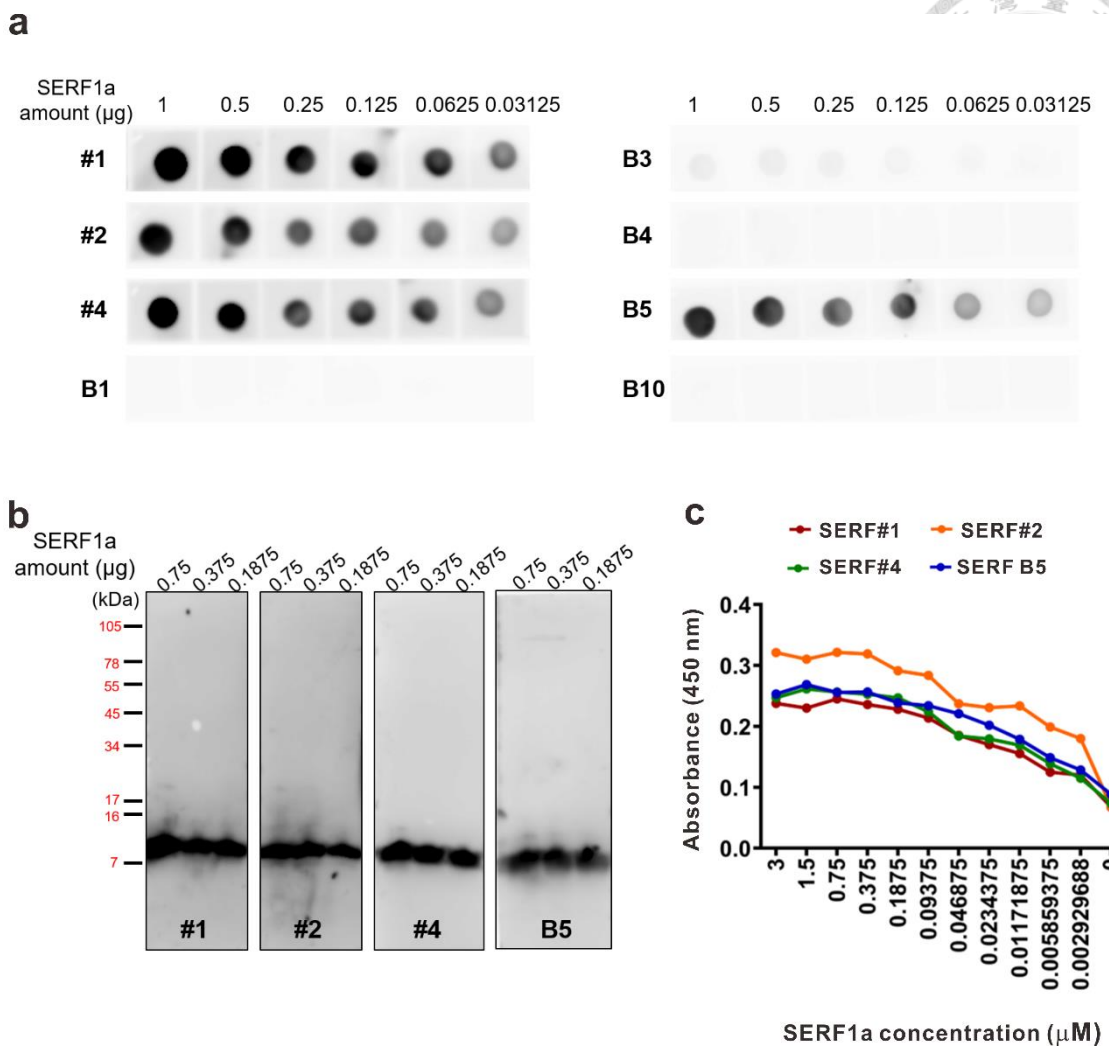


**Figure 21. Validation of the efficiency of SERF1a antibodies.**

**(a)** Dot blot and **(b)** Western blot. Recombinant SERF1a at the indicated amounts were loaded and probed by the tested SERF1a antibodies (1:100). **(c)** ELISA. Recombinant SERF1a was immobilized in the ELISA plate from 0 to 3 μM by serial dilution. The tested SERF1a antibodies were added in 1:100 dilution.



doi:10.6342/NTU202303164

## 3.10 Application and examination of SERF#2

To compare the levels of SERF1a in the brain lysates of normal subjects and AD patients, we performed western blot by using SERF#2 (Figure 22). The results showed bands at ~17 kDa in both of normal control and AD patient cases, which was not consistent with recombinant SERF1a at ~8 kDa (Figure 21b). One possibility is that endogenous SERF1a has higher molecular weight due to certain post-translational modifications. To confirm whether SERF1a expressed in cells has higher molecular weight, we transfected mouse neuroblastoma Neuro-2a (N2a) with EGFP-SERF1a and performed western blot using SERF#2 and anti-EGFP antibody (Figure 23). We found a band were detected by both SERF#2 and anti-EGFP antibody at ~40 kDa, indicating the cell-expressed EGFP-SERF1a. In comparison to the theoretical molecular weight of EGFP-SERF1a, 35.4 kDa, EGFP-SERF1a expressed in cells had higher molecular weight, suggesitng the difference in molecular weight between *E. coli*-expressed (theoretical) and cell-expressed SERF1a. In addition, we also found endogenous protein shown at ~17 kDa in the negative control, N2a mock, and EGFP-SERF1a samples detected by SERF#2. To further examine the 17 kDa proteins, we transfected human embryonic kidney 293T cells (HEK293T) with EGFP-SERF1a and found the bands also shown in human cell line. We lysed the cells and performed IP followed by MS to identify the proteins. The bands we



doi:10.6342/NTU202303164

selected to MS including EGFP-SERF1a, the endogenous protein in cells, and recombinant SERF1a were shown in Figure 24. The MS results confirmed EGFP-SERF1a and recombinant SERF1a according to the sequences we provided, while the endogenous protein did not contain the sequence of SERF (data not shown). These findings indicated that although SERF#2 shows stronger affinity to SERF1a, it has non-specific binding in cells and in brain lysates.



doi:10.6342/NTU202303164

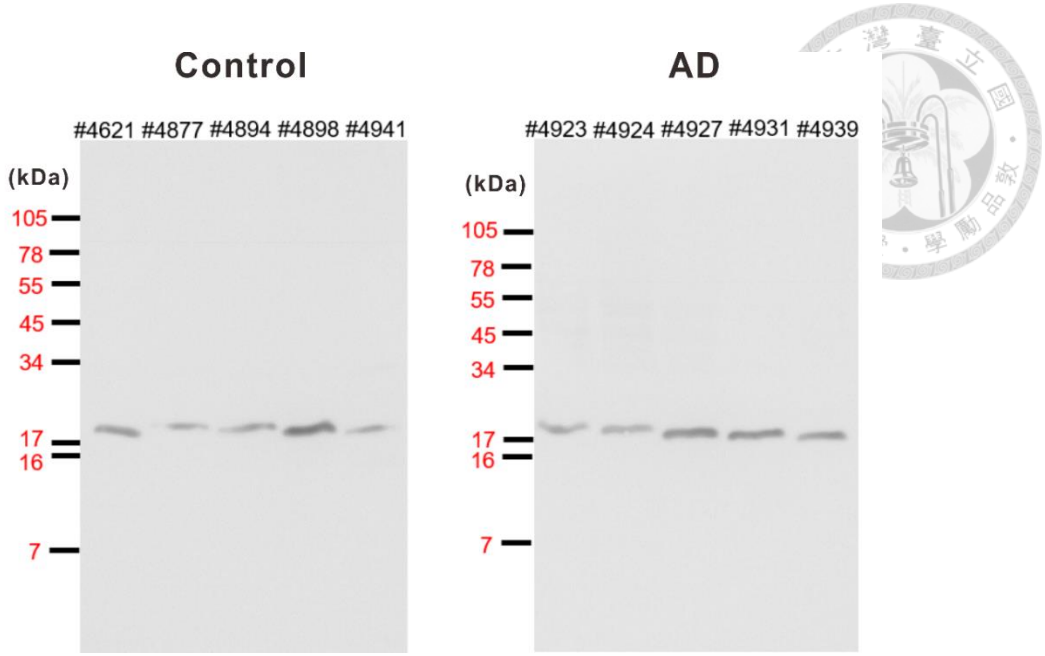


**Figure 22. Detection of SERF1a levels in AD brain (cortex) lysates by SERF#2.**

Western blot for the brain lysates of normal control and AD patients. The samples at 20 μg were loaded and probed by SERF#2 (1:30). The number of each sample are labeled on the top.



doi:10.6342/NTU202303164

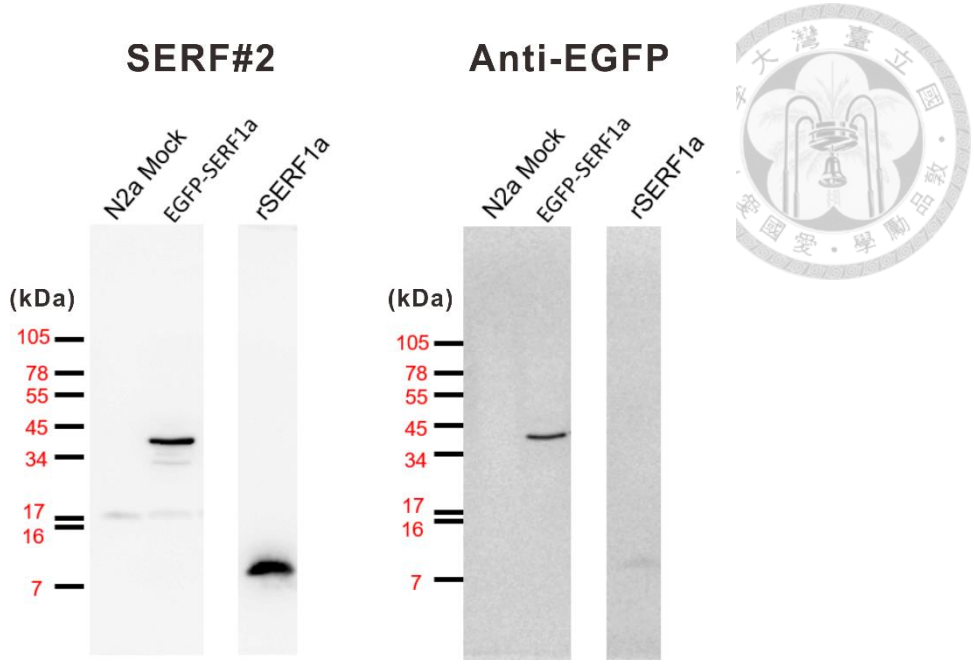


**Figure 23. Examination of SERF1a expressed in cells.**

N2a transfection with EGFP-SERF1a. N2a mock and recombinant SERF1a (rSERF1a) were loaded as a negative control and a positive control, respectively, in the same gel.



doi:10.6342/NTU202303164

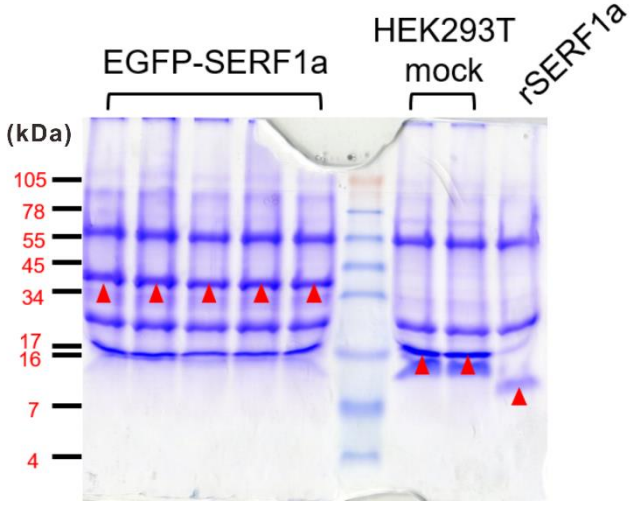


**Figure 24. The band selection from IP for MS.**

HEK293T transfection with EGFP-SERF1a. The bands for EGFP-SERF1a and recombinant SERF1a (rSERF1a) were collected as positive controls. The selected bands are marked with red arrows.



doi:10.6342/NTU202303164

## 3.11 Examination of SERF#1 and SERF B5

Due to the non-specific binding of SERF#2, it was neccesary to find other antibodies for experiments in cells. We therefore tested the specificity of SERF#1, SERF#4, and SERF B5 which showed qualified affinities on the previous tests (Figure 21). By western blot with N2a mock lysates, SERF#4 recognized a non-specific band at ~17 kDa, similar to the band found in the case of SERF#2, while SERF#1 and SERF B5 did not detect the band (Figure 25). In addition to the specificity in cells, we next examined the affinity of SERF#1 and SERF B5 with cell-expressed SERF1a by N2a transfection with EGFP-SERF1a (Figure 26a). Western blot results showed that both SERF#1 and SERF B5 could recognize the cell-expressed EGFP-SERF1a and no non-specific band was detected in N2a mock and HEK293T mock. However, there was no endogenous SERF1a detected in cells, either. To further confirm this, we transfected N2a with flag-SERF1a and performed ICC (Figure 26b). By using Alexa Fluor 594 for SERF#1 and SERF B5 shown in red and Alexa Fluor 488 for anti-flag shown in green, colocalization of SERF#1 or SERF B5 and anti-flag indicated the specificity and affinity of these two antibodies for SERF1a in cells, supporting the observation in western blot. Altogether, we concluded that SERF#1 and SERF B5 can be used for *in vitro* and cell-based experiments instead of SERF#2.



doi:10.6342/NTU202303164

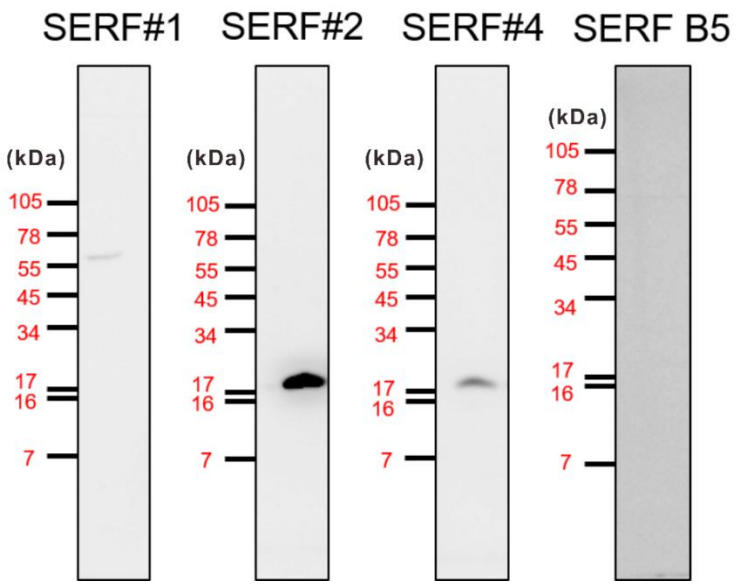


**Figure 25. Examination of the specificity of SERF1a antibodies in cells.**

N2a mock lysates were loaded at 50 μg/well and probed by SERF1a antibodies at 1:100.



doi:10.6342/NTU202303164

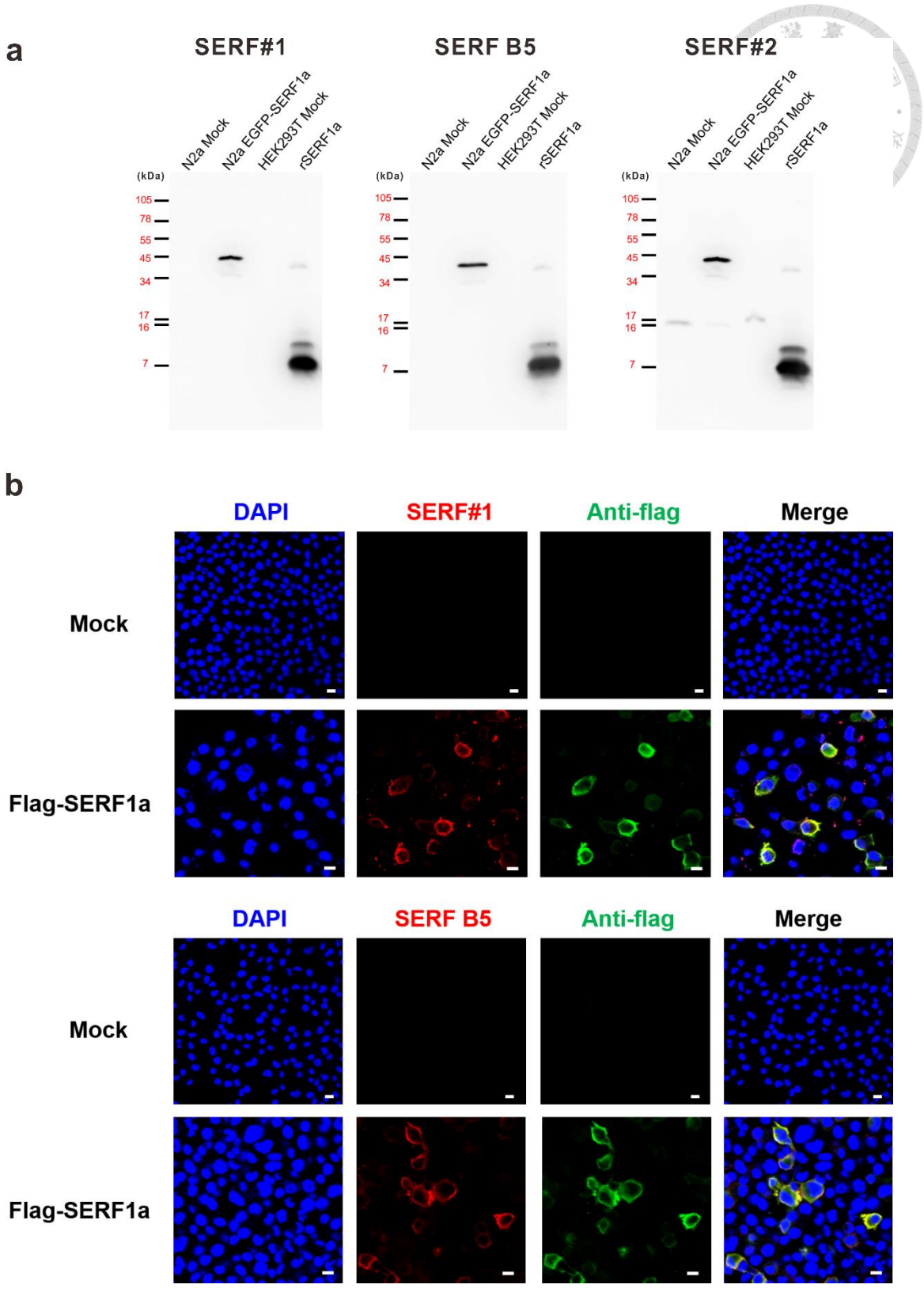


**Figure 26. Examination of the specificity and affinity of SERF1a antibodies in cells.**

**(a)** Western blot. SERF1a antibodies were used at 1:100. rSERF1a: recombinant SERF1a,



doi:10.6342/NTU202303164

loaded as a positive control. **(b)** ICC. N2a was transfected with flag-SERF1a. N2a mock was used as the negative control. SERF#1 and SERF B5 were detected by secondary antibody Alexa Fluor 594. Anti-flag antibody was detected by Alexa Fluor 488. The scale bars are 10 μm.



doi:10.6342/NTU202303164

## 3.12 Validation of SERF B1

Since we found that SERF1a interacts with Aβ40 via its N-terminal region, we need a SERF1a antibody whose epitope is at the N-terminus of SERF1a to block the interaction. SERF B1 is the only one clone recognizing the N-terminus of SERF1a as the epitope among the SERF1a antibodies we produced; therefore, we validated its affinity by ELISA and western blot. Although SERF B1 showed very low efficiency in the first round of selection with other clones (Figure 21), increasing the concentration was able to improve its capacity as shown in Figure 27. The results suggested that SERF B1 can be used for experiments of blocking interaction between SERF1a and Aβ.



doi:10.6342/NTU202303164

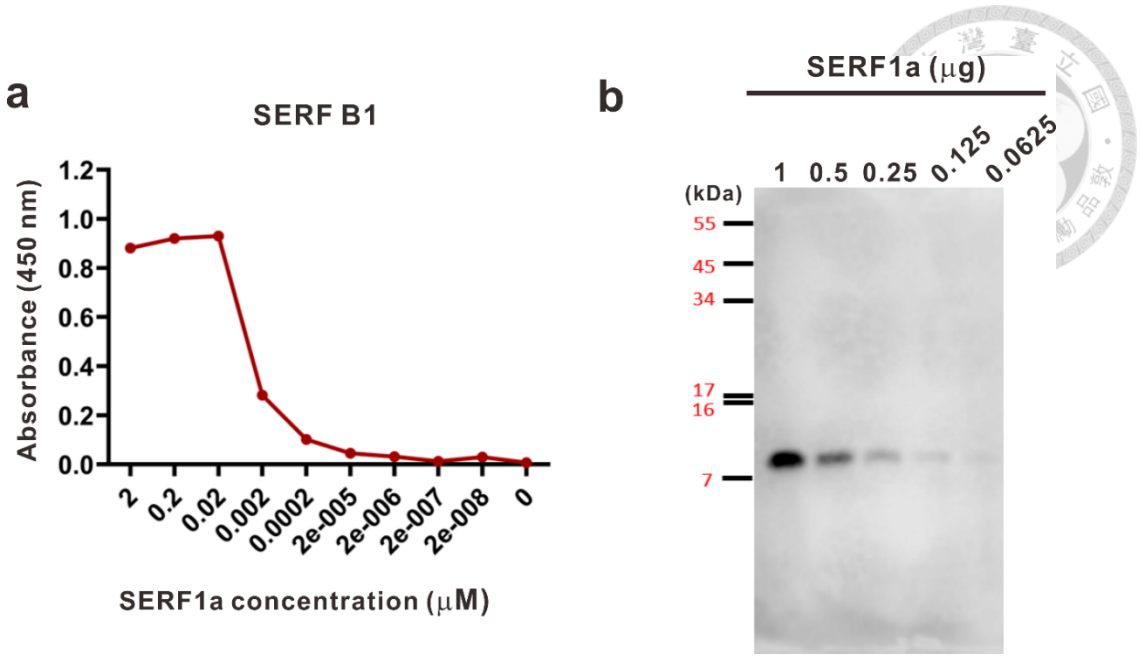


**Figure 27. Validation of SERF B1 by ELISA and western blot.**

**(a)** ELISA. Recombinant SERF1a was immobilized in the ELISA plate from 2 to 0 μM by serial dilution. SERF B1 was added in 1:100 dilution from the stock (5 mg/ml). **(b)** Western blot. Recombinant SERF1a at 1 μg and the serially diluted samples were loaded and subjected to western blot probed by SERF B1 antibody (1:100).



doi:10.6342/NTU202303164

# CHAPTER 4. DISCUSSION

## 4.1 Investigating the role of SERF1a in Aβ40 and Aβ42 fibrillization

MOAG-4/SERF protein is identified as a general amyloid modifier since it has been found to promote the fibrillization of different amyloid proteins, including α-Syn, Aβ40, htt Ex1Q53, and prion proteins[82]. However, the underlying mechanisms by which SERF1a is able to affect a wide range of structurally diverse amyloidogenic proteins/peptides still need to be investigated. In our study, we found that SERF1a dose-dependently expedites the fibril formations of both Aβ40 and Aβ42 but is not related to the final levels of the fibrils. The N-terminal region of SERF1a interacts with Aβ by forming a 1:1 complex, transforming Aβ into more aggregation-prone. SERF1a exacerbates Aβ cytotoxicity owing to its accelerating effect on Aβ aggregation. The cytotoxicity resulting from SERF1a-accelerated Aβ intermediates can be rescued by the SERF1a antibody we produced, suggesting that blocking SERF1a may be a potential therapeutic strategy for AD.

According to the results of FTIR, the spectrum of Aβ42 fibrils showed two peaks at 1628 $cm^{-1}$ denoting parallel β-sheet and 1678 $cm^{-1}$ representing turns connecting β-strands and that is in line with the previous study revealing the 3D structure of Aβ42 fibrils which forms a β-strand–turn–β-strand motif including two intermolecular, parallel β-sheets[108]. However, although the peak at 1678 $cm^{-1}$ was in the range of 1665 $cm^{-1}$ to 1685 $cm^{-1}$



doi:10.6342/NTU202303164

identified as a turn[96,98,99,109,110], the β-turn content was reported around 15-20% for aggregates[98,111] that is inconsistent with our result showing a large peak. It has been revealed that in antiparallel β-sheet structures, in addition to the major peak at 1620 $cm^{-1}$ to 1630 $cm^{-1}$, a minor peak is shown at 1680 $cm^{-1}$ to 1695 $cm^{-1}$ [96,109,112] and that might also contribute to the large peak at 1678 $cm^{-1}$ we observed. Therefore, the Aβ42 alone sample probably contained not only fibrils indicated by parallel β-sheet but also oligomers represented by antiparallel β-sheet.[98] Upon the co-incubation with SERF1a, the peak contributed by β-turn and antiparallel β-sheet was eliminated, attesting that SERF1a induces the conformational change of Aβ42 to be more prone to aggregation. Since Aβ conformation is altered by SERF1a, its way of forming mature fibrils may also be changed. This could probably also be reflected by the differences found in the morphology of Aβ fibrils in TEM.

Intriguingly, our PICUP results demonstrated that Aβ alone formed dimers, trimers, tetramers, and some oligomers themselves, whereas these species were decreased in the presence of SERF1a. In agreement with this observation, our AUC data also showed that Aβ42 trimers and oligomers disappeared in the presence of SERF1a. Since SERF1a has an accelerating effect on Aβ aggregation, we consider the early-formed Aβ oligomers in Aβ alone samples as "off-pathway" oligomers. One possibility is that SERF1a directly disassembles Aβ oligomers into monomers and then alters Aβ conformation to go for



doi:10.6342/NTU202303164

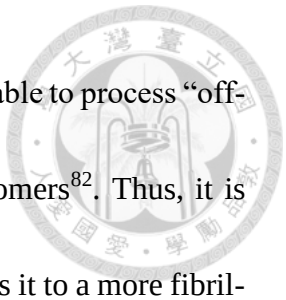

"on-pathway". However, a previous study revealed that SERF1a is unable to process "off-pathway" α-Syn oligomers into fibrils or dissociate them into monomers[82]. Thus, it is more likely that by interacting with the Aβ monomer, SERF1a induces it to a more fibril-prone conformation leading to shifting the equilibrium to disassemble the off-pathway oligomers, and then accelerating the fibril formation.

Although various species of Aβ/SERF1a complexes including Aβ: SERF1a 1:1 and 2:2 in both Aβ40 and Aβ42 and probably 3:1 and 3:2 in Aβ40 (unmarked) were found in the PICUP study, only the 1:1 complex for both Aβ40 and Aβ42 was further verified in the results of ESI-MS and AUC. Together with the NMR data, we propose that SERF1a interacts with the Aβ monomer via its N-terminal region to form a 1:1 complex. In addition, the immunogold labeling and partition analysis results revealed that SERF1a is not incorporated into Aβ fibrils, which means that SERF1a dissociates from Aβ after the interaction. In line with this finding, previous studies have reported that MOAG-4 did not colocalize with polyglutamine aggregates in cells, indicating the exclusion of MOAG-4 from the aggregates[81]. Also, MOAG-4 and SERF1a have been found to transiently bind to α-Syn rather than stably associate with aggregating or fibrillar α-Syn *in vitro*[82,83]. This is reinforced by the fact we observed in ThT assay that even a very low concentration of SERF1a is still capable of affecting Aβ aggregation since SERF1a would dissociate from



doi:10.6342/NTU202303164

Aβ and exert its effect on other Aβ repeatedly. This action is reminiscent of molecular chaperones which can bind to and release substrates efficiently.

SERF2, the other isoform of the human ortholog of MOAG-4, has been reported to drive protein aggregation by charge complementation in which it interacts with negatively charged sections of amyloid proteins via its positively charged N-terminus[113]. By point mutations in the three positively charged residues, $Lys^{16}$, $Lys^{17}$, and $Lys^{23}$ to neutralize the N-terminal region of SERF2 and also lysine-to-arginine mutations in these three residues, they concluded that charge complementation rather than amino acid composition drives the interactions of SERF2 with amyloid proteins. Our NMR study also showed that SERF1a interacts with Aβ40 via its N-terminal region; however, the exact interacting residues we found do not include $Lys^{16}$ or $Lys^{17}$ perhaps owing to the differences in SERF2 and SERF1a, where SERF2 with 170 amino acids is nearly 3 times bigger than SERF1a short form with 62 amino acids. Another possibility is that although $Lys^{16}$, $Lys^{17}$, and $Lys^{23}$ play an important role in the charge of the N-terminal region of SERF2, it does not mean that these three residues directly interact with the binding partners.

In MTT cell viability assay, the samples from the end-point of ThT assay were more toxic to BE2C cells than the samples incubated for 14-18 hr. However, although Aβ fibrils are toxic to the cells, Aβ oligomers and protofibrils are considered the more toxic species[21]. Therefore, we speculate that the end-point products of ThT assay probably



doi:10.6342/NTU202303164

contained not only the fibrils we expected but also other species including oligomers and protofibrils.

Based on our results, we propose a mechanism by which SERF1a accelerates Aβ fibrillization by a transient 1 to 1 interaction with Aβ monomer to convert Aβ into a more aggregation-prone conformation. Then, SERF1a dissociates from Aβ and exerts its effect on other Aβ monomers repeatedly. The SERF1a-induced Aβ intermediates exacerbate the cytotoxicity that can be rescued by targeting SERF1a with our SERF1a antibody. Taken together, our study provides molecular insight into how SERF1a influences Aβ fibril formation and suggests a potential target for therapeutic development for AD in the future.



doi:10.6342/NTU202303164

## 4.2 Examining the effect of SERF1a on HttpolyQ fibrillization

In the HTT peptide study, we found that SERF1a mainly interacts with NT17 and HTT-3 but not those containing proline substitutions in the NT17 region, namely HTT-2, HTT-4, and HTT-5. This result suggests that NT17 is the primary region for SERF1a binding. In addition, the NT17 peptide showed stronger affinity to SERF1a with over fourfold than HTT-3, indicating that the following polyQ region affects the interaction. However, SERF1a did not interact with HTT-0 and HTT-1 even though these two peptides contained unchanged NT17 regions. This might be because the dimerization of HTT-0 and the oligomerization of HTT-1 hindered the binding of SERF1a. Another possibility is that the short polyQ tract with α-helical structure impedes the interaction of the NT17 region since both HTT-0 and HTT-1 contained α-helical and enhanced α-helical polyQ regions, respectively, while this region of HTT-3 was disrupted by the proline mutations. NT17 region was found to adopt different conformations when being attached to different length of polyQ tract[106]. Hence, the interaction between SERF1a and HttpolyQ could be promoted because of conformational changes of NT17 in the long polyQ tract. However, whether full-length HttpolyQ with extended polyQ interacts with SERF1a via NT17 requires further investigations.



doi:10.6342/NTU202303164

Based on our previous data, the promoting effect of SERF1a on HttpolyQ aggregation and the binding affinity of SERF1a to HttpolyQ showed a polyQ length-dependent manner. However, the NT17 region, where SERF1a binds to, was contained in all HttpolyQ samples with different lengths of polyQ tracts in our study. The important role of NT17 in HttployQ aggregation has been reported in previous studies showing that the NT17 region of HttpolyQ triggers rapid polyQ aggregation[106,114]. It has been shown that polyQ attached to NT17 results in a more extended conformation of NT17 in a polyQ length-dependent manner, which greatly promotes its aggregation[106]. Another study revealed that the NT17 region is spatially close to the C-terminal proline-rich domain when polyQ repeats are less than 32, while NT17 is apart from the proline-rich domain with polyQ of more than 37 repeats[115]. Accordingly, SERF1a mainly interacting with the NT17 of mutant HttpolyQ but not that of normal HttpolyQ is probably because of conformational changes or the exposure of the NT17 domain. Taking all our data into account, we propose a model in which SERF1a promotes mutant HttpolyQ fibrillization through binding to the NT17 domain of HttpolyQ proteins via α-helical regions. The interaction where one SERF1a interacts with two HttpolyQ proteins facilitates the conformational conversion of HttpolyQ into an aggregation-prone β-sheet monomer, which rapidly assembles into amyloid fibrils.



doi:10.6342/NTU202303164

Overall, we found that SERF1a affects the fibrillization of Aβ and HttpolyQ protein via different binding sites and probably different mechanisms. For Aβ fibrillization, SERF1a interacts with Aβ via its N-terminal region and forms a 1:1 complex to induce the conformational conversion of Aβ to be more aggregation-prone thereby increasing the cytotoxicity (Figure 28). For HttpolyQ fibril formation, one SERF1a binds to two HttpolyQ via α-helical regions to facilitate the conformational change of HttpolyQ monomer from α-helix to β-sheet which is prone to fibrillization (Figure 29). In addition, the previous study proposed that in the case of α-Syn, MOAG-4 and SERF1a enhance α-Syn fibrillization by using positively charged N-terminal region to compete with the positively charged N-terminus of α-Syn for its negatively charged C-terminus thereby exposing the middle aggregation-prone region[83]. It is interesting and necessary to further investigate why SERF1a affects the fibrillization of amyloid proteins with different structures and the mechanisms by which it affects other amyloid proteins.

However, although the human protein atlas shows that the RNA levels of SERF1a and SERF2 are relatively high in brain, there is no protein expression level available, indicating that SERF protein level is quite low in human. Indeed, we could not detect endogenous SERF neither in human neuroblastoma cell lines nor in human brain lysates by our SERF antibodies. Therefore, it is difficult to conclude the correlation between the



doi:10.6342/NTU202303164

SERF expression level and the diseases. Also, the importance of SERF in human needs to be further confirmed in the future.



doi:10.6342/NTU202303164

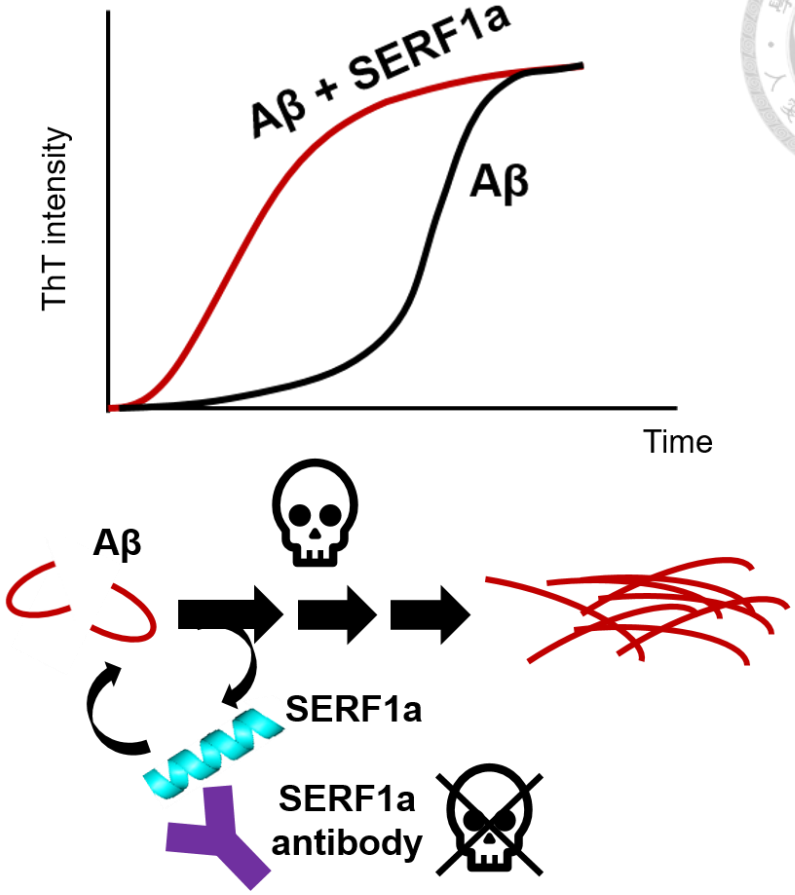


**Figure 28. Proposed model of SERF1a effect on Aβ aggregation.**

SERF1a reduces the lag time of Aβ fibrillization by transiently binding to Aβ monomers in a 1:1 ratio to transform Aβ to a more fibril-prone conformation. SERF1a then dissociates from Aβ and applies its effect on other Aβ monomers repeatedly. The SERF1a-accelerated Aβ intermediates exacerbate the cytotoxicity that can be rescued by targeting SERF1a by SERF1a antibody.



doi:10.6342/NTU202303164

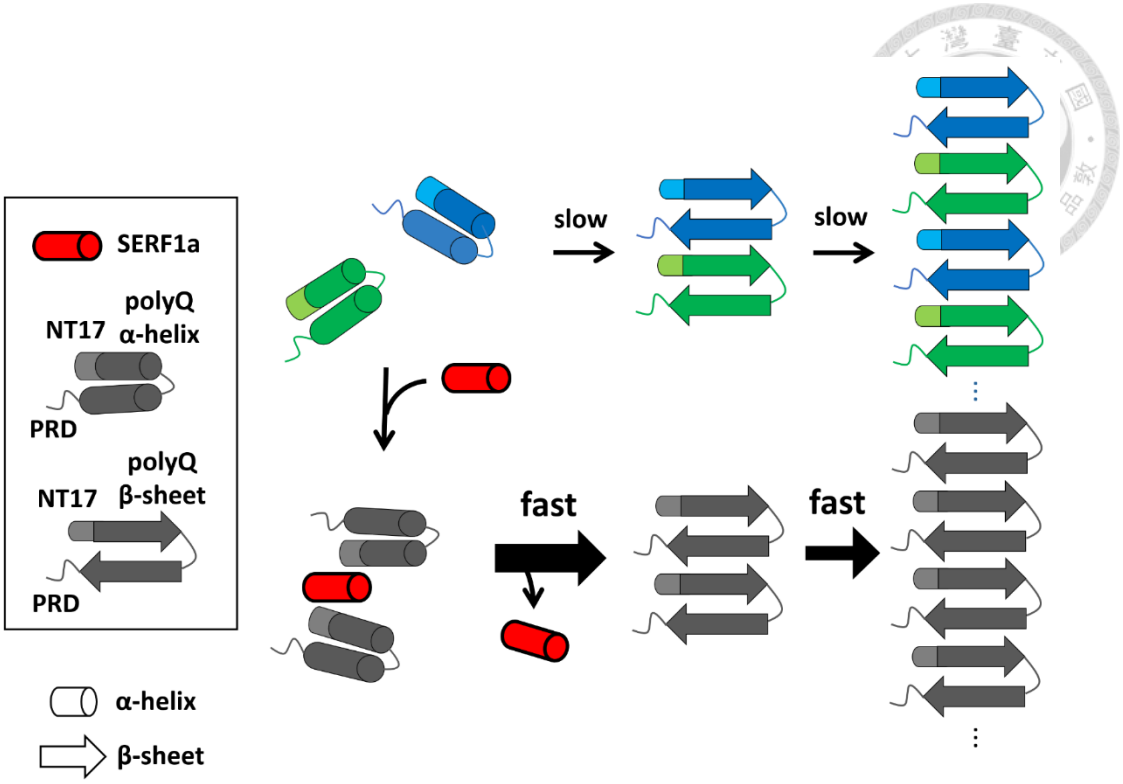


**Figure 29. Mechanisms of SERF1a and HttpolyQ assembly.**

HttpolyQ undergoes conformational change from α-helical to β-sheet-rich conformation and then aggregates to amyloid fibrils. In the presence of SERF1a, the conformational change is facilitated by interaction between α-helical regions of SERF1a and NT17 of HttpolyQ protein in a 1:2 ratio to accelerate formation of a β-sheet species that enhances fibrillization.



doi:10.6342/NTU202303164

# REFERENCES


1 Ruz, C., Alcantud, J. L., Vives Montero, F., Duran, R. & Bandres-Ciga, S. Proteotoxicity and neurodegenerative diseases. *Int J Mol Sci* **21**, doi:10.3390/ijms21165646 (2020).

2 Erkkinen, M. G., Kim, M. O. & Geschwind, M. D. Clinical neurology and epidemiology of the major neurodegenerative diseases. *Cold Spring Harb Perspect Biol* **10**, doi:10.1101/cshperspect.a033118 (2018).

3 Gan, L., Cookson, M. R., Petrucelli, L. & La Spada, A. R. Converging pathways in neurodegeneration, from genetics to mechanisms. *Nat Neurosci* **21**, 1300-1309, doi:10.1038/s41593-018-0237-7 (2018).

4 Taylor, J. P., Hardy, J. & Fischbeck, K. H. Toxic proteins in neurodegenerative disease. *Science* **296**, 1991-1995, doi:10.1126/science.1067122 (2002).

5 Stroo, E., Koopman, M., Nollen, E. A. & Mata-Cabana, A. Cellular regulation of amyloid formation in aging and disease. *Front Neurosci* **11**, 64, doi:10.3389/fnins.2017.00064 (2017).

6 Koga, H., Kaushik, S. & Cuervo, A. M. Protein homeostasis and aging: The importance of exquisite quality control. *Ageing Res Rev* **10**, 205-215, doi:10.1016/j.arr.2010.02.001 (2011).

7 Eisenberg, D. & Jucker, M. The amyloid state of proteins in human diseases. *Cell* **148**, 1188-1203, doi:10.1016/j.cell.2012.02.022 (2012).

8 Knowles, T. P., Vendruscolo, M. & Dobson, C. M. The amyloid state and its association with protein misfolding diseases. *Nat Rev Mol Cell Biol* **15**, 384-396, doi:10.1038/nrm3810 (2014).

9 Iadanza, M. G., Jackson, M. P., Hewitt, E. W., Ranson, N. A. & Radford, S. E. A new era for understanding amyloid structures and disease. *Nat Rev Mol Cell Biol* **19**, 755-773, doi:10.1038/s41580-018-0060-8 (2018).

10 Chiti, F. & Dobson, C. M. Protein misfolding, amyloid formation, and human disease: A summary of progress over the last decade. *Annu Rev Biochem* **86**, 27-68, doi:10.1146/annurev-biochem-061516-045115 (2017).

11 Eichner, T. & Radford, S. E. A diversity of assembly mechanisms of a generic amyloid fold. *Mol Cell* **43**, 8-18, doi:10.1016/j.molcel.2011.05.012 (2011).

12 Westermark, P., Andersson, A. & Westermark, G. T. Islet amyloid polypeptide, islet amyloid, and diabetes mellitus. *Physiol Rev* **91**, 795-826, doi:10.1152/physrev.00042.2009 (2011).

13 Livingston, G. *et al.* Dementia prevention, intervention, and care: 2020 report of the Lancet Commission. *Lancet* **396**, 413-446, doi:10.1016/S0140-




doi:10.6342/NTU202303164

6736(20)30367-6 (2020).

14 Breijyeh, Z. & Karaman, R. Comprehensive review on Alzheimer's disease: Causes and treatment. *Molecules* **25**, doi:10.3390/molecules25245789 (2020).

15 Bertram, L., Lill, C. M. & Tanzi, R. E. The genetics of Alzheimer disease: back to the future. *Neuron* **68**, 270-281, doi:10.1016/j.neuron.2010.10.013 (2010).

16 Barber, R. C. The genetics of Alzheimer's disease. *Scientifica (Cairo)* **2012**, 246210, doi:10.6064/2012/246210 (2012).

17 Huang, Y. & Mucke, L. Alzheimer mechanisms and therapeutic strategies. *Cell* **148**, 1204-1222, doi:10.1016/j.cell.2012.02.040 (2012).

18 Corder, E. H. *et al.* Gene dose of apolipoprotein E type 4 allele and the risk of Alzheimer's disease in late onset families. *Science* **261**, 921-923, doi:10.1126/science.8346443 (1993).

19 Farrer, L. A. *et al.* Effects of age, sex, and ethnicity on the association between apolipoprotein E genotype and Alzheimer disease. A meta-analysis. APOE and Alzheimer Disease Meta Analysis Consortium. *JAMA* **278**, 1349-1356 (1997).

20 Agarwal, M., Alam, M. R., Haider, M. K., Malik, M. Z. & Kim, D. K. Alzheimer's disease: An overview of major hypotheses and therapeutic options in nanotechnology. *Nanomaterials-Basel* **11**, doi:ARTN 59 10.3390/nano11010059 (2021).

21 Hampel, H. *et al.* The Amyloid-beta pathway in Alzheimer's disease. *Mol Psychiatr* **26**, 5481-5503, doi:10.1038/s41380-021-01249-0 (2021).

22 Haass, C., Kaether, C., Thinakaran, G. & Sisodia, S. Trafficking and proteolytic processing of APP. *Cold Spring Harb Perspect Med* **2**, a006270, doi:10.1101/cshperspect.a006270 (2012).

23 Zhao, J., Liu, X., Xia, W., Zhang, Y. & Wang, C. Targeting amyloidogenic processing of APP in Alzheimer's disease. *Front Mol Neurosci* **13**, 137, doi:10.3389/fnmol.2020.00137 (2020).

24 Vassar, R. ADAM10 prodomain mutations cause late-onset Alzheimer's disease: not just the latest FAD. *Neuron* **80**, 250-253, doi:10.1016/j.neuron.2013.09.031 (2013).

25 Esch, F. S. *et al.* Cleavage of amyloid beta peptide during constitutive processing of its precursor. *Science* **248**, 1122-1124, doi:10.1126/science.2111583 (1990).

26 Sisodia, S. S., Koo, E. H., Beyreuther, K., Unterbeck, A. & Price, D. L. Evidence that beta-amyloid protein in Alzheimer's disease is not derived by normal processing. *Science* **248**, 492-495, doi:10.1126/science.1691865 (1990).

27 Wang, R., Meschia, J. F., Cotter, R. J. & Sisodia, S. S. Secretion of the beta/A4 amyloid precursor protein. Identification of a cleavage site in cultured mammalian cells. *J Biol Chem* **266**, 16960-16964 (1991).



doi:10.6342/NTU202303164

28 Suzuki, N. *et al.* An increased percentage of long amyloid beta protein secreted by familial amyloid beta protein precursor (beta APP717) mutants. *Science* **264**, 1336-1340, doi:10.1126/science.8191290 (1994).

29 Iwatsubo, T. *et al.* Visualization of A beta 42(43) and A beta 40 in senile plaques with end-specific A beta monoclonals: evidence that an initially deposited species is A beta 42(43). *Neuron* **13**, 45-53, doi:10.1016/0896-6273(94)90458-8 (1994).

30 Gravina, S. A. *et al.* Amyloid beta protein (A beta) in Alzheimer's disease brain. Biochemical and immunocytochemical analysis with antibodies specific for forms ending at A beta 40 or A beta 42(43). *J Biol Chem* **270**, 7013-7016, doi:10.1074/jbc.270.13.7013 (1995).

31 Gu, L. & Guo, Z. Alzheimer's Abeta42 and Abeta40 peptides form interlaced amyloid fibrils. *J Neurochem* **126**, 305-311, doi:10.1111/jnc.12202 (2013).

32 De Jonghe, C. *et al.* Pathogenic APP mutations near the gamma-secretase cleavage site differentially affect Abeta secretion and APP C-terminal fragment stability. *Hum Mol Genet* **10**, 1665-1671, doi:10.1093/hmg/10.16.1665 (2001).

33 Selkoe, D. J. Alzheimer's disease: genes, proteins, and therapy. *Physiol Rev* **81**, 741-766, doi:10.1152/physrev.2001.81.2.741 (2001).

34 Chen, W. *et al.* Familial Alzheimer's mutations within APPTM increase Abeta42 production by enhancing accessibility of epsilon-cleavage site. *Nat Commun* **5**, 3037, doi:10.1038/ncomms4037 (2014).

35 Sun, L., Zhou, R., Yang, G. & Shi, Y. Analysis of 138 pathogenic mutations in presenilin-1 on the in vitro production of Abeta42 and Abeta40 peptides by gamma-secretase. *Proc Natl Acad Sci U S A* **114**, E476-E485, doi:10.1073/pnas.1618657114 (2017).

36 Walker, E. S., Martinez, M., Brunkan, A. L. & Goate, A. Presenilin 2 familial Alzheimer's disease mutations result in partial loss of function and dramatic changes in Abeta 42/40 ratios. *J Neurochem* **92**, 294-301, doi:10.1111/j.1471-4159.2004.02858.x (2005).

37 Smith, D. G., Cappai, R. & Barnham, K. J. The redox chemistry of the Alzheimer's disease amyloid beta peptide. *Biochim Biophys Acta* **1768**, 1976-1990, doi:10.1016/j.bbamem.2007.02.002 (2007).

38 Cerpa, W., Dinamarca, M. C. & Inestrosa, N. C. Structure-function implications in Alzheimer's disease: effect of Abeta oligomers at central synapses. *Curr Alzheimer Res* **5**, 233-243, doi:10.2174/156720508784533321 (2008).

39 Carrillo-Mora, P., Luna, R. & Colin-Barenque, L. Amyloid beta: multiple mechanisms of toxicity and only some protective effects? *Oxid Med Cell Longev* **2014**, 795375, doi:10.1155/2014/795375 (2014).



doi:10.6342/NTU202303164

40 Schmidt, C. *et al.* Amyloid precursor protein and amyloid beta-peptide bind to ATP synthase and regulate its activity at the surface of neural cells. *Mol Psychiatry* **13**, 953-969, doi:10.1038/sj.mp.4002077 (2008).

41 Puzzo, D. *et al.* Endogenous amyloid-beta is necessary for hippocampal synaptic plasticity and memory. *Ann Neurol* **69**, 819-830, doi:10.1002/ana.22313 (2011).

42 Abramov, E. *et al.* Amyloid-beta as a positive endogenous regulator of release probability at hippocampal synapses. *Nat Neurosci* **12**, 1567-1576, doi:10.1038/nn.2433 (2009).

43 Giuffrida, M. L. *et al.* Monomeric ß-amyloid interacts with type-1 insulin-like growth factor receptors to provide energy supply to neurons. *Front Cell Neurosci* **9**, 297, doi:10.3389/fncel.2015.00297 (2015).

44 Paulson, H. Repeat expansion diseases. *Handb Clin Neurol* **147**, 105-123, doi:10.1016/B978-0-444-63233-3.00009-9 (2018).

45 Tabrizi, S. J., Flower, M. D., Ross, C. A. & Wild, E. J. Huntington disease: new insights into molecular pathogenesis and therapeutic opportunities. *Nat Rev Neurol* **16**, 529-546, doi:10.1038/s41582-020-0389-4 (2020).

46 Lee, J. K. *et al.* Effect of trinucleotide repeats in the Huntington's gene on intelligence. *EBioMedicine* **31**, 47-53, doi:10.1016/j.ebiom.2018.03.031 (2018).

47 Saudou, F. & Humbert, S. The biology of Huntingtin. *Neuron* **89**, 910-926, doi:10.1016/j.neuron.2016.02.003 (2016).

48 Aylward, E. H. *et al.* Longitudinal change in regional brain volumes in prodromal Huntington disease. *J Neurol Neurosurg Psychiatry* **82**, 405-410, doi:10.1136/jnnp.2010.208264 (2011).

49 Rosas, H. D. *et al.* Cerebral cortex and the clinical expression of Huntington's disease: complexity and heterogeneity. *Brain* **131**, 1057-1068, doi:10.1093/brain/awn025 (2008).

50 Bessert, D. A., Gutridge, K. L., Dunbar, J. C. & Carlock, L. R. The identification of a functional nuclear localization signal in the Huntington disease protein. *Brain Res Mol Brain Res* **33**, 165-173, doi:10.1016/0169-328x(95)00124-b (1995).

51 Zheng, Z., Li, A., Holmes, B. B., Marasa, J. C. & Diamond, M. I. An N-terminal nuclear export signal regulates trafficking and aggregation of Huntingtin (Htt) protein exon 1. *J Biol Chem* **288**, 6063-6071, doi:10.1074/jbc.M112.413575 (2013).

52 Xia, J., Lee, D. H., Taylor, J., Vandelft, M. & Truant, R. Huntingtin contains a highly conserved nuclear export signal. *Hum Mol Genet* **12**, 1393-1403, doi:10.1093/hmg/ddg156 (2003).

53 Zala, D., Hinckelmann, M. V. & Saudou, F. Huntingtin's function in axonal transport is conserved in Drosophila melanogaster. *Plos One* **8**, doi:ARTN e60162



doi:10.6342/NTU202303164

10.1371/journal.pone.0060162 (2013).

54 Wong, Y. C. & Holzbaur, E. L. The regulation of autophagosome dynamics by huntingtin and HAP1 is disrupted by expression of mutant huntingtin, leading to defective cargo degradation. *J Neurosci* **34**, 1293-1305, doi:10.1523/JNEUROSCI.1870-13.2014 (2014).

55 Caviston, J. P., Zajac, A. L., Tokito, M. & Holzbaur, E. L. Huntingtin coordinates the dynein-mediated dynamic positioning of endosomes and lysosomes. *Mol Biol Cell* **22**, 478-492, doi:10.1091/mbc.E10-03-0233 (2011).

56 Steffan, J. S. *et al.* The Huntington's disease protein interacts with p53 and CREB-binding protein and represses transcription. *P Natl Acad Sci USA* **97**, 6763-6768, doi:DOI 10.1073/pnas.100110097 (2000).

57 Takano, H. & Gusella, J. F. The predominantly HEAT-like motif structure of huntingtin and its association and coincident nuclear entry with dorsal, an NF-kB/Rel/dorsal family transcription factor. *BMC Neurosci* **3**, 15, doi:10.1186/1471-2202-3-15 (2002).

58 Legendre-Guillemin, V. *et al.* HIP1 and HIP12 display differential binding to F-actin, AP2, and clathrin. Identification of a novel interaction with clathrin light chain. *J Biol Chem* **277**, 19897-19904, doi:10.1074/jbc.M112310200 (2002).

59 Engqvist-Goldstein, A. E. *et al.* The actin-binding protein Hip1R associates with clathrin during early stages of endocytosis and promotes clathrin assembly in vitro. *J Cell Biol* **154**, 1209-1223, doi:10.1083/jcb.200106089 (2001).

60 White, J. K. *et al.* Huntingtin is required for neurogenesis and is not impaired by the Huntington's disease CAG expansion. *Nat Genet* **17**, 404-410, doi:DOI 10.1038/ng1297-404 (1997).

61 Reiner, A. *et al.* Neurons lacking huntingtin differentially colonize brain and survive in chimeric mice. *J Neurosci* **21**, 7608-7619, doi:10.1523/JNEUROSCI.21-19-07608.2001 (2001).

62 Elias, S. *et al.* Huntingtin regulates mammary stem cell division and differentiation. *Stem Cell Reports* **2**, 491-506, doi:10.1016/j.stemcr.2014.02.011 (2014).

63 Lo Sardo, V. *et al.* An evolutionary recent neuroepithelial cell adhesion function of huntingtin implicates ADAM10-Ncadherin. *Nat Neurosci* **15**, 713-721, doi:10.1038/nn.3080 (2012).

64 Strehlow, A. N. T., Li, J. Z. & Myers, R. M. Wild-type huntingtin participates in protein trafficking between the Golgi and the extracellular space. *Human Molecular Genetics* **16**, 391-409, doi:10.1093/hmg/ddl467 (2007).

65 Ho, L. W., Brown, R., Maxwell, M., Wyttenbach, A. & Rubinsztein, D. C. Wild type Huntingtin reduces the cellular toxicity of mutant Huntingtin in mammalian cell



doi:10.6342/NTU202303164

models of Huntington's disease. *J Med Genet* **38**, 450-452, doi:10.1136/jmg.38.7.450 (2001).

66 Zhang, Y. *et al.* Huntingtin inhibits caspase-3 activation. *EMBO J* **25**, 5896-5906, doi:10.1038/sj.emboj.7601445 (2006).

67 Kim, M. W., Chelliah, Y., Kim, S. W., Otwinowski, Z. & Bezprozvanny, I. Secondary structure of Huntingtin amino-terminal region. *Structure* **17**, 1205-1212, doi:10.1016/j.str.2009.08.002 (2009).

68 Urbanek, A. *et al.* Flanking regions determine the structure of the poly-glutamine in Huntingtin through mechanisms common among glutamine-rich human proteins. *Structure* **28**, 733-746 e735, doi:10.1016/j.str.2020.04.008 (2020).

69 Baias, M. *et al.* Structure and dynamics of the Huntingtin exon-1 N-terminus: A solution NMR perspective. *J Am Chem Soc* **139**, 1168-1176, doi:10.1021/jacs.6b10893 (2017).

70 Scherzinger, E. *et al.* Huntingtin-encoded polyglutamine expansions form amyloid-like protein aggregates in vitro and in vivo. *Cell* **90**, 549-558 (1997).

71 Tobin, A. J. & Signer, E. R. Huntington's disease: the challenge for cell biologists. *Trends Cell Biol* **10**, 531-536 (2000).

72 Chen, S., Berthelier, V., Hamilton, J. B., O'Nuallain, B. & Wetzel, R. Amyloid-like features of polyglutamine aggregates and their assembly kinetics. *Biochemistry* **41**, 7391-7399 (2002).

73 Matlahov, I. & van der Wel, P. C. Conformational studies of pathogenic expanded polyglutamine protein deposits from Huntington's disease. *Exp Biol Med (Maywood)* **244**, 1584-1595, doi:10.1177/1535370219856620 (2019).

74 Breydo, L., Redington, J. M. & Uversky, V. N. Effects of intrinsic and extrinsic factors on aggregation of physiologically important intrinsically disordered proteins. *Int Rev Cell Mol Biol* **329**, 145-185, doi:10.1016/bs.ircmb.2016.08.011 (2017).

75 Chen, W. T., Liao, Y. H., Yu, H. M., Cheng, I. H. & Chen, Y. R. Distinct effects of Zn2+, Cu2+, Fe3+, and Al3+ on amyloid-beta stability, oligomerization, and aggregation: amyloid-beta destabilization promotes annular protofibril formation. *J Biol Chem* **286**, 9646-9656, doi:10.1074/jbc.M110.177246 (2011).

76 Lovell, M. A., Robertson, J. D., Teesdale, W. J., Campbell, J. L. & Markesbery, W. R. Copper, iron and zinc in Alzheimer's disease senile plaques. *J Neurol Sci* **158**, 47-52, doi:Doi 10.1016/S0022-510x(98)00092-6 (1998).

77 Lopez del Amo, J. M. *et al.* Structural properties of EGCG-induced, nontoxic Alzheimer's disease Abeta oligomers. *J Mol Biol* **421**, 517-524, doi:10.1016/j.jmb.2012.01.013 (2012).

78 Thapa, A., Jett, S. D. & Chi, E. Y. Curcumin attenuates Amyloid-beta aggregate



doi:10.6342/NTU202303164

toxicity and modulates Amyloid-beta aggregation pathway. *ACS Chem Neurosci* **7**, 56-68, doi:10.1021/acschemneuro.5b00214 (2016).

79 Sahoo, B. R. & Bardwell, J. C. A. SERF, a family of tiny highly conserved, highly charged proteins with enigmatic functions. *FEBS J*, doi:10.1111/febs.16555 (2022).

80 Scharf, J. M. *et al.* Identification of a candidate modifying gene for spinal muscular atrophy by comparative genomics. *Nat Genet* **20**, 83-86, doi:10.1038/1753 (1998).

81 van Ham, T. J. *et al.* Identification of MOAG-4/SERF as a regulator of age-related proteotoxicity. *Cell* **142**, 601-612, doi:10.1016/j.cell.2010.07.020 (2010).

82 Falsone, S. F. *et al.* SERF protein is a direct modifier of amyloid fiber assembly. *Cell Rep* **2**, 358-371, doi:10.1016/j.celrep.2012.06.012 (2012).

83 Yoshimura, Y. *et al.* MOAG-4 promotes the aggregation of alpha-synuclein by competing with self-protective electrostatic interactions. *J Biol Chem* **292**, 8269-8278, doi:10.1074/jbc.M116.764886 (2017).

84 Merle, D. A. *et al.* Increased aggregation tendency of alpha-synuclein in a fully disordered protein complex. *J Mol Biol* **431**, 2581-2598, doi:10.1016/j.jmb.2019.04.031 (2019).

85 Meyer, N. H. *et al.* Structural fuzziness of the RNA-organizing protein SERF determines a toxic gain-of-interaction. *J Mol Biol* **432**, 930-951, doi:10.1016/j.jmb.2019.11.014 (2020).

86 Nielsen, L. *et al.* Effect of environmental factors on the kinetics of insulin fibril formation: elucidation of the molecular mechanism. *Biochemistry* **40**, 6036-6046, doi:10.1021/bi002555c (2001).

87 Sattler, M., Schleucher, J. & Griesinger, C. Heteronuclear multidimensional NMR experiments for the structure determination of proteins in solution employing pulsed field gradients. *Prog Nucl Mag Res Sp* **34**, 93-158, doi:Doi 10.1016/S0079-6565(98)00025-9 (1999).

88 Markley, J. L. *et al.* Recommendations for the presentation of NMR structures of proteins and nucleic acids--IUPAC-IUBMB-IUPAB Inter-Union Task Group on the standardization of data bases of protein and nucleic acid structures determined by NMR spectroscopy. *Eur J Biochem* **256**, 1-15, doi:10.1046/j.1432-1327.1998.2560001.x (1998).

89 Kumar, S., Henning-Knechtel, A., Chehade, I., Magzoub, M. & Hamilton, A. D. Foldamer-mediated structural rearrangement attenuates Abeta oligomerization and cytotoxicity. *J Am Chem Soc* **139**, 17098-17108, doi:10.1021/jacs.7b08259 (2017).

90 Liu, D. G. *et al.* Optical design and performance of the biological small-angle X-



doi:10.6342/NTU202303164

ray scattering beamline at the Taiwan Photon Source. *J Synchrotron Radiat* **28**, 1954-1965, doi:10.1107/S1600577521009565 (2021).

91 Shih, O. *et al.* Performance of the new biological small- and wide-angle X-ray scattering beamline 13A at the Taiwan Photon Source. *J Appl Crystallogr* **55**, 340-352, doi:10.1107/S1600576722001923 (2022).

92 Petoukhov, M. V. *et al.* New developments in the ATSAS program package for small-angle scattering data analysis. *J Appl Crystallogr* **45**, 342-350, doi:10.1107/S0021889812007662 (2012).

93 Biancalana, M. & Koide, S. Molecular mechanism of Thioflavin-T binding to amyloid fibrils. *Biochim Biophys Acta* **1804**, 1405-1412, doi:10.1016/j.bbapap.2010.04.001 (2010).

94 Kayed, R. *et al.* Fibril specific, conformation dependent antibodies recognize a generic epitope common to amyloid fibrils and fibrillar oligomers that is absent in prefibrillar oligomers. *Mol Neurodegener* **2**, 18, doi:10.1186/1750-1326-2-18 (2007).

95 Wu, J. W. *et al.* Fibrillar oligomers nucleate the oligomerization of monomeric amyloid beta but do not seed fibril formation. *J Biol Chem* **285**, 6071-6079, doi:10.1074/jbc.M109.069542 (2010).

96 Bramanti, E., Lenci, F. & Sgarbossa, A. Effects of hypericin on the structure and aggregation properties of beta-amyloid peptides. *Eur Biophys J* **39**, 1493-1501, doi:10.1007/s00249-010-0607-x (2010).

97 Goormaghtigh, E., Ruysschaert, J. M. & Raussens, V. Evaluation of the information content in infrared spectra for protein secondary structure determination. *Biophys J* **90**, 2946-2957, doi:10.1529/biophysj.105.072017 (2006).

98 Cerf, E. *et al.* Antiparallel beta-sheet: a signature structure of the oligomeric amyloid beta-peptide. *Biochem J* **421**, 415-423, doi:10.1042/BJ20090379 (2009).

99 Cerda-Costa, N., De la Arada, I., Aviles, F. X., Arrondo, J. L. & Villegas, S. Influence of aggregation propensity and stability on amyloid fibril formation as studied by Fourier transform infrared spectroscopy and two-dimensional COS analysis. *Biochemistry* **48**, 10582-10590, doi:10.1021/bi900960s (2009).

100 Bitan, G., Lomakin, A. & Teplow, D. B. Amyloid beta-protein oligomerization: prenucleation interactions revealed by photo-induced cross-linking of unmodified proteins. *J Biol Chem* **276**, 35176-35184, doi:10.1074/jbc.M102223200 (2001).

101 Loo, J. A. Studying noncovalent protein complexes by electrospray ionization mass spectrometry. *Mass Spectrom Rev* **16**, 1-23, doi:10.1002/(SICI)1098-2787(1997)16:1<1::AID-MAS1>3.0.CO;2-L (1997).

102 Liu, J. & Konermann, L. Protein-protein binding affinities in solution determined



doi:10.6342/NTU202303164

by electrospray mass spectrometry. *J Am Soc Mass Spectrom* **22**, 408-417, doi:10.1007/s13361-010-0052-1 (2011).

103 Heck, A. J. & Van Den Heuvel, R. H. Investigation of intact protein complexes by mass spectrometry. *Mass Spectrom Rev* **23**, 368-389, doi:10.1002/mas.10081 (2004).

104 Fiumara, F., Fioriti, L., Kandel, E. R. & Hendrickson, W. A. Essential role of coiled coils for aggregation and activity of Q/N-rich prions and PolyQ proteins. *Cell* **143**, 1121-1135, doi:10.1016/j.cell.2010.11.042 (2010).

105 Lupas, A., Van Dyke, M. & Stock, J. Predicting coiled coils from protein sequences. *Science* **252**, 1162-1164, doi:10.1126/science.252.5009.1162 (1991).

106 Thakur, A. K. *et al.* Polyglutamine disruption of the huntingtin exon 1 N terminus triggers a complex aggregation mechanism. *Nat Struct Mol Biol* **16**, 380-389, doi:10.1038/nsmb.1570 (2009).

107 Nelson, P. N. *et al.* Monoclonal antibodies. *Mol Pathol* **53**, 111-117, doi:10.1136/mp.53.3.111 (2000).

108 Luhrs, T. *et al.* 3D structure of Alzheimer's amyloid-beta(1-42) fibrils. *Proc Natl Acad Sci U S A* **102**, 17342-17347, doi:10.1073/pnas.0506723102 (2005).

109 Berthelot, K., Ta, H. P., Gean, J., Lecomte, S. & Cullin, C. In vivo and in vitro analyses of toxic mutants of HET-s: FTIR antiparallel signature correlates with amyloid toxicity. *J Mol Biol* **412**, 137-152, doi:10.1016/j.jmb.2011.07.009 (2011).

110 Krimm, S. & Bandekar, J. Vibrational analysis of peptides, polypeptides, and proteins. V. Normal vibrations of beta-turns. *Biopolymers* **19**, 1-29, doi:10.1002/bip.1980.360190102 (1980).

111 Sarroukh, R. *et al.* Transformation of amyloid beta(1-40) oligomers into fibrils is characterized by a major change in secondary structure. *Cell Mol Life Sci* **68**, 1429-1438, doi:10.1007/s00018-010-0529-x (2011).

112 Sarroukh, R., Goormaghtigh, E., Ruysschaert, J. M. & Raussens, V. ATR-FTIR: a "rejuvenated" tool to investigate amyloid proteins. *Biochim Biophys Acta* **1828**, 2328-2338, doi:10.1016/j.bbamem.2013.04.012 (2013).

113 Pras, A. *et al.* The cellular modifier MOAG-4/SERF drives amyloid formation through charge complementation. *EMBO J* **40**, e107568, doi:10.15252/embj.2020107568 (2021).

114 Bhattacharyya, A. *et al.* Oligoproline effects on polyglutamine conformation and aggregation. *J Mol Biol* **355**, 524-535, doi:10.1016/j.jmb.2005.10.053 (2006).

115 Caron, N. S., Desmond, C. R., Xia, J. & Truant, R. Polyglutamine domain flexibility mediates the proximity between flanking sequences in huntingtin. *Proc Natl Acad Sci U S A* **110**, 14610-14615, doi:10.1073/pnas.1301342110 (2013).



doi:10.6342/NTU202303164

# APPENDIX

**List of antibodies**

| Application | Reagent or Resource | Source | Catalog no. |
|---|---|---|---|
| **Filter-trap assay** | OC | Sigma-Aldrich | AB2286 |
| | Goat anti- rabbit IgG antibody (HRP) | GeneTex | GTX213110-01 |
| **ICC** | Anti-flag (D6W5B) | Cell Signaling | 14793 |
| | Alexa Fluor 594 anti-mouse | Invitrogen | A-11005 |
| | Alexa Fluor 488 anti-rabbit | Invitrogen | A-21206 |
| **Immunogold labeling** | SERF#1 | In house | n/a |
| | Goat pAb to Ms IgG (Gold 10 nm) | abcam | ab39619 |
| **Partition analysis** | SERF#1 | In house | n/a |
| | Goat anti-mouse IgG antibody (HRP) | GeneTex | GTX213111-01 |
| **PICUP** | 4G8 | BioLegend | 800702 |
| | 6E10 | BioLegend | 803003 |
| | SERF#1 | In house | n/a |
| | Goat anti-mouse IgG antibody (HRP) | GeneTex | GTX213111-01 |



doi:10.6342/NTU202303164

**List of commercial reagents**

| Application | Reagent or Resource | Source | Catalog no. |
|---|---|---|---|
| **Cell transfection** | Lipofectamine 2000 | Invitrogen | 11668-019 |
| | Lipofectamine 3000 | Invitrogen | L3000015 |
| **MTT assay** | MTT | Sigma-Aldrich | M5655 |
| **ELISA** | TMB | seracare | 5120-0083 |
| **ICC** | Hoechst 33258 | Invitrogen | H1398 |
| | formaldehyde | Invitrogen | FB002 |
| **IP** | Protein G magnetic beads | GE Healthcare | GE28-9670-70 |
| **PICUP** | RuBpy | Sigma-Aldrich | 224758-250MG |
| **Purification** | Ampicillin | VWR Life Science | 0339-25G |
| | Kanamycin | Calbiochem | 420311 |
| | IPTG | PROTECH | PT-0487-10G |
| | Thrombin | GE Healthcare | 27-0846-01 |
| **Quantification** | BCA assay kit | Thermo | 23225 |
| **SDS-PAGE** | SeeBlue Plus2 Prestained Standard | Invitrogen | LC5925 |
| **TEM** | Uranyl acetate | SPI-Chem | 6159-44-0 |
| **ThT assay** | Thioflavin T | Sigma-Aldrich | T3516-25G |
| **Tricine gel** | APS | VWR Life Science | 0486-25G |
| | TEMED | Millipore | 1.10732.0100 |
| **Western blot** | ECL | Millipore | WBKLS0500 |
| | PVDF membrane 0.2 μm | GE | 10600021 |



doi:10.6342/NTU202303164